Control-Relevant Upscaling

Control-Relevant Upscaling

PROEFSCHRIFT

ter verkrijging van de graad van doctor
aan de Technische Universiteit Delft,
op gezag van de Rector Magnificus Prof. ir. K.C.A.M. Luyben,
voorzitter van het College voor Promoties,
in het openbaar te verdedigen op

dinsdag 9 november 2010 om 10:00 uur

door

Seyed Ali VAKILI GHAHANI

ingenieur technische aardwetenschappen

geboren te Ghom, Iran.

Dit proefschrift is goedgekeurd door de promotor:

Prof. dr. ir. J.D. Jansen

Samenstelling promotiecommissie:

Rector Magnificus,	voorzitter
Prof. dr. ir. J.D. Jansen,	Technische Universiteit Delft, promotor
Prof. dr. D.C. Sorensen,	Rice University
Prof. dr. J. Bruining,	Technische Universiteit Delft
Prof. dr. R.J. Arts,	Technische Universiteit Delft
Prof. dr. ir. A.W. Heemink,	Technische Universiteit Delft
Prof. dr. ir. P.M.J. Van den Hof,	Technische Universiteit Delft
dr. ir. M.D.L.C. Rojas Larrazabal,	Technische Universiteit Delft

This research was carried out within the context of the Integrated Systems Approach to Petroleum Production (ISAPP) knowledge centre. ISAPP is a joint project between Delft University of Technology (TU Delft), Shell International Exploration and Production (SIEP), and the Dutch Organization for Applied Scientific Research (TNO).

ISBN: 978-90-9025826-3

Keywords: reservoir simulation, systems and control, model reduction, upscaling

Printed in the Netherlands.

to my parents

to Elaheh

to Tara

ACKNOWLEDGEMENTS

This thesis would not have been possible without supports and contributions by many people who deserve special mention.

In the first place, I am sincerely grateful to Jan Dirk Jansen, for his supervision, advice, and guidance from the beginning of my PhD research, as well as providing me encouragement and support in various ways. I am also thankful to Rob Arts and Cor Hofstee for their advice in the early stage of this research.

I am indebted to many friends and colleagues at the department of Geotechnology and ISAPP group, who provided me a stimulating and fun environment to work. I am especially grateful to Lydia, Margot, Marlijn, Hannie and Ralph for their logistical supports, to Anke for ISAPP-related arrangements, and to Renato, Farzad, Hamidreza, Ehsan, Jorn, Sippe, Rouhi, Gerbon, Elham, Maryam and Gosia for all constructive discussions and contributions. Renato Markovinović also helped me with the Dutch translation of the summary and he was supportive in various scientific, philosophical, intellectual and humorous debates.

During my PhD research, I had the pleasant opportunity to visit Sanford University for about three months. I gratefully acknowledge professor Durlofsky for giving me this opportunity, as well as his advice and supervision during my stay. I am thankful to everybody who made my stay pleasant. In particular, I wish to thank Margot Gerritsen, James Lambers, Marco Cardoso, Jincong He and Jon Sætrom for insightful discussions and for their contributions to my research.

I also would like to thank all my friends, as well as expressing my apology that I could not mention them one by one. Without you it would definitely not have been such a fantastic personal and professional experience in Delft.

Finally, I wish to express my love and gratitude to my parents, who raised me, taught me, encouraged me, and supported me; my wife who has always stood by me, helped me, and believed me; and our little angel, Tara, who granted us a new perspective on life. To them I dedicate this thesis.

Delft, October 2010

Ali Vakili

CONTENTS

LIST OF TABLES

LIST OF FIGURES

1. CHAPTER: INTRODUCTION

This thesis concerns the application of system-theoretical techniques in reduced-order modeling, to upscaling of grid-based reservoir models. The main research question is related to the optimal level of complexity required to simulate, predict and control the flow behaviour in porous media. We start from an overview of the classical upscaling techniques in reservoir simulation, and then we develop a modified grid-based upscaling algorithm that is based on control-relevant properties of the reservoir model. Finally, we explain several order-reduction techniques and investigate the potential benefit of using them in combination with our control-relevant upscaling approach.

1.1. Petroleum production

'Petroleum production' involves diverse technologies for exploration, drilling, and production of oil and gas from a petroleum reservoir. A 'reservoir' is a body of porous sedimentary rock formations that contain naturally occurring hydrocarbons (mainly oil and gas). These hydrocarbons have been trapped by impermeable rock layers in the deep subsurface, resulting in a very high pressure and temperature of the order of hundreds of bars and hundreds of degrees centigrade, respectively. Initially, the oil is produced by natural drive mechanisms of the pressurized reservoir, referred to as 'primary production'. As the oil and the gas are produced, the reservoir pressure is depleted. Injecting of another fluid (mostly water or gas) can maintain the pressure and push the hydrocarbons out of the reservoir. Nevertheless, the typical ultimate oil recovery for a reservoir is up to around 40 percent of its initial oil-in-place.

The increase in worldwide energy demand and the decline of easy-to-produce oil and gas resources in recent years have motivated the exploration and production (E&P) industry to look for expensive enhanced oil recovery (EOR) solutions, such as foam and polymer injections and thermal methods, and to move to high-risk development areas like offshore production in deep water. This has also resulted in an intense research in understanding complex fluid flow mechanisms and, in particular, advanced numerical reservoir simulators.

The goal of a 'reservoir simulator' is to build a model of the reservoir that represents the true system such that it can be used to predict and control the flow behaviour in the subsurface. The simulator is built on a reservoir model that includes physical flow relations and different data from geological interpretation, seismic interpretation and reservoir characterization, as well as the associated uncertainty. Usually, the simulator is scaled up to a coarser representation during an 'upscaling' step and it is calibrated based on historic pressure and production data in a process referred to as 'history matching'. Figure 1.1 shows the schematic workflow of reservoir modeling. Multiple geological and production scenarios then can be simulated to understand the behaviour of fluid flow over time in each setting.

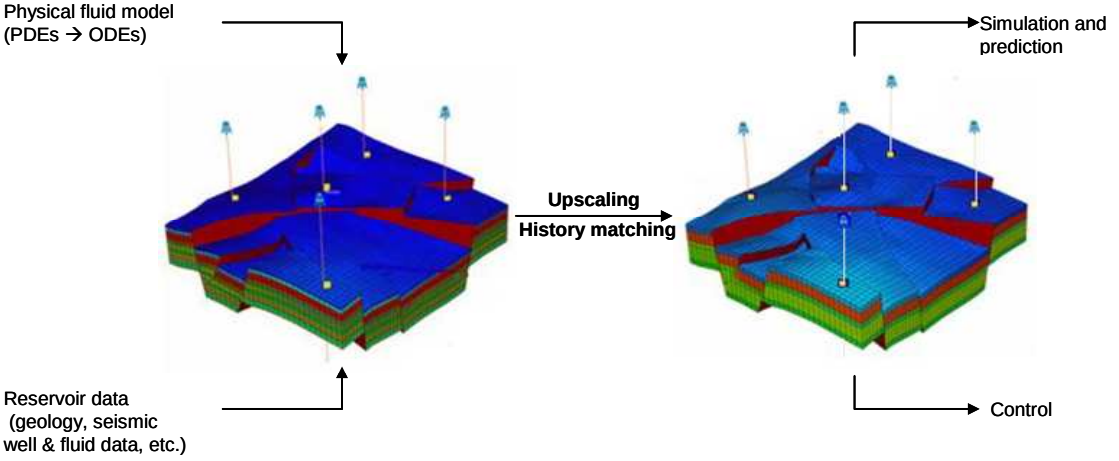

Figure 1.1 Reservoir modeling workflow.

1.1.1. Reservoir management

Nowadays, 'reservoir management' is an integrated workflow that covers reservoir life-cycle from exploration to abandonment. The ultimate goal is to maximize the oil production or another economic objective and reduce the risk of failure, particularly in expensive high-risk E&P projects. In this workflow, reservoir simulation plays a central role in aligning the primary seismic, geological and geophysical data with the production data through 'model-based optimization' and 'model updating'.

In model-based optimization, the oil recovery process is optimized using the predictions from the reservoir model. This optimization can be performed for different objectives (e.g., the number and locations of wells, or injection/production rates), as well as different time cycles to improve the field performance and economics. A typical application is in dynamic water flooding optimization over the life-cycle of the reservoir,

where the scope of the flooding process can be investigated through a model-based optimization framework (Brouwer & Jansen 2004). In such a process, an objective function (e.g., cumulative oil production or Net Present Value) of the scenario is optimized by changing the controls of the model (i.e., water injection rates or down-hole valve settings). More details of this activity can be found in, e.g., Ramirez (1987), Brouwer (2004), Sarma et al. (2005), Jansen et al. (2008), Markovinović (2009), and Zandvliet (2008).

As the oil and gas are produced from the reservoir, new pressure and production data become available. In particular, the introduction of 'smart wells', with down-hole measurement sensors, and '4D (time-lapse) seismic' provides an abundance of measurement data. This data can be used for the model updating step, also referred to as 'data assimilation' or 'automated history matching', to obtain a more accurate and reliable simulator. A systematic approach is to form a 'variational' problem, in which the controls are formed by unknown reservoir parameters, e.g., permeability and porosity values, while the objective function is defined in terms of the mismatch between simulated and measured production data (Li et al. 2003; Rommelse 2009). Another approach that allows the updating of uncertain states in large nonlinear models is ensemble Kalman filtering (EnKF). This technique includes the model error by taking an ensemble of model realizations, and updates the state vector at every time that a new measurement is available. For the application of EnKF in reservoir engineering see Nævdal et al. (2005), Evensen (2009) and Rommelse (2009), where in the latter an overview of different data assimilation techniques is also provided.

Closing the loop

Sequential data assimilation and computer-assisted optimization at every time that new measurements become available leads to a 'closed-loop' reservoir management approach (Jansen et al. 2005). The process involves the use of several realizations of simulation models during the producing life of a reservoir for near-continuous flooding optimization based on frequently updated reservoir models (see Figure 1.2). Brouwer et al. (2004), Naevdal et al. (2006), Sarma et al. (2006), Jansen et al. (2009) and Chen & Oliver (2009) reported successful application of the closed-loop control approach, although the resulting reservoir performance has been only evaluated by numerical simulations.

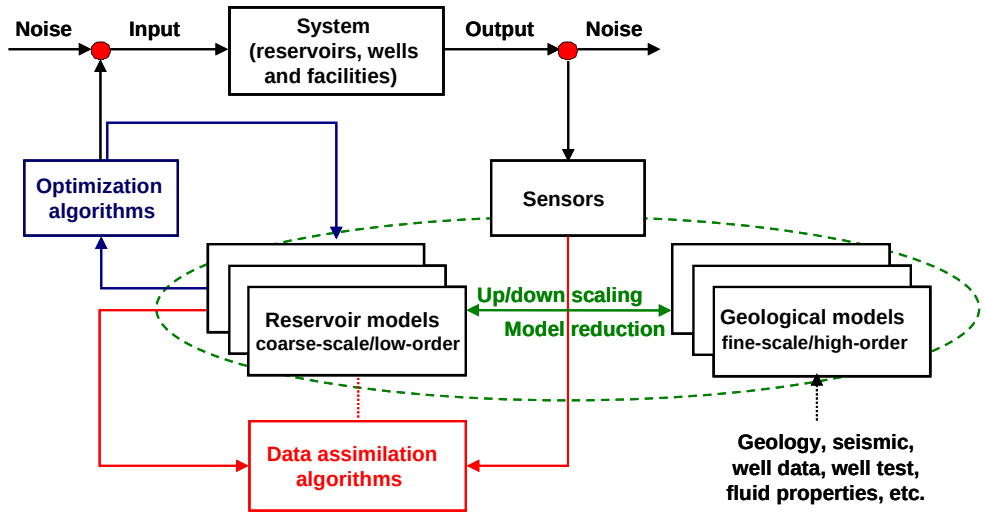

Figure 1.2 Closed-loop reservoir management (after Jansen et al. 2009).

The outcome of closed-loop reservoir management is, in the ideal case, a set of multiple potential development scenarios with associated risk and economic analysis, resulting in improved decision makings and increased returns on human asset and capital investments.

1.1.2. Upscaling/model reduction

As a precursor to flow simulation, reservoir data are collected from different sources with various temporal and spatial scales. For example, there are core measurements in the order of centimetres, well log measurements in the order of tens of centimetres, and well test and seismic data in the order of meters. These data are integrated into a system of numerical grid blocks that should represent the high complexity of the geological environment with heterogeneities of different spatial scales, and also the associated uncertainties. The results are geological realizations with tens to hundred layers and around 10^6 to 10^9 grid cells. Adding nonlinear dynamical flow relations with different flow mechanisms that vary over spatial and temporal scales makes the efficient and accurate modeling of the flow behaviour on such detailed models computationally extremely challenging. Therefore, in addition to the model updating and the optimization elements, reducing the complexity of reservoir models through an ‘upscaling/model reduction’ step is another essential part of the closed-loop reservoir management concept. This part, as depicted with the dashed oval in Figure 1.2, is the main focus of our research.

1.2. Problem statement

1.2.1. Issues with large-scale models

Geological subsurface models often represent the subsurface heterogeneity with 10^6 to 10^9 parameters ('voxels'). The major issues with such high-order[1] (large-scale) systems are related to computational costs such as CPU time and storage requirements, and system-theoretical properties like controllability, observability and identifiability of the system.

Computational costs

Notwithstanding the rapid increase in cluster computing power is facilitating the simulation of more sophisticated and detailed reservoir models, the increasing resolution and multi-scale complexity of geological models over time keep the quest for faster and more efficient reservoir simulators ongoing. Moreover, the uncertainty of the geological parameters is increasingly taken into account by simulating an ensemble of model realizations which significantly increases the computational demands, especially when it is also required to perform repeated simulations for computer-assisted flooding optimization or history matching (e.g., application of reservoir simulation in closed-loop reservoir management). This requires an 'upscaling/order-reduction' solution that transfers the relevant features of a geological model to a flow simulation model such that cost-efficient simulation, prediction and control of the fluid flow in the reservoir become feasible. The model size is often determined such that the flow simulation can be performed within a practical time frame. At present, computational limits of reservoir flow simulators restrict the model order to typically 10^4 to 10^6 (depending on the type of the model).

System-theoretical properties

The input into the upscaling/model-reduction problem is itself an uncertain set of data which are often obtained by geostatistical interpolations of a limited amount of direct measurements (mainly adjacent to the wells), and sometimes from indirect global measurements such as seismic inversions. Therefore, for a given configuration of wells, there are only a limited number of degrees of freedom in the input-output dynamics of a reservoir system. From a system-theoretical point of view, this means that a large number

[1] Here, the model order (dimension) is defined as the number of time-dependent variables (i.e., state variables such as grid block pressures, saturations or component accumulations) which is typically equal to the number of active grid blocks times the number of components (i.e., hydrocarbon components and water) in the simulation. The number of time-independent model parameters is usually of the same order of magnitude because they are also proportional to the number of grid blocks (e.g. grid block permeabilities and porosities).

of combinations of the state variables (pressure and saturation values) are not actually 'controllable' and 'observable' from the wells, and accordingly, they are not affecting the input-output behavior of the system (Zandvliet et al. 2008).

The problem with the uncontrollable/unobservable modes is two-fold. Firstly, they may waste computational effort. Secondly, they may lead to ill-posed inverse problems and even wrong answers (Skogestad & Postlethwaite 2005; Antoulas 2005). More specifically, in model updating or in history matching we are dealing with a very large number of model parameters and states that need to be adjusted to match the model predicted data with the real measurements. This is inherently an ill-posed problem due to the relatively small number of measurements and, therefore, presence of an uncontrollable/unobservable system.

In conclusion, in most reservoir applications, the controllable and observable subspaces are rather small compared to the total system state-space, in which case the complexity level of the model can be reduced by leaving out the uncontrollable/unobservable subspaces.

1.2.2. Research objective

Although considerable research has been devoted to upscaling techniques in reservoir engineering to overcome the computational limits of the simulator, fewer efforts have been put on studying the issues related to the control-relevant properties and adjusting the complexity of the reservoir model to the available amount of control and information. Therefore, the main objective of this research project is to replace a fine-scale (high-order) reservoir model with an 'optimal' representation, based on the control-relevant properties of the system. The optimal model should be a coarse-scale (low-order) system that preserves the essential properties of the original model in terms of input-output behaviour, while reducing its computational complexity.

1.2.3. Approach

Various approaches have been developed over the past decades to reduce the complexity of a system model. The most widely used techniques for reservoir simulations are classical grid-based upscaling methods that vary from simple averaging methods on uniform Cartesian cells to sophisticated flow-based techniques on adaptive and unstructured grids (for an overview see e.g., Wen et al. 1996; Renard & Marsily 1997; Durlofsky 2005). In most cases, the coarse-scale parameters are approximated based on fine-scale parameters and/or some local flow calculations, subjected to generic boundary conditions. Therefore, the performance of these methods often depends on the choice of

the local boundary conditions and may not adequately capture the key features of the fine-scale flow behaviour, especially in the near-well region (Durlofsky et al. 2000).

System-theoretical model reduction techniques such as proper orthogonal decomposition (POD) appear to provide another helpful tool to reduce the complexity of a large-scale model (Heijn et al., 2004; Antoulas 2005; Gildin 2006; Markovinović 2002 and 2009). In these methods, we use the spatial correlation in the states (pressures and saturations) to compute a limited number of spatial patterns (directions) in the state-space coordinates, which can be used to characterize the dominant dynamical variations of the system. These dominant patterns are obtained by selecting the leading eigen vectors of the covariance (correlation) matrix of several fine-scale simulation data. We can then project the high-order system of reservoir equations onto the dominant spatial patterns to obtain a reduced-order model. Reparameterization of the permeability field is somehow a similar technique that benefits from the spatial correlation in the model parameters to reduce the dimension of the parameter space (Sahni & Horne 2005; Sarma et al. 2007; Jafarpour & McLaughlin 2007; Van Doren et al. 2008). Although these methods might outperform the grid-based upscaling techniques in terms of issues related to the system properties, they often lead to a non-physical reduced-order model. Moreover, in strongly nonlinear cases, reducing the dynamical order might not necessarily reduce the computational complexity as the expensive nonlinear reduction step may need to be repeated during the simulation.

Recent advances in multi-scale methods also seem to be promising to address the issue of scales. In this approach, different grid blocks are used for flow and transport computations. Therefore, fine-scale information may be used at various stages of the simulation, though it might require a large memory capacity to carry the fine-scale data through the multi-scale simulation (Hou & Wu 1997; Aarnes 2004, Gerritsen & Durlofsky 2005).

The present study focuses on system-theoretical aspects of grid-based upscaling, whereby we develop an upscaling methodology that coarsens the reservoir model based on the relevant level of control and information; i.e., controllability and observability properties of the system. The main benefit of this approach is that, unlike in most reduction techniques, the approximated model is still in a physical space, while for most cases that we investigated it outperforms the classical grid-based upscaling techniques in terms of input/output behavior. Different algorithms, requirements and limitations of this control-relevant approach are presented in this thesis.

1.2.4. Thesis structure

We started the thesis by a general introduction to petroleum production and a brief description of the research problem. In **Chapter 2**, we present the governing flow equations, followed by an overview and discussion of various upscaling methods that have been developed in both hydrology and reservoir simulation. **Chapter 3** is devoted to derivation of linear 'state-space formulation' of a reservoir system. Furthermore, some system-theoretical properties like controllability and observability are discussed to understand how much of the state-space can be reached from the input side, and how the internal behaviour of the system can be obtained from the output information. We use these properties in **Chapter 4** to develop a 'control-relevant upscaling (CRU) algorithm' that indirectly uses the controllable and observable part of the system to determine the coarse-scale parameters. The accuracy of the control-relevant approach is further improved in **Chapter 5** by leaving out the controllable/observable parts of the reservoir domain and scaling up only the uncontrollable/unobservable parts. This is referred to as 'control-relevant selective coarsening' or, in short, the 'CRSC algorithm'. **Chapter 6** explains some system-theoretical reduction techniques and investigates the potential benefit of using them in combination with the CRU and CRSC methods. Finally, the conclusions and the recommendations for the future research are given in **Chapter 7**.

2. CHAPTER: FLOW MODELING AND UPSCALING FOR RESERVOIR SIMULATIONS

This chapter provides a brief explanation of the governing equations that describe the fluid flow behaviour in porous media, followed by an overview of current upscaling techniques in reservoir simulation. Particular attention is paid to single-phase flow equations and single-phase numerical upscaling methods as they are frequently used throughout this thesis.

2.1. Flow modeling

We consider simplified partial differential flow equations and their spatial and temporal discretization to model fluid flow in porous media. Derivations of the equations are mainly borrowed form Aziz & Settari (1979) and Peaceman (1977).

2.1.1. Governing equations

The fundamental equation that models the isothermal and immiscible multi-phase flow in porous media is the continuity (mass conservation) equation, given by

$$\frac{\partial}{\partial t}(\phi \rho_\alpha S_\alpha) + \nabla.(\rho_\alpha \mathbf{u}_\alpha) = \rho_\alpha q_\alpha, \tag{2.1}$$

where t is time, ϕ is porosity, ρ is density, S is the phase saturation, q represents source (sink) term expressed as volumetric flow rate (negative for production), and **u** denotes the fluid velocity. In a two-phase flow system, subscript α refers to o for the oil phase and w for the water phase. For low velocities, instead of the momentum balance, we may relate the fluid velocity for each phase to the fluid pressure p and gravity forces through the empirical relation of Darcy, written as

$$\mathbf{u}_\alpha = -\frac{k_{r\alpha}}{\mu_\alpha}\mathbf{K}.\nabla(p_\alpha - \rho_\alpha g z). \tag{2.2}$$

In this equation, μ is viscosity, $k_{r\alpha}$ is the relative permeability of phase α, **K** is a diagonal absolute permeability tensor, g represents the gravitational acceleration, and z is the distance in the direction of gravity. Note that even though the permeability tensor is

generally a full tensor, we can often align the coordinate directions to the geological layering in the reservoir such that we obtain a diagonal permeability tensor $\mathbf{K}(x, y, z) = diag(K_x, K_y, K_z)$.

More equations are given by closure relations for the phase saturations and capillary pressures written, respectively, as

$$S_o + S_w = 1, \tag{2.3}$$

$$p_c = p_o - p_w. \tag{2.4}$$

For simplicity, we assume that the parameters $\mathbf{K}$ and μ are pressure independent, while ϕ and ρ are related to the pressure by isothermal relations

$$c_l(p) = \frac{1}{\rho}\frac{\partial \rho}{\partial p}, \tag{2.5}$$

$$c_r(p) = \frac{1}{\phi}\frac{\partial \phi}{\partial p}, \tag{2.6}$$

where c_l is the isothermal liquid compressibility and c_r is the rock compressibility. Moreover, the phase mobility is defined as $\lambda_\alpha = k_{r\alpha}/\mu_\alpha$, and the fractional flow is $f_w(S_w) = \lambda_w/(\lambda_w + \lambda)$. Therefore, from Eqs. (2.1) to (2.6), the pressure (flow) and the saturation (transport) equations are correspondingly given by

$$\phi c_t \frac{\partial p}{\partial t} + \nabla.\left[-\lambda_w \mathbf{K}.\nabla(p_w - \rho_w g z) - \lambda_o \mathbf{K}.\nabla(p_o - \rho_o g z)\right] = q, \tag{2.7}$$

$$\phi \frac{\partial S_w}{\partial t} + \nabla.\left[f_w(\mathbf{u} + \lambda_o \mathbf{K}.\nabla p_c + \lambda_o(\rho_w - \rho_o) g \mathbf{K}.\nabla z)\right] = q_w. \tag{2.8}$$

Here, the total flow rate, velocity and compressibility are correspondingly defined as $q = q_w + q_o$, $\mathbf{u} = \mathbf{u}_w + \mathbf{u}_o$ and $c_t = S_w c_w + (1 - S_w)c_o + c_r$. The saturation equation clearly explains three different forces involved in fluid flow. These are viscous forces, expressed by the term $q_v = \nabla.[f_w \mathbf{u}]$, capillary forces, represented by the term $q_c = \nabla.[f_w \lambda_o \mathbf{K}.\nabla p_c]$, and gravity forces, given by $q_g = \nabla.[f_w \lambda_o (\rho_w - \rho_o) g \mathbf{K}.\nabla z]$. The influence of each force depends on flow rates and reservoir heterogeneities (Aarnes et al. 2007). In the absence of the capillary and gravity forces (i.e., $p_w = p_o$, $\nabla z = 0$), the simplified pressure equation describing an immiscible incompressible two-phase flow is written as

$$c_t \frac{\partial p}{\partial t} - \nabla.(\lambda \mathbf{K}.\nabla p) = q. \tag{2.9}$$

2.1.2. Single-phase flow equation

In most cases, there is more than one fluid phase present in the reservoir system. Nevertheless, there are some examples such as gas reservoirs, or oil reservoirs in an early production stage, for which there is only one phase present. Moreover, single-phase flow simulation, as the simplest way of describing flow in a porous medium, is used in simplified fundamental studies such as upscaling.

Combining Eqs. (2.1) and (2.2) for slightly compressible rock and fluid, and in the absence of the gravity force, we obtain the simplified single-phase pressure equation as

$$c_t \frac{\partial p}{\partial t} - \nabla.(\frac{1}{\mu}\mathbf{K}.\nabla p) = q. \tag{2.10}$$

This form of the pressure equation is very similar to the two-phase pressure equation (2.9), except for λ that is replaced by $1/\mu$. They also take the same form in case of a unit mobility ratio, where $\mu_o = \mu_w$, $k_{r\alpha} = S_\alpha$, and $\lambda = 1/\mu_w = 1/\mu_o$. From the similarity between single- and two-phase pressure equations, one can conclude that single-phase upscaling approaches might be sufficient and applicable for more general cases of multi-phase flow simulations. This is particularly valid for low degree of coarsening, i.e., one or two orders of magnitude reduction in the number of grid cells (Durlofsky 2005). Therefore, a simplified form of Eq. (2.10) for steady-state incompressible single-phase flow is often used in upscaling procedures.

2.1.3. Discretization

Spatial discretization

Consider a two-dimensional horizontal reservoir domain with regular rectangular grid cells, where the grids are aligned with the principal coordinate axes. We use a flux-continuous finite volume discretization (FVD) to solve the single-phase flow equation over the given domain (Edwards & Roger 1998; Pal et al 2006). In this method, physical values are represented as averaged values over a finite number of control volumes denoted here by Ω. Conservation of mass, thus integrating Eq. (2.1) over each control volume, gives

$$\int_{\Omega_i} \left(\frac{\partial}{\partial t}(\phi\rho) \right) dV + \int_{\Omega_i} \left(\nabla.(\rho\mathbf{u}) \right) dV = \int_{\Omega_i} (\rho q) dV, \tag{2.11}$$

where *dV* denotes a volume element. Using the divergence theorem and Darcy's law, and assuming slightly compressible rock and fluid with total compressibility of c_t, we obtain

$$c_t \phi V_i \dot{p}_i + \sum_{k=1}^{4} \int_{\partial\Omega_{ik}} (-\frac{1}{\mu}\mathbf{K}(x,y).\nabla p).\mathbf{n}_i dS = q_i V_i, \tag{2.12}$$

where dS denotes a surface element, $\mathbf{n}_i$ is a unit outward normal vector on $\partial\Omega_{ik}$, and $\partial\Omega_{ik}$ (i=1,2,3,4) surrounds the control volume Ω_i. This equation simply states that the total fluxes to or from the four neighboring control volumes are equal to the source and accumulation terms. For a diagonal permeability tensor the flux integral at each boundary can be approximated by a two-point flux approximation (TPFA) approach, resulting in the classical five-point scheme in a two-dimensional problem. In case of a full permeability tensor, a 9-point scheme in 2D and 27-point scheme in 3D can be implemented (Aavatsmark 2002).

In TPFA the flux of each boundary is related to the cell-centered pressures of two blocks that share that boundary. For grid blocks i and i-1, this relation can be derived from the continuity of the pressure at the interface and can be written as

$$q_{i-1/2,j} = -T_{i-1/2,j}(p_{i-1,j} - p_{i,j}), \tag{2.13}$$

where $T_{i-1,j}$ is the transmissibility between two grid blocks, defined as

$$T_{i-1/2,j} = \frac{1}{\mu}\frac{2K_{i-1,j}K_{i,j}}{\Delta x_i K_{i-1,j} + \Delta x_{i-1} K_{i,j}}\Delta y \Delta z \tag{2.14}$$

This can also be seen as a local upscaling problem in two adjacent half grid blocks, where the upscaled permeability at their interface is obtained by distance-weighted harmonic average of the x component of the permeability tensor in the grid blocks i and i-1 (Edwards & Roger 1998). The transmissibility relation for other interfaces is defined similarly. Eventually, for a system of n grid blocks, we can compute the flux integral in (2.12) by Eq. (2.13) and write n relations in the matrix form of

$$\mathbf{V}_{n\times n}\dot{\mathbf{p}}_{n\times 1} + \mathbf{T}_{n\times n}\mathbf{p}_{n\times 1} = \mathbf{q}_{n\times 1}, \tag{2.15}$$

where $\mathbf{V}$ is a diagonal accumulation matrix, $\mathbf{T}$ is a symmetric transmissibility matrix, $\mathbf{p}$ is the pressure vector, and $\mathbf{q}$ represents the source/sink vector that includes $q_i V_i$ values for all grid blocks.

Furthermore, we need to set boundary conditions of the model. For reservoir simulation purposes, the boundary conditions are usually prescribed in two types (see Aziz & Settari 1979). In the first one the pressure values at the boundaries are specified (Dirichlet), whereas in the second type $\partial p / \partial \mathbf{n}$ over the boundaries is given (Neumann). Here, $\mathbf{n}$ is an

outward normal unit vector. Using Darcy's law, both Dirichlet and Neumann boundary conditions can directly or indirectly be expressed in terms of fluxes and added to the source/sink term in the right hand side of Eq. (2.15). The simplest boundary condition is to assume no flow across all boundaries. This means that the velocity vector normal to the boundaries of the reservoir as well as the transmissibility through them is zero. Consequently, the flow into or out of the system is only occurring through source/sink terms (wells). Nevertheless, for incompressible single-phase flow equation, a pressure value has to be specified in at least one point to obtain a unique solution.

Time discretization

We approximate the accumulation term in Eq. (2.12) by

$$\frac{dp}{dt}(k+1) = \frac{p(k+1) - p(k)}{\Delta t}, \tag{2.16}$$

where k is the time-step number. Moreover, we choose vector $\mathbf{p}_0$ as the initial condition (pressure) of the reservoir. Eq. (2.16) is solved by an implicit Euler method that in contrary to an explicit Euler approximation requires no limitation on the time step size to guarantee the stability of the numerical model. However, even in the implicit time discretization scheme, we need to be aware of non-physical smearing effects due to very large time-step sizes.

2.2. Upscaling

2.2.1. Introduction

Reservoir simulators are established from detailed geological models, which are themselves often a result of several geostatistical realizations of petrophysical and geological data with different temporal and spatial scales. Even though the resulting high-resolution geo-model (that typically consists of 10^6 to 10^9 cells) is still unable to present all existing small-scale heterogeneities in the system, it is simply too fine to be used in existing simulators, which can typically handle models with grid cells of the order of up to 10^6. Therefore, 'upscaling' for reservoir simulation is defined as a procedure of transferring flow and transport processes from a detailed fine-scale model to a more practical and courser one (Durlofsky 2005). This procedure includes both equations and properties of the reservoir system. The properties to be scaled up are static parameters such as absolute permeability, porosity, net to gross and connate water saturation, and dynamic properties like relative permeability and capillary curves. The upscaling process should be implemented in a way that it is manageable by existing reservoir simulators,

yet take into account the effect of heterogeneities and geological complexities in the flow and transport simulation. In other words, an appropriate upscaling technique aims at an optimum compromise between the quality of simulation and the required computational time.

The correctness criterion of an upscaling procedure is often the equality of flow for a given potential (Renard & Marsily 1997; Gueguen et al. 2006). Accordingly, the coarse model should be capable of reproducing the main aspects of the fine-scale flow behavior such as flow rates, averaged pressures, averaged saturations, and breakthrough times. However, all coarsening procedures introduce a discrepancy and loss of detail in the numerical model due to the uncertain definition of the boundary conditions and the geological heterogeneities in the coarse-scale model. Study of upscaling techniques is not new, but still an ongoing research area as it can be a significant source of the simulation error, when it is done improperly.

2.2.2. Coarse-scale equations

In general, there are some flow features such as dynamical or non-equilibrium effects in the coarse-scale processes that are not present in the small-scale description (Hassanizadeh et al. 2005). Therefore, in an appropriate upscaling procedure, both equations and parameters need to be scaled up. Coarse-scale equations are often derived by using procedures such as homogenization and volume averaging. Nevertheless, in most reservoir practices, the resulting coarse-scale equations from homogenization analysis follow mathematically the same form as the fine-scale equations with the difference that the fine-scale parameters are replaced by upscaled (effective) ones (Saez et al. 1989; Durlofsky 1998). Therefore, it is quite common to assume that, for instance, Darcy's law is valid for both fine- and coarse-scale simulations, and only new upscaled permeability values need to be calculated. Accordingly, Eq. (2.10) for course-scale modelling of a steady-state incompressible single-phase flow can be rewritten as

$$-\nabla.(\frac{1}{\mu}\mathbf{K}^{*}.\nabla p^{c}) = q^{c}, \tag{2.17}$$

where superscripts asterisk and *c* designate an upscaled parameter and upscaled variable, respectively. In fact, during the upscaling process, variations of the permeability tensor $\mathbf{K}$ in Eq. (2.10) over the scale at which the fine-scale equations are valid, are averaged or homogenized to obtain an equivalent or effective $\mathbf{K}^{*}$ over the coarse grid block scale. Note that depending on the upscaling technique, the resulting permeability matrix might

be a full tensor even if the original fine-scale permeability tensor is diagonal (see e.g. Durlofsky 1991).

The terms ‘effective’, ‘equivalent’ and ‘block’ parameters have been frequently used in the literature. Effective permeability is used for media, which are statistically homogeneous in the coarse scale (Renard & Marsily 1997; Gueguen et al. 2006). This means that the scale, over which the flow properties are averaged, is large enough to include all heterogeneity scales present in the reservoir (Begg et al. 1989). Therefore, the fine grid model can be replaced by a single coarse grid block with a constant ‘effective’ permeability. The concept of effective permeability is an intrinsic physical magnitude independent of the boundary and flow conditions. In most cases, however, the conditions for existence of an effective permeability value are not met. Thus, fine scale permeability values are often replaced by a set of ‘equivalent’ permeability values instead of a single one. This set is computed based on the equality of flow (or equality of dissipated energy by different forces) between the fine- and the course-grid models (Gueguen et al. 2006). Unlike the effective permeability, the equivalent permeability depends on the flow and boundary conditions and, hence is not unique in different calculations. It goes without saying that equivalent permeability tends to the effective one as the size of the coarse block become larger. Finally, if averaged permeability is calculated over the scale of simulator grid blocks, it is called the ‘block’ permeability. Henceforth, we simply refer to all effective, equivalent and block parameters as ‘upscaled’ or ‘coarse scale’ parameters, while we keep in mind the differences. A wide variety of upscaling techniques is available to calculate the coarse-scale parameters considering the effect of geological features and small-scale heterogeneities on the flow behavior.

2.2.3. Single- and two-phase upscaling

There are several classifications of upscaling techniques in the literature (see, e.g., Wen & Gomez-Hernandez 1996; Renard & Marsily 1997; Farmer 2002; Durlofsky 2005). An important classification is based on the type of the parameters that have to be upscaled (Durlofsky 2005). In a ‘single-phase upscaling’ procedure, we only calculate equivalent permeability and porosities for the coarse-scale flow equation, whereas in a ‘two-phase upscaling’ method both flow and transport equations are considered and relative permeability curves and capillary pressures are also scaled up.

Even though, in most cases, there are more than one phase present in the reservoir, the coarse-scale flow parameters are commonly computed by using a single-phase upscaling method, and the two-phase-flow upscaling is less frequently applied in practical reservoir

simulations (Christie & Blunt 2001). One reason for that is the similarity of the single-phase and two-phase flow equations, as we mentioned before. Therefore, it is often reasonable to use only a single-phase upscaling procedure for two-phase flow simulations, particularly for low degree of coarsening (Durlofsky 2005). The other reason is related to the inefficiency of existing two-phase upscaling techniques. In 'dynamic' two-phase upscaling methods, for instance, the fine-scale flow simulations are used to calculate pseudo-functions or pseudo-relative permeability curves, which are used to correct for numerical dispersion and account for the effect of small-scale heterogeneities in the coarse-scale model. However, the calculation of the pseudo-functions is often computationally expensive, yet not robust and reliable (Barker & Thibeau 1997; Darman et al. 2002). In addition, 'steady-state' methods have been introduced, in which the steady-state assumption is used to calculate the saturation distribution. Once the saturation distribution is known, any single-phase upscaling technique can be used to calculate the upscaled relative permeability and capillary pressure curves (Ekrann & Aasen 2000). Unlike dynamic pseudo-functions, steady-state methods do not refer to expensive transient flow simulations on the fine-scale grid blocks, but only to the steady-state saturation distribution. Nevertheless, they often assume viscous and capillary limits which are correspondingly valid for high and low flow rate areas. Unfortunately the domains, on which these assumptions are valid, are generally unknown or limited to small parts of the reservoir (Virnovsky et al. 2004). For a more detail description of dynamic upscaling methods, see e.g., Kyte & Berry (1975), Barker & Thibeau (1997), Christie (2001), Darman et al. (2002), and Artus & Noetinger (2004), and for the steady-state techniques see e.g., Dale et al. (1997), Ekrann & Aasen (2000), Pickup & Stephen (2000) and Virnovsky et al. (2004).

In any case, upscaling of absolute permeability (or transmissibility) values is always a key step (even in a multi-phase upscaling problem) and that is done through a single-phase upscaling procedure. Therefore, in this thesis we only focus on single-phase upscaling of the absolute permeability, with the understanding that its results can be used for both single- and or multi-phase problems. We should also mention that a lot of topics such as multi-scale methods, dual-gridding techniques, upscaling with flow-based gridding and near-well upscaling are also related to the upscaling problem in reservoir simulation, but they are not discussed here. For an overview of those topics see Gerritsen & Durlofsky (2005) and references therein.

2.3. Overview of single-phase upscaling techniques

'Single-phase upscaling' refers to an upscaling procedure that only includes static parameters such as the absolute permeability and porosity values. Porosity ϕ in a coarse grid block with bulk volume V is usually upscaled using a simple volume averaging

$$\phi^* = \frac{1}{V}\int_V \phi(x)dV. \tag{2.18}$$

Calculating the upscaled permeability (or transmissibility) values is more challenging, as we shall discuss here.

Depending on how we calculate the upscaled equations and parameters, we can categorize the existing single-phase upscaling techniques. These techniques vary between purely numerical methods based on the discrete fine-scale properties to more analytical and physical approaches that focus on the algebraic form of the equations. Here, we only mention several common single-phase upscaling techniques that are presented as averaging techniques, theoretical methods and flow-based numerical techniques. Particular attention is paid to the averaging, and flow-based numerical methods, seeing that they are widely used in the reservoir simulation. The material presented here is mainly borrowed from more extensive reviews in Mansoori (1994), Wen & Gomez-Hernandez (1996), Christie (1996), Renard & Marsily (1997), Farmer (2002), He et al (2002), Hartanto (2004), Durlofsky (2002 and 2005), Gerritsen & Durlofsky (2005), Dasheng & Hesketh (2005) and Noetinger et al. (2005).

2.3.1. Averaging methods

We consider a reservoir with N layers of isotropic permeability K_i and thickness h_i, assuming that the fluid flows only in the x-direction parallel to the permeable layers (Figure 2.1). Therefore, there is no flux from the top or bottom of the reservoir and the pressure is constant at both inlet and outlet of the system. Our objective is to calculate the coarse-scale permeability value in the x-direction K_x^*, such that the same flow rate of the layered system is recovered from the coarse model. Therefore, using Darcy's law for an incompressible single-phase flow, we can write the total flux through the reservoir as

$$Q_x = -\frac{1}{\mu}\sum_{i=1}^{N}\left(K_i h_i\right)\frac{(P_{out}-P_{in})}{l_x} = -\frac{K_x^*}{\mu}\frac{(P_{out}-P_{in})}{l_x}\sum_{i=1}^{N}h_i. \tag{2.19}$$

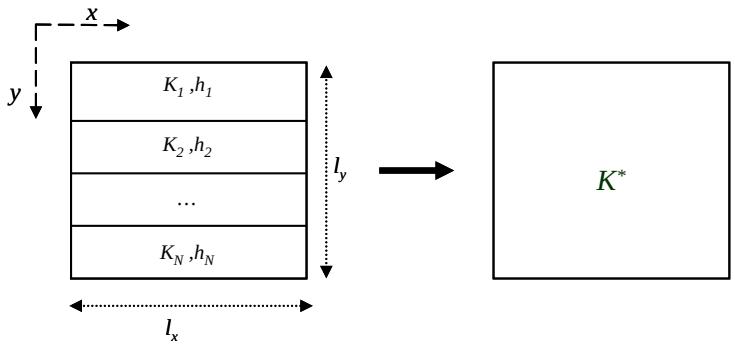

Figure 2.1 Layered reservoir with flow direction parallel to the permeable layers.

From this equation, the calculated equivalent permeability is given by weighted arithmetic averaging

$$K_x^* = K_a = \frac{\sum_{i=1}^{N} K_i h_i}{\sum_{i=1}^{N} h_i}. \tag{2.20}$$

The same procedure for the flow perpendicular to the layers gives the equivalent permeability K_y^* as the weighted harmonic averaging of the layers permeability values (Cardwell and Parsons 1945). This upscaling procedure results in a diagonal permeability tensor due to heterogeneity (layering) of the fine-scale model.

A more general algebraic relation for calculating the averaged permeability is the power-law averaging method introduced by Journel et al. (1986) and Deutsch (1989). In this method the effective permeability is defined as

$$K_p^* = \left(\frac{1}{V_b} \int_{V_b} k(x)^{\omega} dV \right)^{\frac{1}{\omega}}. \tag{2.21}$$

Here, V_b is bulk volume and exponent ω is obtained by tuning it against numerical upscaling results. The same exponent can then be used for similar permeability fields. The value of ω can vary between 1 and -1. Basically, ω=1 represents the arithmetic average, whereas ω=-1 gives the harmonic average. This also states that the upscaled permeability is bounded above and below by arithmetic and harmonic means,

respectively. These upper and lower permeability bounds are often referred to as 'Wiener bounds'.

The geometric average is also obtained when exponent ω goes to zero. Mathematically, the geometric average contains both arithmetic and harmonic effects of the permeability field and it is an appropriate method when the permeability field is isotropic, but randomly distributed regarding to the flow direction. For cases of large variations in permeability or finite fraction of zero permeability however, this is not a suitable method (King 1989; Renard & Marsily 1997).

Simple averaging methods are known to be fast methods for upscaling. However, their main drawback is the limited range of application, compared to other methods such as numerical upscaling tourniquets. Furthermore, zero permeability domains cause an error in upscaled permeability obtained by these methods.

2.3.2. Theoretical methods

In theoretical methods, it is assumed that the geological model, in particular, permeability field and boundary conditions are known. Then, some theories are applied to calculate an approximation of the upscaled equations and parameters. Examples of them, which are mainly adapted from the field theory,[2] are 'perturbation theory' and the 'theory of effective media' (King 1987, 1989; Drummond & Horgan 1987; Gueguen et al. 2006). However, the application of perturbation and effective medium theories is limited to very small fluctuations in permeability values. More interesting theories for reservoir applications are renormalization, percolation and homogenization as we describe them here.

Renormalization

The drawback of perturbation and effective medium theory leads to an alternative approach, which does not make any assumption about the scale of the fluctuations. Such a method was developed in permeability upscaling by King (1989), and was named 'renormalization technique'. The idea came again from field theory, but this time King used the analogy of a resistor network to represent the porous medium. In this method, the upscaling is performed successively, such that in each sequence permeability values

[2] In mathematical physics, fields are used to describe systems with infinite degrees of freedom. They can be scalar, vector or tensor, and they are functions of position, so that we are able to integrate and differentiate them. A reservoir is considered as a large disordered system, where permeability is a random stochastic variable with a probability distribution and an infinite number of degrees of freedom. King (1987) used this analogy to develop theories for calculating effective properties and modeling the flow in heterogeneous porous media.

are averaged over a smaller region in the reservoir to form a permeability field with lower permeability variance. For each small region (a region of two-by-two grid blocks in a two-dimensional problem), a single value for block permeability is calculated, so that it gives the same flow as the fine-grid simulation across the corresponding region. The process is repeated until we reach the desired coarse grid.

To calculate the effective permeability of renormalized blocks, they are modeled by an equivalent resistor network. The equivalent resistor between the midpoint of a block with permeability *K* and its edge is *1/K*. Thus, we can replace each grid block with a cross of resistors.

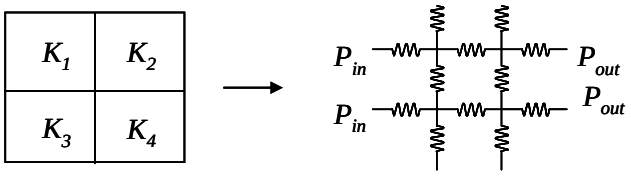

Figure 2.2 Resistor analogues in renormalization (after King 1989).

For instance, consider an isotropic two-dimensional medium with uniform pressures at the sides of the blocks and no-flow boundaries at the top and bottom of the blocks (see Figure 2.2). We can replace each block with a cross of resistors and we can join the nodes with the same pressure. This network is further simplified using a star-triangle transformation[3] and finally the effective permeability of the single equivalent resistance is given as

$$K_{eff} = \frac{4\left(K_1+K_3\right)\left(K_2+K_4\right)\left[K_2K_4\left(K_1+K_3\right)+K_1K_3\left(K_2+K_4\right)\right]}{\left\{\left[K_2K_4\left(K_1+K_3\right)+K_1K_3\left(K_2+K_4\right)\right]\left(K_1+K_2+K_3+K_4\right)\right.} \\ \left.+3\left(K_1+K_2\right)\left(K_3+K_4\right)\left(K_1+K_3\right)\left(K_2+K_4\right)\right\}. \qquad (2.22)$$

Renormalization techniques are seen to be accurate in comparison to the simple averaging methods and they can handle large permeability fluctuations. Nevertheless, Peaceman (1997) found out that the renormalization approach is less accurate for non-rectangular grids and in the presence of anisotropy. Moreover, like any other local method, errors arise from the boundary conditions, particularly for highly anisotropic and heterogeneous media (King 1996; Yeo & Zimmerman 2001).

[3] Star-triangle or Y-Δ transformation is a technique of simplifying an electrical network by establishing equivalences for resistor networks with three terminals. The name refers to two star-shape and triangle-shape resistor networks, which are equivalent (see Appendix 1 in King 1989)

Percolation theory

Percolation theory is a mathematical theory of connectivity between different objects in a complex system (Berkowitz & Balberg 1993; Renard & Marsily 1997, King et al. 2002). In many reservoirs flow is strongly controlled by the connectivity between different geological features, e.g., shale layers and sand bodies distributed randomly in space. Therefore, percolation theory can give an approximate measurement of the connectivity in a porous medium. Then, effective permeability in that medium can be calculated by the following relations:

$$p < p_t \rightarrow K_{eff} = 0, \tag{2.23}$$

$$p > p_t \rightarrow K_{eff} \sim \left(p - p_t \right)^{\mu}. \tag{2.24}$$

Here, p is the proportion of permeable medium to the total bulk volume, and p_t is a fundamental characteristic of percolation theory, known as the percolation threshold. In our case, the percolation threshold is a particular value of proportion of permeable medium, such that for $p > p_t$ there is a continuous pathway through the medium. The exact value of p_t depends on the type and the dimension of the grid blocks. μ is an exponent that depends only on the space dimension, but not on the shape of flow units (μ ≈1.3 in two-dimensions and μ ≈1.8 in three-dimensions). Hence, this exponent is also referred to as a universal exponent (King et al. 2002).

Homogenization

The basic hypothesis in homogenization is the spatial periodicity in a medium. From there, the medium can be represented by small basic cells, subject to periodic boundary conditions. Therefore, space scales in the model have to be separated into two distinct scales. One is the coarse scale or the observation scale, L, and the other one is the permeability oscillation scale, l. Moreover, a length scale parameter, denoted by ε, is defined as the ratio between these two scales. The second assumption is that basic cells are very small compared to the given medium, i.e., $\varepsilon \rightarrow 0$. As a consequence, any space dependent quantity in the system is a function of both scales and the gradient operator should be written as $\nabla = \nabla_L + \nabla_l$.

In order to obtain the coarse-scale equations, the fine-scale equations are rewritten based on an expansion in the length scale parameter. Then, they are solved for different orders of ε separately. The lowest order of ε gives the upscaled equation. In single-phase flow homogenization, the upscaled equation keeps essentially the same form, although coarse-

scale parameters are different from the fine-scale ones. The upscaled parameters of the model are also defined from the basic cell problem.

A benefit of this method is that we can use homogenization to upscale both equations and their parameters. This method is also applied in two-phase flow, although the procedure is then more complicated (see e.g., Van Duijn et al 2002; Salimi & Bruining 2009). Homogenization is a very useful tool to improve our understanding of the processes in porous media. However, we have to be aware of the strong assumptions and approximations made. For further details and reviews of homogenization applications in porous media, we refer to Renard & Marsily (1997), Farmer (2002), Hornung (1997), Van Duijn et al (2002), Neuweiler & Cirpka (2005), and Salimi & Bruining (2009).

2.3.3. Flow-based numerical methods

In many cases, geological complexities and strong heterogeneity in oil reservoirs allows none of the assumptions made in averaging, theoretical, or any other such approximation methods to be valid. In other words, those approaches are useful in very limited numbers of cases, where their hypothesis is met, or in fundamental studies. In general reservoir simulation, however, flow-based numerical methods are required to transfer the flow properties of a fine-grid model to a coarser one. Common numerical methods are based on the criterion of flow equality between fine- and coarse-scale models. Therefore, the upscaling procedure is divided into two steps:

Step (1): the first step implies the solution of the flow equation over the fine-scale grid blocks. From Eq. (2.10) and assuming zero source (sink) terms, the simplified incompressible single-phase flow equation is given by

$$-\nabla.(\frac{1}{\mu}\mathbf{K}.\nabla p) = 0. \tag{2.25}$$

Flow-based numerical upscaling techniques are classified based on the domain, over which this equation is solved (see e.g., Wen & Gomez-Hernandez 1996; Renard & Marsily 1997; Farmer 2002; Durlofsky 2005). If this domain is only limited to the target course grid block, it is called a local upscaling technique. When it also includes some neighboring grids of that coarse grid, the upscaling technique is called an extended-local method. Finally, when the flow equation is solved over the entire fine-grid model, the upscaling procedure is called a global upscaling method (Figure 2.3).

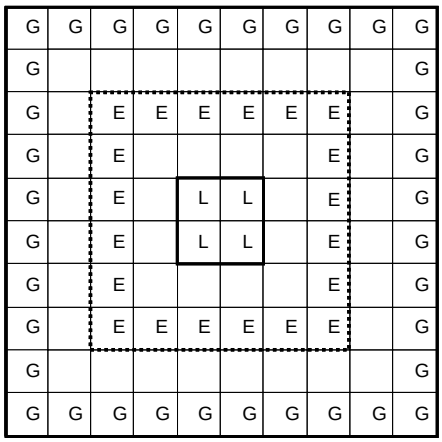

Figure 2.3 Different domains, over which the flow equation is solved in local (L), extended-local (E) and global (G) numerical upscaling. Here, the target coarse grid block corresponds to four fine grid blocks in the middle.

Step (2): in this step, we solve the coarse-scale flow Eq. (2.17) and then, from the flow equality criterion between fine- and coarse-scale models, we calculate the upscaled permeability tensor $\mathbf{K}^*$. When this is done only from the coarse-scale flow over the target course grid, the procedure is called a local technique; otherwise it is a non-local method. The classification of local-local, local-global, global-local, and global-global upscaling is also related to steps (1) and (2).

We should mention that most numerical upscaling techniques are able to directly compute the coarse-scale transmissibility values (see e.g., Romeu & Noetinger 1995). However, the procedure is similar to the above described permeability upscaling. In the following, we present a brief overview of local and non-local upscaling techniques to compute the upscaled permeability values on structured Cartesian grids.

Local methods

In local upscaling methods, coarse scale parameters are computed by considering only the fine-scale region corresponding to the target coarse block. However, flow directions and proper local boundary conditions have to be specified. In fact, the resulting upscaled parameters are dependent on the selected boundary conditions.

One approach is to assume pressure-no-flow boundary conditions, which are originally taken from pressure solver methods of Warren & Price (1961). In this approach, a constant pressure (potential) is assigned to two opposing sides, while no-flow boundary conditions are assumed on the other sides. Figure 2.4 depicts this type of boundary conditions for a part of the fine-scale model, corresponding to a coarse grid block.

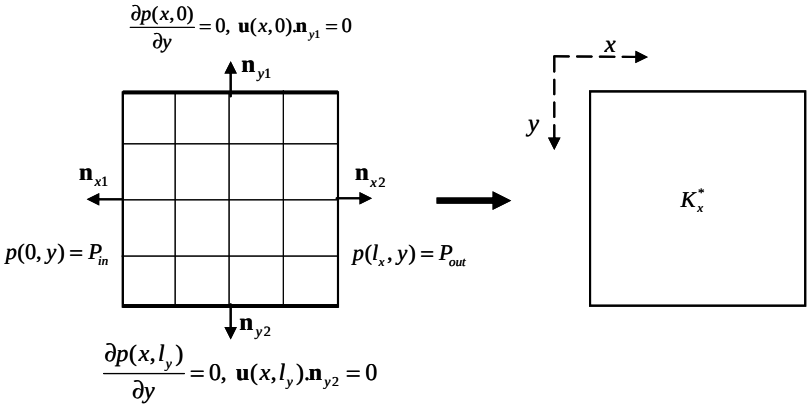

Figure 2.4 Constant pressure and no-flow boundary conditions.

In order to calculate the upscaled permeability for this domain, first, we solve the flow Eq. (2.25) over the fine grid domain of Figure 2.4 to obtain the pressure distribution. It is assumed that the pressure gradient is constant along the x-direction and, therefore, analogous to averaging method for a layered reservoir, we can write the total flow rate in the x-direction as

$$Q_x = -\frac{1}{\mu}\sum_{j=1}^{n_y}\left(K_{i-1/2,j}\frac{p_{i,j}-p_{i-1,j}}{l_x}\Delta y\right) = -\frac{K_x^*}{\mu}\frac{(P_{out}-P_{in})}{l_x}l_y, \tag{2.26}$$

where n_y is the number of grid blocks in the y-direction, l_x and l_y are the coarse grid block lengths in the x- and y-directions, respectively, and $K_{i-1/2,j}$ is the distance-weighted harmonic average of the fine-scale permeability values in blocks *i* and *i-1*. Therefore, the equivalent coarse-scale permeability is given by

$$K_x^* = \frac{\sum_{j=1}^{n_y}\left(K_{i-1/2,j}\frac{p_{i,j}-p_{i-1,j}}{l_x}\Delta y\right)}{(P_{out}-P_{in})l_y}l_x = -\mu\frac{Q_x l_x}{(P_{out}-P_{in})l_y}. \tag{2.27}$$

Now, we rotate the boundary conditions so that the flow occurs in the y-direction. Similarly we can write

$$K_y^* = \frac{\sum_{i=1}^{n_x}\left(K_{i,j-1/2}\frac{p_{i,j}-p_{i,j-1}}{l_y}\Delta x\right)}{(P_{out}-P_{in})l_x}l_y = -\mu\frac{Q_y l_y}{(P_{out}-P_{in})l_x}, \tag{2.28}$$

where n_x is the number of grid blocks in the x-direction. The local upscaling procedure with pressure-no-flow boundary conditions results in a diagonal permeability tensor. In

other words, the cross terms of the permeability tensor are assumed to be zero. Consequently, the method is less accurate for grid blocks, in which the directional flow is significant.

An alternative solution to compute the full tensor permeability is to choose periodic boundary conditions, in which it is assumed that the reservoir domain is a periodic cell in a periodic medium. The assumption of periodicity relates the pressures and velocities at opposite boundaries of the reservoir domain to each other (Durlofsky 1991):

$$p(x,0) = p(x,l_y), \tag{2.29}$$

$$p(0,y) = p(l_x,y) - G_x l_x, \tag{2.30}$$

$$\mathbf{u}(x,0).\mathbf{n}_{y1} = -\mathbf{u}(x,l_y).\mathbf{n}_{y2}, \tag{2.31}$$

$$\mathbf{u}(0,y).\mathbf{n}_{x1} = -\mathbf{u}(l_x,y).\mathbf{n}_{x2}, \tag{2.32}$$

where G_x is an arbitrary pressure gradient in the x-direction. Like in the pressure-no-flow boundary conditions, we need to rotate the boundary conditions and solve the flow problem again. The main advantage of this method is that it can compute a full symmetric and positive definite permeability tensor[4]. However, this method is only accurate if the assumption of periodicity is valid, otherwise the large-scale permeability connectivity may be lost (Durlofsky 2005).

Non-local methods

In general, the resulting upscaled parameters from local methods depend on the choice of boundary conditions, which are often unknown. As a consequence, these generic boundary conditions might lead to a significant error in approximation of the upscaled permeability field. In addition, the assumption of a constant pressure gradient over a coarse grid block is not valid for a highly heterogeneous or channelized reservoir (Chen et al. 2003). In such cases, the behaviour of the coarse-scale reservoir depends on some global flow patterns that cannot be captured by local techniques. This leads to the development of non-local methods that consider all the fine-scale grid blocks (global methods) or at least the neighboring grid cells (extended-local methods) in the calculation of the coarse-scale parameters. Extended-local methods, as depicted in Figure 2.3, reduce the effect of the boundary conditions by including the neighboring grids into the

[4] For a symmetric permeability tensor $K^*_{xy} = K^*_{yx}$, and for a positive definite tensor $K^*_{xx}, K^*_{yy} > 0$ and $\left(K^*_{xy}\right)^2 < K^*_{xx}K^*_{yy}$.

upscaling calculations (see e.g., Wen et al. 2003). However, in order to resolve the global permeability connectivity in some cases, particularly in strongly channelized systems, we may need to use a global technique that includes the flow information from a global fine-scale simulation into the calculations (White & Horne 1987; Holden & Nielsen 2000).

Another alternative to expensive global fine-scale flow calculations is a 'local-global' or 'quasi-global' approach, in which the generic boundary conditions are only used to obtain an initial coarse-scale flow solution. The interpolation of the coarse-scale solution then gives more accurate local boundary conditions to find the new coarse-scale parameters and the process is iterated until the solution converges (see Chen et al. 2003; Chen and Durlofsky 2006). Generally, the non-local methods are computationally more accurate, but also more expensive than the local techniques.

2.4. Summary of upscaling techniques

Upscaling techniques are classified in terms of the types of the parameters that are scaled up (Single- or two-phase upscaling), and the fine-scale domain, over which these parameters are computed (local or non-local methods).

The earliest upscaling techniques were local methods based on some form of averaging of the fine-block permeability values. Cardwell and Parsons (1945) found that the arithmetic and harmonic averages are, respectively, the upper and lower limits of the equivalent permeability for a heterogeneous block (Wiener bounds). Later, this observation was used to develop a power-law averaging relation that gives the equivalent permeability of a group of heterogeneous grid blocks as a value between the upper and lower bounds by varying the power exponent (Journel et al. 1986; Deutsch 1989). Because the equivalent permeability depends on fine-scale permeability distributions with respect to the flow directions, averaging methods are reliable only for particular reservoirs and flow geometries.

Theoretical methods, like perturbation and effective medium theory, resolved the problem of simple averaging methods, in which zero permeability fractions cause an error. However, they both fail when the permeability fluctuations become larger. Renormalization, overcomes this problem, since it does not make any assumption about the scale of fluctuations. Nevertheless, its accuracy reduces for non-rectangular grid blocks and in the presence of anisotropy. Homogenization techniques also provide a mathematic tool to derive both upscaled equations and parameters, assuming a periodic medium, although no natural medium is periodic. Thus the theoretical methods are based on strong assumptions and approximations about the permeability field and boundary

conditions, which can be useful and efficient in their specified cases. They can also be a valuable tool in a better understanding of the basics and theories related to the upscaling issues in porous media. However, just like the averaging methods, they lack generality of the numerical techniques.

In flow-based numerical local methods, the equivalent permeability is calculated from the equality of flow through a coarse grid block and its corresponding fine grid cells for a given potential. However, a flow direction and proper local boundary conditions have to be selected a-priori to solve the pressure equation (Warren & Price 1961; Durlofsky 1991). The coarse-scale parameters from the local numerical methods are, therefore, heavily dependent on the choice of the generic local boundary conditions, which are in general unknown. This can lead to a significant error, particularly in highly heterogeneous cases in which the behavior of the coarse-scale model may depend on global flow patterns and large-scale permeability connectivities that cannot be captured by local techniques. More recently, non-local methods were developed to overcome this problem by considering the flow behavior of an extended domain around the fine-scale grid blocks that make up the target coarse block (extended-local methods), or of the entire fine-scale model (global methods) (see Durlofsky 2005; Wen et al. 2003; White & Horne 1987; Holden & Nelson 2000; Chen et al. 2003). Because of their more extensive applications, the flow-based numerical methods are preferable in reservoir simulation.

In conclusion, although there are different single-phase upscaling techniques available, most of them lack generality and case independency, as they are only valid under certain reservoir and boundary conditions. Moreover, in most techniques, it is assumed that the computed coarse-scale parameters, based on a specified set of boundary conditions often with no sink/source terms, will be applicable to all other flow scenarios. The validity of this assumption is not warranted, seeing that in a real reservoir the global flow is often driven by wells rather than by fixed-pressure or fixed-rate boundary conditions. This is also a motivation for us to develop a control-relevant upscaling approach that is related to a particular configuration of wells in the reservoir.

3. CHAPTER: SYSTEM-THEORETICAL CONCEPTS

State-space representation of a reservoir system and the relating system-theoretical notations are briefly discussed in this chapter. In particular, we define the controllability and the observability properties to understand how the system inputs influence the state variables, and how the outputs give information about the states. Hankel singular values of the system are then defined to obtain a measure of the combined controllability and observability of the state variables, and from there, to identify those linear combinations of the states that represent the most important input-output characteristics of the system.

3.1. State-space representation of a reservoir model

In system theory, a reservoir model is considered as a dynamic system that evolves with time. The relation between the initial conditions, the inputs of the system, the internal variables (states), and the outputs are expressed in a state-space form that is discussed briefly here (see also Figure 3.1). To simplify our study, we only consider a single-phase flow reservoir that leads to a linear time-invariant (LTI) system. For a more detailed derivation of the state-space representation of reservoir models, in particular, in case of a two-phase flow system see Jansen (2009).

3.1.1. Continuous time

Consider an isothermal weakly compressible single-phase flow model with a given set of boundary and well conditions. In Chapter 2, we described the flow behavior of such a model through Eq. (2.13). This equation can be rewritten in a partitioned form as

$$\begin{bmatrix} \mathbf{V}_{11} & 0 & 0 \\ 0 & \mathbf{V}_{22} & 0 \\ 0 & 0 & \mathbf{V}_{33} \end{bmatrix} \begin{bmatrix} \dot{\mathbf{p}}_1 \\ \dot{\mathbf{p}}_2 \\ \dot{\mathbf{p}}_3 \end{bmatrix} + \begin{bmatrix} \mathbf{T}_{11} & \mathbf{T}_{12} & \mathbf{T}_{13} \\ \mathbf{T}_{21} & \mathbf{T}_{22} & \mathbf{T}_{23} \\ \mathbf{T}_{31} & \mathbf{T}_{32} & \mathbf{T}_{33} + \mathbf{J}_p \end{bmatrix} \begin{bmatrix} \mathbf{p}_1 \\ \mathbf{p}_2 \\ \mathbf{p}_3 \end{bmatrix} = \begin{bmatrix} 0 \\ \breve{\mathbf{q}}_w \\ \mathbf{J}_p \breve{\mathbf{p}}_w \end{bmatrix}, \tag{3.1}$$

where the diagonal block matrices $\mathbf{V}_{ii}$, $i = 1, 2, 3$ are accumulation matrices with entries that depend on the grid block size, grid block porosities, and the total compressibility, and the band-diagonal block matrices $\mathbf{T}_{ij}$, $i = 1, 2, 3$, $j = 1, 2, 3$ are transmissibility matrices with entries that depend on the grid block size, grid block permeabilities, and the fluid viscosity. The elements of vector $\mathbf{p}_1$ are the pressures in those grid blocks (elements) that

are not penetrated by a well. The elements of $\mathbf{p}_2$ are the pressures in the blocks where the source terms are prescribed well flow rates $\breve{\mathbf{q}}_w$, and those of $\mathbf{p}_3$ are the pressures in the blocks where the source terms are obtained through prescription of the bottomhole pressures with the aid of a well model,

$$\bar{\mathbf{q}}_w = \mathbf{J}_p \left(\breve{\mathbf{p}}_w - \mathbf{p}_3 \right). \tag{3.2}$$

Here $\mathbf{J}_p$ is a diagonal matrix of well indices, the elements of $\breve{\mathbf{p}}_w$ are the prescribed pressures, and the elements of $\bar{\mathbf{q}}_w$ are the resulting well flow rates. To compute the bottomhole pressures $\bar{\mathbf{p}}_w$ in the wells where the flow rates have been prescribed, we need an additional diagonal matrix $\mathbf{J}_q$ of well indices such that

$$\breve{\mathbf{q}}_w = \mathbf{J}_q \left(\bar{\mathbf{p}}_w - \mathbf{p}_2 \right). \tag{3.3}$$

Eqs. (3.2) and (3.3) can be combined to give

$$\begin{bmatrix} 0 \\ \bar{\mathbf{p}}_w \\ \bar{\mathbf{q}}_w \end{bmatrix} = \begin{bmatrix} 0 & 0 & 0 \\ 0 & \mathbf{I} & 0 \\ 0 & 0 & -\mathbf{J}_p \end{bmatrix} \begin{bmatrix} \mathbf{p}_1 \\ \mathbf{p}_2 \\ \mathbf{p}_3 \end{bmatrix} + \begin{bmatrix} 0 & 0 & 0 \\ 0 & \mathbf{J}_q^{-1} & 0 \\ 0 & 0 & \mathbf{J}_p \end{bmatrix} \begin{bmatrix} 0 \\ \breve{\mathbf{q}}_w \\ \breve{\mathbf{p}}_w \end{bmatrix}. \tag{3.4}$$

If we define the vectors

$$\mathbf{x} = \begin{bmatrix} \mathbf{p}_1 \\ \mathbf{p}_2 \\ \mathbf{p}_3 \end{bmatrix}, \tag{3.5}$$

$$\mathbf{u} = \begin{bmatrix} \breve{\mathbf{q}}_w \\ \breve{\mathbf{p}}_w \end{bmatrix}, \tag{3.6}$$

$$\mathbf{y} = \begin{bmatrix} \bar{\mathbf{p}}_w \\ \bar{\mathbf{q}}_w \end{bmatrix}, \tag{3.7}$$

Eqs. (3.1) and (3.4) can be rewritten, respectively, as

$$\dot{\mathbf{x}} = \mathbf{A}_c \mathbf{x} + \mathbf{B}_c \mathbf{u}, \tag{3.8}$$

$$\mathbf{y} = \mathbf{C}\mathbf{x} + \mathbf{D}\mathbf{u}, \tag{3.9}$$

Where

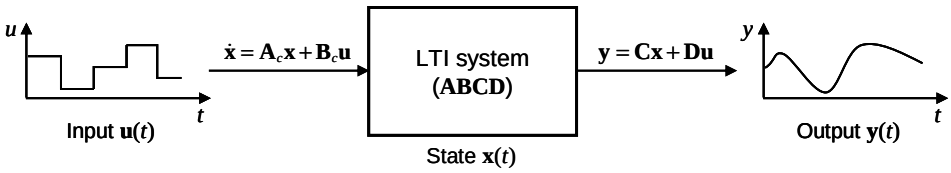

Figure 3.1 Schematic description of the state-space representation of a dynamic system.

$$\mathbf{A}_c = -\begin{bmatrix} \mathbf{V}_{11}^{-1}\mathbf{T}_{11} & \mathbf{V}_{11}^{-1}\mathbf{T}_{12} & \mathbf{V}_{11}^{-1}\mathbf{T}_{13} \\ \mathbf{V}_{22}^{-1}\mathbf{T}_{21} & \mathbf{V}_{22}^{-1}\mathbf{T}_{22} & \mathbf{V}_{22}^{-1}\mathbf{T}_{23} \\ \mathbf{V}_{33}^{-1}\mathbf{T}_{31} & \mathbf{V}_{33}^{-1}\mathbf{T}_{32} & \mathbf{V}_{33}^{-1}\left(\mathbf{T}_{33}+\mathbf{J}_p\right) \end{bmatrix}, \tag{3.10}$$

$$\mathbf{B}_c = \begin{bmatrix} 0 & 0 \\ \mathbf{V}_{22}^{-1} & 0 \\ 0 & \mathbf{V}_{33}^{-1}\mathbf{J}_p \end{bmatrix}, \tag{3.11}$$

$$\mathbf{C} = \begin{bmatrix} 0 & \mathbf{I} & 0 \\ 0 & 0 & -\mathbf{J}_p \end{bmatrix}, \tag{3.12}$$

$$\mathbf{D} = \begin{bmatrix} \mathbf{J}_q^{-1} & 0 \\ 0 & \mathbf{J}_p \end{bmatrix}. \tag{3.13}$$

Eqs. (3.8) and (3.9) give the standard continuous-time (CT) 'state-space representation' of a LTI system, as used in systems and control theory. The matrices $\mathbf{A}_c \in \mathbb{R}^{n\times n}$, $\mathbf{B}_c \in \mathbb{R}^{n\times m}$, $\mathbf{C} \in \mathbb{R}^{p\times n}$, and $\mathbf{D} \in \mathbb{R}^{p\times m}$ are respectively referred to as the 'system matrix' as it contains the properties of the system, the 'input matrix' since it maps the inputs to the states, the 'output matrix' as it maps the states to the outputs, and the 'direct-throughput matrix'. Here, the subscript *c* refers to the CT form. Moreover, for a system with *m* inputs, *p* outputs and *n* state variables, the input vector $\mathbf{u}(t) \in \mathbb{R}^m$ and the output vector $\mathbf{y}(t) \in \mathbb{R}^p$ include the flow rate or bottom-hole pressure in each well. The state vector $\mathbf{x}(t) \in \mathbb{R}_+^n$ represents the state variables i.e. pressure values in all grid blocks that are a function of time ($t \in \mathbb{R}$) and other independent variables e.g. space. The order (or dimension) of the system is also equal to *n*.

3.1.2. Discrete time

In order to derive the discrete-time (DT) LTI state-space representation of the reservoir system, we use an implicit time discretization with a fixed time step Δt. Therefore, Eqs. (3.8) and (3.9) can be rewritten in DT form as

$$\mathbf{x}_{k+1} = \mathbf{A}\mathbf{x}_k + \mathbf{B}\mathbf{u}_k, \tag{3.14}$$

$$\mathbf{y}_k = \mathbf{C}\mathbf{x}_k + \mathbf{D}\mathbf{u}_k \tag{3.15}$$

where

$$\mathbf{A} = \left(\mathbf{I} - \Delta t \mathbf{A}_c\right)^{-1}, \tag{3.16}$$

$$\mathbf{B} = \left(\mathbf{I} - \Delta t \mathbf{A}_c\right)^{-1} \Delta t \mathbf{B}_c. \tag{3.17}$$

Eqs. (3.14) and (3.15) are also referred to as the 'system' and 'output' equations, respectively. LTI state-space models are sometimes designated with $\sum := (\mathbf{ABCD})$, because the matrices **A**, **B**, **C** and **D** can completely describe the system.

We note that although Eq. (3.14) appears to be explicit in time, the underlying implicit discretization scheme results in the need to solve a system of equations at each time step. Moreover, in a practical computational scheme the inverse matrices in Eqs. (3.10), (3.11), (3.16) and (3.17) will not actually be computed, and a computationally more efficient approach will be followed. In the sequel, we assume that the system is stable (i.e., the discrete eigen values of **A** have a norm smaller than unity). Moreover, we present the analysis only for a DT system as most of the reservoir models are given in discrete time. However, also in a CT case, the theory discussed here remains valid.

3.2. Controllability and observability

In order to improve the dynamical behavior of a system, we need to observe and control the inaccessible internal (state) variables through the available inputs and outputs. More specifically, in a reservoir system, our success in optimizing the model predictions by manipulating the inputs (e.g., well settings), and updating the reservoir model by assimilating measured data (e.g., production data) depends on how much of the state-space can be reached from the input side (i.e., the degree to which the system is 'controllable'), and how the internal behaviour of the system can be obtained from the output information (i.e., the degree to which the reservoir is 'observable')[5]. We formulate the controllability and observability concepts in this section. The system-theoretical material presented here is well-established and can be found in related textbooks such as Kailath (1980), DeCarlo (1989), Polderman & Willems (1998), Olsder & Van der Woude (2005), Antoulas (2005), and Skogestad & Postlethwaite (2005). For recent applications

[5] Another important property, which is excluded here, is 'identifiability'. A system is 'identifiable' if its parameters can be uniquely estimated from the measured data by a suitable choice of the admissible inputs.

of systems theory to reservoir modeling see Markovinovic et al. (2002), Heijn et al. (2004), Gildin et al. (2006), Zandvliet (2008), Zandvliet et al. (2008), Van Doren et al. (2008), Cardoso et al. (2009), Markovinovic (2009), and Vakili-Ghahani & Jansen (2010a, 2010b).

3.2.1. Controllability matrix

Consider a stable LTI system with m inputs, n state variables and p outputs. Roughly speaking, this system is 'state controllable' if we can steer it from an arbitrary initial state to an arbitrary final state by choosing a proper set of admissible inputs (Olsder & van der Woude, 2005). From Eq. (3.14), the system trajectories, i.e. the set of state variable values as a function of time, for k time steps are obtained by simply integrating in time

$$\begin{bmatrix} \mathbf{x}_1 \\ \mathbf{x}_2 \\ \vdots \\ \mathbf{x}_k \end{bmatrix} = \begin{bmatrix} \mathbf{A} \\ \mathbf{A}^2 \\ \vdots \\ \mathbf{A}^k \end{bmatrix} \mathbf{x}_0 + \begin{bmatrix} \mathbf{B} & 0 & \cdots & 0 \\ \mathbf{AB} & \mathbf{B} & \ddots & 0 \\ \vdots & \ddots & \ddots & \\ \mathbf{A}^{k-1}\mathbf{B} & \mathbf{A}^{k-2}\mathbf{B} & \cdots & \mathbf{B} \end{bmatrix} \begin{bmatrix} \mathbf{u}_0 \\ \mathbf{u}_1 \\ \vdots \\ \mathbf{u}_{k-1} \end{bmatrix}, \tag{3.18}$$

or in short

$$\mathbf{x}_k = \mathbf{A}^k \mathbf{x}_0 + \sum_{k=0}^{n-1} \mathbf{A}^{n-k-1} \mathbf{B} \mathbf{u}_k . \tag{3.19}$$

The first term of this equation is related to the initial state, which is known. The states are then fully controllable if the second term has a full rank equal to n. The second term that gives a linear map between the inputs and the states, is called the 'controllability matrix' of the system, written as

$$\mathcal{C} = \begin{bmatrix} \mathbf{B} & \mathbf{AB} & \mathbf{A}^2\mathbf{B} & \cdots & \mathbf{A}^{n-1}\mathbf{B} \end{bmatrix}, \tag{3.20}$$

with n rows and $n \times m$ columns[6]. Therefore, the system is fully state controllable if the controllability matrix has a full rank equal to n or, in general cases that $\mathbf{x}(t) \in \mathbb{R}^n$, the controllable subspace $\mathbb{X}^{con} = \text{image}(\mathcal{C}) = \mathbb{R}^n$.

[6] According to the Cayley-Hamilton theorem, $\mathbf{A}^n$ for $k \geq n$ can be expressed as a linear combination of $\mathbf{A}^0, \mathbf{A}^1, ..., \mathbf{A}^{n-1}$ and therefore $\text{image}(\mathcal{C}_k) = \text{image}(\mathcal{C}_n)$ and $\text{kernel}(\mathcal{C}_k) = \text{kernel}(\mathcal{C}_n)$ for $k \geq n$. Accordingly, the rank of the controllability matrix and the span of its columns can be determined by the first n terms. An immediate consequence is that for a DT system, every controllable state can be reached in (at most) n time step (Antoulas 2005). Similarly, for an observable system, the initial state can be reconstructed from n output measurements.

3.2.2. Observability matrix

The full 'state observability' means that we can construct the initial state from the knowledge of the inputs and the outputs. From the integration of the output equation (3.15), we get

$$\begin{bmatrix} \mathbf{y}_0 \\ \mathbf{y}_1 \\ \vdots \\ \mathbf{y}_{k-1} \end{bmatrix} = \begin{bmatrix} \mathbf{C} \\ \mathbf{CA} \\ \vdots \\ \mathbf{CA}^{k-1} \end{bmatrix} \mathbf{x}_0 + \begin{bmatrix} \mathbf{D} & 0 & \cdots & 0 \\ \mathbf{CB} & \mathbf{D} & \ddots & 0 \\ \vdots & \ddots & \ddots & \\ \mathbf{CA}^{k-1}\mathbf{B} & \mathbf{CA}^{k-2}\mathbf{B} & \cdots & \mathbf{D} \end{bmatrix} \begin{bmatrix} \mathbf{u}_0 \\ \mathbf{u}_1 \\ \vdots \\ \mathbf{u}_{k-1} \end{bmatrix}. \tag{3.21}$$

Since the inputs are known, the second term is also known and the relation between the outputs and the initial state variables are given by the 'observability matrix' with n columns and $n \times p$ rows, defined as

$$\mathcal{O} = \begin{bmatrix} \mathbf{C} & \mathbf{CA} & \mathbf{CA}^2 & \cdots & \mathbf{CA}^{n-1} \end{bmatrix}^T. \tag{3.22}$$

Therefore, the system is observable if the observability matrix has full rank n or the unobservable subspace $\mathbb{X}^{unobs} = \text{kernel}(\mathcal{O}) = \varnothing$. Note that the controllability and observability concepts for a LTI system depend only on properties of the pairs (**A**,**B**) and (**A**,**C**), and not on time or the input function. This is irrespective of whether we are dealing with DT or CT systems.

3.2.3. Gramians

We define the finite square symmetric controllability and observability Gramian as

$$\mathbf{W}_c = \mathcal{C}\mathcal{C}^T = \sum_{k=0}^{n-1} \mathbf{A}^k \mathbf{B}\mathbf{B}^T \left(\mathbf{A}^T\right)^k, \tag{3.23}$$

$$\mathbf{W}_o = \mathcal{O}^T\mathcal{O} = \sum_{k=0}^{n-1} (\mathbf{A}^T)^k \mathbf{C}^T \mathbf{C}\mathbf{A}^k. \tag{3.24}$$

The controllability Gramian measures to what degree a state is excited by an input, while the observability Gramian measures to what degree each states excites future outputs. A system is controllable/observable if and only if the controllability/observability Gramian is positive definite. Instead of computing the sum of Eqs. (3.23) and (3.24), the Gramians can be found as solutions of the DT Lyapunov (Stein) equations

$$\mathbf{A}\mathbf{W}_c\mathbf{A}^T + \mathbf{B}\mathbf{B}^T = \mathbf{W}_c, \tag{3.25}$$

$$\mathbf{A}^T\mathbf{W}_o\mathbf{A} + \mathbf{C}^T\mathbf{C} = \mathbf{W}_o. \tag{3.26}$$

For a brief overview of numerical techniques to compute the solutions of Lyapunov equations, see section 6.4.

3.2.4. Control and observation energy

The degree of controllability for a given state $\mathbf{x}$, is also defined in terms of 'control energy', i.e., the minimum energy of the input signal that is required to bring the system to state $\mathbf{x}$, given by [7]

$$E_{\mathscr{C}}(\mathbf{x}) = \| \mathbf{u} \|_2^2 = \mathbf{x}^T \mathbf{W}_{\mathscr{C}}^{-1} \mathbf{x}. \tag{3.27}$$

This means that, for two states $\mathbf{x}_1$ and $\mathbf{x}_2$ with $\|\mathbf{x}_1\| = \|\mathbf{x}_2\|$, if $\mathbf{x}_1^T \mathbf{W}_{\mathscr{C}}^{-1} \mathbf{x}_1 < \mathbf{x}_2^T \mathbf{W}_{\mathscr{C}}^{-1} \mathbf{x}_2$ then state $\mathbf{x}_1$ is 'more controllable', i.e., it takes a smaller input to bring the system from the initial state to state $\mathbf{x}_1$. Mathematically, if $\mathbf{W}_{\mathscr{C}}^{-1}$ is large, there will be some states that require a large control (input) energy to reach (Glover 1984). Accordingly, the combination of states that needs the minimum energy to reach, is corresponding to the largest eigen value of $\mathbf{W}_{\mathscr{C}}$. Similarly, the 'observation energy', i.e., the energy of the output function caused by the initial state $\mathbf{x}$, is defined as

$$E_{\mathscr{O}}(\mathbf{x}) = \| \mathbf{y} \|_2^2 = \mathbf{x}^T \mathbf{W}_{\mathscr{O}} \mathbf{x}. \tag{3.28}$$

Hence, the combinations of states that release the maximum observation energy, i.e., they excite larger output signals, are 'more observable'. Mathematically, these states are related to the largest eigen value of $\mathbf{W}_{\mathscr{O}}$. The definition of the control and observation energy in terms of the Gramians can be used to obtain a measure of the degree of controllability and observability of individual combinations of states, i.e., the degree to which a combination of states is influenced by the inputs, and the effect that changes in a combination of states has on the outputs. In this sense, 'more controllable' and 'more observable, states are dynamically more important. A more detailed discussion of controllability and observability concepts in reservoir engineering can be found in Zandvliet et al. (2008).

[7] Note that the term 'energy' is used loosely here, motivated by the fact that energy can often be written as a quadratic form (e.g. potential energy as a function of squared pressure).

3.3. Balanced realization of a linear system

By balancing we aim at finding a state-space coordinate system, in which the states are equally controllable and observable. This means that the states that are least influenced by the inputs have least influence on the outputs. Such a balanced realization is obtained by finding a transformation matrix $\mathbf{T}$, such that the state-coordinate transformation, $\bar{\mathbf{x}} = \mathbf{T}\mathbf{x}$, produces an equivalent model with equal and diagonal controllability and observability Gramians. This transformation can be obtained by a Cholesky factorization of $\mathbf{W}_c = \mathbf{L}_c\mathbf{L}_c^T$ and a eigen value decomposition of $\mathbf{L}_c^T\mathbf{W}_o\mathbf{L}_c = \mathbf{U}\boldsymbol{\Sigma}^2\mathbf{U}^T$. Then, it can be shown that the balanced Gramians are given by

$$\bar{\mathbf{W}}_c = \mathbf{T}\mathbf{W}_c\mathbf{T}^T, \tag{3.29}$$

$$\bar{\mathbf{W}}_o = \mathbf{T}^{-T}\mathbf{W}_o\mathbf{T}^{-1}, \tag{3.30}$$

where $\mathbf{T} = \boldsymbol{\Sigma}^{1/2}\mathbf{U}^T\mathbf{L}_c^{-1}$ and $\mathbf{T}^{-1} = \mathbf{L}_c\mathbf{U}\boldsymbol{\Sigma}^{-1/2}$. This transformation leads to

$$\bar{\mathbf{W}}_c = \bar{\mathbf{W}}_o = \boldsymbol{\Sigma} = diag(\sigma_1, \sigma_2, \cdots, \sigma_n) = diag(\boldsymbol{\sigma}_h), \tag{3.31}$$

where $\sigma_1 \geq \sigma_1 \geq \cdots \geq \sigma_n$ and the diagonal entries of the balanced Gramians, $\boldsymbol{\sigma}_h$, are known as Hankel singular values (HSVs) of the system. According to Eqs. (3.27), (3.28) and (3.31), each HSV offers a measure of the energy contribution of a component of the transformed (balanced) state to the input-output behavior, where the transformed (balanced) state is itself a linear combination of the original states. Therefore, the HSVs can be used to identify those linear combinations of the states that represent the most important input-output characteristics of the system.

For a DT system, the Hankel matrix[8], which represents a mapping from the past inputs to the future outputs, is written as

$$\mathcal{H} = \mathcal{O}\mathcal{C}, \tag{3.32}$$

and, therefore, the Hankel singular values can also be obtained as

$$\boldsymbol{\sigma}_h = \sqrt{\lambda(\mathcal{H}^T\mathcal{H})} = \sqrt{\lambda(\mathcal{C}^T\mathcal{O}^T\mathcal{O}\mathcal{C})} = \sqrt{\lambda(\mathcal{C}\mathcal{C}^T\mathcal{O}^T\mathcal{O})} = \sqrt{\lambda(\mathbf{W}_c\mathbf{W}_o)}. \tag{3.33}$$

Note that from Eqs. (3.29), (3.30) and (3.33), it turns out that, for the product of the Gramians, the similarity transformation $(\bar{\mathbf{W}}_c\bar{\mathbf{W}}_o) = \mathbf{T}(\mathbf{W}_c\mathbf{W}_o)\mathbf{T}^{-1}$ holds. As a result, the eigen values of the product of the Gramians, i.e., the HSVs, are coordinate-independent

[8] This is called a Hankel matrix since it has a block Hankel structure, i.e. $\mathcal{H}_{i,j} = \mathcal{H}_{i+j-1}$.

or ‘input-output invariant’, whereas the eigen values of the controllability and observability Gramians are coordinate-dependent and will change as the coordinates are changed (see also Moore 1981). Furthermore, the HSVs are identical for the DT and CT forms of a system. This makes the HSVs a system property rather than a model property, and gives a promising tool in determining the optimal complexity of a model for describing the system’s dynamics. We demonstrate the behavior of the HSVs for a reservoir system in the following example.

3.3.1. Example 3.1

Consider the small reservoir system given in Test Case (1), which is a 2D horizontal reservoir with a heterogeneous and isotropic permeability field depicted in Figure 3.2.

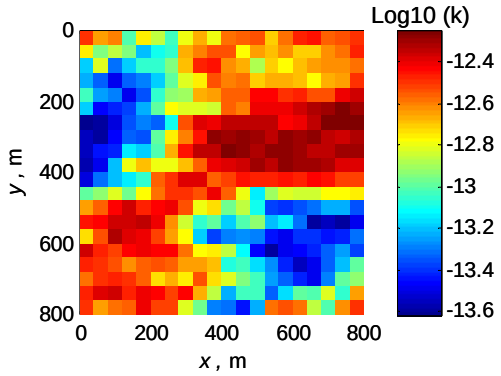

Figure 3.2 Log10 permeability field for Test Case (1).

Table 3.1 Reservoir model parameters and fluid properties for Test Case (1).

parameter	value	unit
reservoir length	800	m
reservoir width	800	m
reservoir height	2	m
fluid density	1000	kg/m^3
fluid viscosity	1.0e-03	Pa s
porosity	0.3	-
total compressibility	2.0e-08	1/Pa
initial reservoir pressure	3.0e07	Pa

This simulation model has 20×20 grid blocks with injection and production wells controlled by time-varying bottomhole pressures. The well flow rates are then measured as the system outputs. Rock and reservoir properties are given in Table 5.2.

Figure 3.3 displays the first 150 diagonal entries of the balanced Gramians (i.e., the HSVs) for the given reservoir system. Note that the y-axis is represented on a logarithmic scale, and that the smallest singular values of the system are smaller than the machine precision in Matlab (10^{-16}). We performed the simulation for different numbers of wells including one injector in the middle and one producer in the corner (2 wells), one injector in the middle and two producers in the opposite corners (3 wells), one injector in the middle and three producers in the corners (4 wells), and one injector in the middle and four producers in the corners (5 wells). Different markers, therefore, represent the HSV plots for simulations with the different number of wells.

Given that each HSV provides a measure of the energy contribution, i.e., the degree of combined controllability and observability of a balanced state, the rapid decline in the magnitude of HSVs shows that a large number of the states are weakly controllable/observable, hence, they weakly influence the input-output behavior of the system. Therefore, the intrinsic order of the system, i.e. the number of balanced states required to describe the input-output behavior of the system, is much smaller than 400, which is the total number of the original states. This is also in line with earlier results in Markovinović et al (2002), Heijn et al. (2004) and Zandvliet et al. (2008).

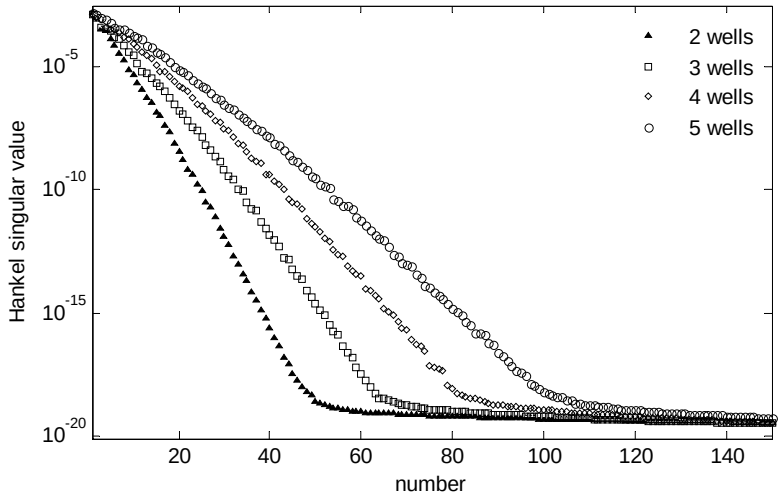

Figure 3.3 HSV plots for different number of wells in Test Case (1).

The second observation is that the slope of the HSV plot decreases as the number of wells (i.e., the number of inputs and outputs[9]) increases. Accordingly, any change in the number of wells and, consequently, the number of inputs/outputs will influence the degree of controllability and observability of the system. This mathematically means that the lower the rank of the input and output matrices **B** and **C**, the lower the number of required linear combinations of the states to represent the system dynamics. On the other hand, the order reduction is modest when there are a large number of inputs/outputs.

Finally, to demonstrate the effect of well locations on the controllability and observability of the system, we present the HSV plots for two different simulations of Test Case (1) in Figure 3.4. The first simulation was performed with one injector in the middle and one producer in the corner (middle-corner), while the second one is related to a simulation run with one injector and one producer at the opposite corners (corner-corner). The figure shows that the slope of the HSV plots is slightly altered as the well locations are changed, though the variation is less, compared to the one due to a change in the number of wells. The effect of the well locations is more pronounced in case of a reservoir with a more heterogeneous permeability field.

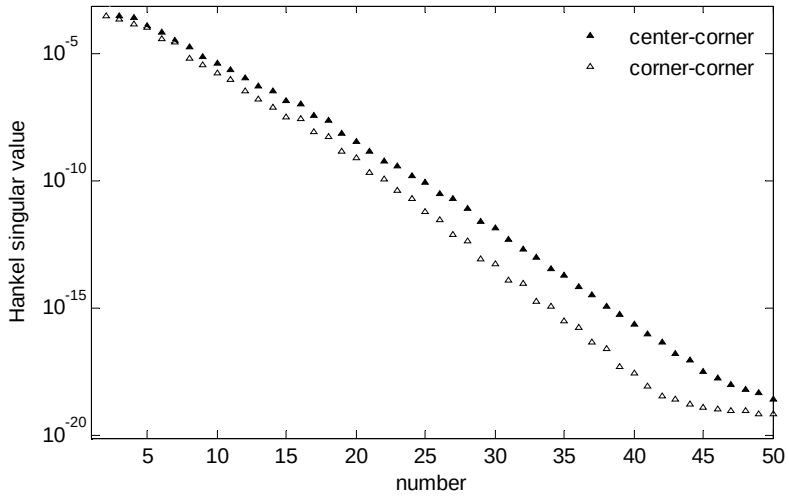

Figure 3.4 HSV plots for different well locations in Test Case (1).

[9] Here, we assume one input (bottomhole pressure) and one measurement (flow rate) at each well location. Accordingly, the numbers of both inputs and outputs are equal to the number of wells for each simulation.

3.4. Markov parameters

Consider the LTI system $\sum := (\mathbf{ABCD})$. Assuming a zero initial state vector[10], the impulse response of this system (for a unit input impulse) is easily calculated by using Eqs. (3.14) and (3.15):

$$\begin{aligned}
&\mathbf{M}_0 = \mathbf{y}_0 = \mathbf{D}\mathbf{u}_0 = \mathbf{D} \\
&\mathbf{M}_1 = \mathbf{y}_1 = \mathbf{C}\mathbf{x}_1 = \mathbf{CB} \\
&\vdots \\
&\mathbf{M}_k = \mathbf{y}_k = \mathbf{C}\mathbf{x}_k = \mathbf{C}\mathbf{A}^{k-1}\mathbf{B}.
\end{aligned}$$

The impulse response terms are known as the Markov parameters (**M**) of the system[11], where $\mathbf{M}_0 = \mathbf{D}$ and $\mathbf{M}_k = \mathbf{C}\mathbf{A}^{k-1}\mathbf{B}$, ($k$ = 1, 2, …) or

$$\mathbf{M} = \begin{bmatrix} \mathbf{M}_0 & \mathbf{M}_1 & \cdots & \mathbf{M}_k \end{bmatrix} = \begin{bmatrix} \mathbf{D} & \mathbf{CB} & \cdots & \mathbf{C}\mathbf{A}^{k-1}\mathbf{B} \end{bmatrix}. \tag{3.34}$$

Note that the Markov parameters are directly related to the Hankel matrix and, therefore, the HSVs of the system as the following relation holds

$$\mathscr{H} = \begin{bmatrix} \mathbf{M}_1 & \mathbf{M}_2 & \cdots \\ \mathbf{M}_2 & \mathbf{M}_3 & \cdots \\ \vdots & \vdots & \ddots \end{bmatrix}. \tag{3.35}$$

Given an arbitrary input **u**, the output vector of the system is obtained by the convolution[12] of the input signal with the impulse response (Markov parameters), written as

$$\mathbf{y}_k = \mathbf{D}\mathbf{u}_k + \sum_{i=1}^{k} \mathbf{C}\mathbf{A}^{i-1}\mathbf{B}\mathbf{u}_{k-i} = \begin{bmatrix} \mathbf{D} & \mathbf{CB} & \cdots & \mathbf{C}\mathbf{A}^{k-1}\mathbf{B} \end{bmatrix} \begin{bmatrix} \mathbf{u}_k & \mathbf{u}_{k-1} & \ldots & \mathbf{u}_0 \end{bmatrix}^T. \tag{3.36}$$

Furthermore, the z-transform of the output vector is given by

$$\hat{\mathbf{y}}(z) = \mathbf{H}(z)\hat{\mathbf{u}}(z), \tag{3.37}$$

---

[10] In the case of a nonzero initial state vector $\mathbf{x}_0$, we can redefine the state-variables such that the initial state vector becomes zero through a translation by an amount $\mathbf{x}_0$.

[11] In a single-input/single-output (SISO) system, Markov parameters are scalars, whereas for a multi-input/multi-output (MIMO) case, they are matrices.

[12] For our linear system, the convolution sum of **M** and **u** for time sequences of length k is given by $(\mathbf{M} * \mathbf{u})(k) = \sum_{i=0}^{k-1} \mathbf{M}_i \mathbf{u}_{k-i} = \mathbf{M}_0\mathbf{u}_k + \mathbf{M}_1\mathbf{u}_{k-1} + \cdots$ (Antoulas 2005).

where $\hat{\mathbf{u}}(z)$ depicts the z-transform of the input vector, and $\mathbf{H}(z)$ is the z-transform of the impulse response (Markov parameters) or the 'transfer function' of the system defined as

$$\mathbf{H}(z) = \mathbf{C}(z\mathbf{I} - \mathbf{A})^{-1}\mathbf{B} + \mathbf{D}. \tag{3.38}$$

The Markov parameters (as well as the transfer function) of a system completely determine its dynamic behavior, and, therefore, two equivalent systems in terms of input-output behavior have the same Markov parameters (transfer function) (Antoulas, 2005).

3.5. System norms

System norms provide a helpful tool to quantify the input-output behavior of a given system. Consequently, they can be used to investigate whether two systems are close or far apart. In this section, we briefly define three system norms. A more detailed description can be found in, e.g., Antoulas (2005).

3.5.1. H2-norm

The H_2-norm of a DT LTI system is defined as the L2-norm of its impulse response, written as

$$\|\Sigma\|_{\mathrm{H}_2}^2 = tr(\mathbf{M}^T\mathbf{M}) = tr(\mathbf{C}\mathbf{W}_c\mathbf{C}^T + \mathbf{D}\mathbf{D}^T) = tr(\mathbf{B}^T\mathbf{W}_o\mathbf{B} + \mathbf{D}^T\mathbf{D}). \tag{3.39}$$

The second equality denotes the Frobenius norm, which is also equal to the root mean square value of the Markov parameters (i.e., of the impulse responses) and, hence, it can be interpreted as the energy of the impulse responses of the system.

3.5.2. HSH-norm

Hilbert-Schmidt-Hankel norm (HSH-norm) is defined as the Hilbert-Schmidt norm of the Hankel Matrix (Hanzon 1992), and it is also equal to the square root of the sum of squares of the HSVs, and, equivalently, to the trace of the product of controllability and observability Gramians:

$$\|\Sigma\|_{\mathrm{HSH}}^2 = tr(\mathcal{H}\mathcal{H}^T) = \sigma_{h,1}^2 + \ldots + \sigma_{h,n}^2 = tr(\mathbf{W}_c\mathbf{W}_o). \tag{3.40}$$

The second equality shows that the HSH-norm is equal to the Frobenius norm of the impulse response matrix (Hankel matrix) of the system and, therefore, it can be considered as the total energy transferred through the system. Note that the transformation between the DT and CT cases leaves the controllability and observability Gramians and, consequently, the HSH-norm invariant (see e.g., Antoulas 2005).

3.5.3. Hankel norm

The Hankel norm or H-norm of a system is defined as the $l2$ -induced norm of its impulse matrix, given by

$$\left\|\Sigma\right\|_{\mathrm{H}} = \left\|\mathscr{H}\right\|_{2-\mathrm{ind}} = \sigma_1(\mathscr{H}) = \sigma_{h,\max}, \tag{3.41}$$

where $\sigma_{h,\max}$ is the largest HSV of he system. As a result, the H-norm gives the maximum energy gain from the past inputs to the future outputs. Summary of the system norms is given in Table 3.2.

Table 3.2 Summary of the system norms.

system norm	expression	interpretation
$\left\|\Sigma\right\|_{\mathrm{H}_2}^2$	$tr(\mathbf{C}\mathbf{W}_c\mathbf{C}^T + \mathbf{D}\mathbf{D}^T) = tr(\mathbf{B}^T\mathbf{W}_o\mathbf{B} + \mathbf{D}^T\mathbf{D})$	energy of the impulse response
$\left\|\Sigma\right\|_{\mathrm{HSH}}^2$	$tr(\mathbf{W}_c\mathbf{W}_o) = \sigma_{h,1}^2 + \ldots + \sigma_{h,n}^2$	the total energy transferred through the system
$\left\|\Sigma\right\|_{\mathrm{H}}^2$	$\lambda_{\max}(\mathbf{W}_c\mathbf{W}_o)$	maximum energy gain

3.6. Summary

The dynamic behavior of a reservoir model can be described by $(\mathbf{A},\mathbf{B},\mathbf{C},\mathbf{D})$ matrices through the state-space relations, the Markov parameters, or the transfer function of the system. The degree of combined controllability and observability of such a system can be obtained by computing the HSVs, which can be used to identify those linear combinations of the states that represent the most important input-output characteristics of the system. As demonstrated in Example 3.1, a rapid decline in the HSV plot indicates that there are a large number of uncontrollable/unobservable states that are not affecting the input-output behaviour of the reservoir system. Therefore, they can be used to adjust (reduce) the level of the model complexity (or model order) to the available amount of control and information. Note that the controllability and observability of a linear system is independent of the specific values of the time-variant inputs **u**, but dependent on well configuration. This means that any change in the well configuration (i.e., any change in either the number of wells or the well locations) will affect the controllability and the observability of the system. The controllability and observability analysis presented here

forms the basis for the development of control-relevant upscaling algorithms in the next two chapters.

4. CHAPTER: CONTROL-RELEVANT UPSCALING (CRU)

In this chapter, we consider a control-relevant upscaling approach, which is based on the controllability and the observability of a reservoir system. More specifically, we aim at minimizing the difference between fine- and coarse-scale models of a reservoir in terms of several system norms that characterize the input-output behaviour of the system.

4.1. Introduction

4.1.1. Motivation

The primary objective of conventional upscaling techniques is to overcome the computational limit of the reservoir simulator. Therefore, in the most common techniques, a coarser model is created of which the coarse-scale parameters are calculated on the basis of the fine-scale parameters and/or some local flow calculations (see Chapter 2). The upscaled parameters are, therefore, heavily dependent on the choice of the local boundary conditions, which are, in general, unknown. Moreover, even in non-local methods that consider extended-local (global) flow properties of the system, often the assumption is that the coarse-scale parameters computed based on a set of generic (e.g., fixed-pressure and no-flow) boundary conditions will be applicable to all other flow scenarios. This can lead to a significant error, knowing that in reservoir simulation the global flow is largely driven by wells rather than the fixed boundary conditions[13]. Moreover, as demonstrated in example 3.1, any change in the well configuration can significantly change the system properties like controllability and observability, thus resulting in wrong input-output predictions if the coarse-scale model is not adapted for that.

Therefore, in this thesis, we look at the upscaling problem from a system-theoretical perspective. We argue that, in addition to the computational difficulties, a more fundamental reason for upscaling is that, for a given configuration of wells in a reservoir, there is only a limited degree of freedom in the input/output dynamics of the system [i.e.,

[13] The assumption of fixed boundary conditions might also lead to a poor capturing of near-well effects on the global flow pattern unless a near-well upscaling technique is added (Ding 1995 and 2004; Durlofsky et al. 2000).

there is only a limited amount of information (output) that can be observed from production data, while there is also a limited amount of control (input) that can be exercised by adjusting the well parameters]. This means that a large number of combinations of the state variables (pressure and saturation values in the grid blocks) are not actually controllable and observable, and, accordingly, they are not affecting the input/output behavior of the model (see Chapter 3, Markovinović et al 2002, Heijn et al. 2004, and Zandvliet et al. 2008). Therefore, the complexity level of a model should be adjusted to the amount of available information and the extent of control that is possible in the reservoir system.

The problem with uncontrollable states and the associated parameters is two-fold. First, they lead to an ill-posed parameter-updating problem; and second, they increase the computational time. A potential approach to address these issues is through model-order reduction using system-theoretical methods (Markovinović et al 2002; Heijn et al. 2004; Cardoso et al. 2009). Alternatively, the number of state variables and parameters and, consequently, the computational time, may be decreased through a control-relevant grid-based upscaling. The former is briefly discussed in Chapter 6, and the latter is described in this chapter.

4.1.2. Behavior of HSVs for fine- and coarse-scale models

In reservoir simulation, we use a spatial discretization method to solve the flow equation over a given reservoir domain, (see Chapter 2). The maximum number of grid blocks that are used to generate the grid system is usually determined by the computational power and the storage capacity of our simulator. On the other hand, a straightforward way to reduce the simulation time of our model is to choose a smaller number of grid blocks for the spatial discretization. However, the parameters for the resulting coarse-scale model need to be computed such that the input-output behavior of the coarse-scale model is as close as possible to the fine-scale one.

Figure 4.1 and Figure 4.2 show the behavior of the HSVs for three different reservoir models. All models describe the input-out behavior of the reservoir system given as Test Case (1) in Chapter 3. However, each model has been discretized by a different number of grid blocks. The coarse-scale parameters were obtained from a local flow-based upscaling method (described in section 2.3.3). We consider a production scenario with one injector and one producer that are controlled by prescribed flow rates and bottomhole pressures, respectively. For both homogenous (Figure 4.1) and heterogeneous (Figure 4.2) permeability fields, the first few HSVs are close, but not identical. Actually, since the

controllability and the observability are reservoir properties and not just the properties of the coarse- or fine-scale models, the spatial discretization should not have a significant effect on them (Zandvliet 2008). Accordingly, the HSVs of three mentioned models, as a measure of the combined controllability and observability of the system, are also expected to be similar. However, we observe that the discrepancies in the HSV plots increase for smaller HSVs as well as for a higher degree of coarsening. Both homogenous and heterogeneous cases follow the same trend, although the HSV plots are less steep in the latter, indicating a more complex system.

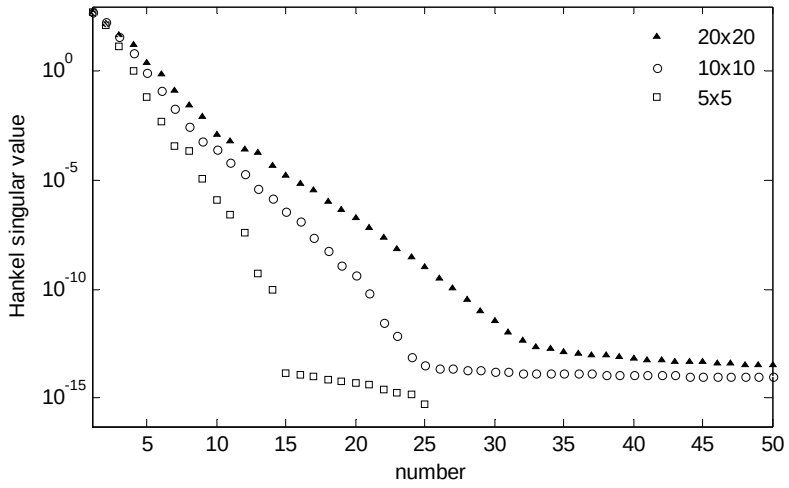

Figure 4.1 Behavior of HSVs for the homogenous fine-scale model and two different coarse-scale representations of Test Case (1).

Note that, as we mentioned in Chapter 3, any change in the state-space coordinates through, e.g., change in the grid numbering will not affect the HSVs as they are system-invariant. However, a different model representation in terms of a different number of grid blocks gives a different HSV plot. The discrepancies mainly arise from the errors associated with the computation of the equivalent upscaled parameters and equations as well as the error due to the numerical dispersion[14]. In fact, because of these inevitable errors, our coarse-scale models might unintentionally describe a slightly different physical system from the one represented by the original fine-scale model.

[14] In this thesis, we refer to the both errors as the ‘upscaling error’.

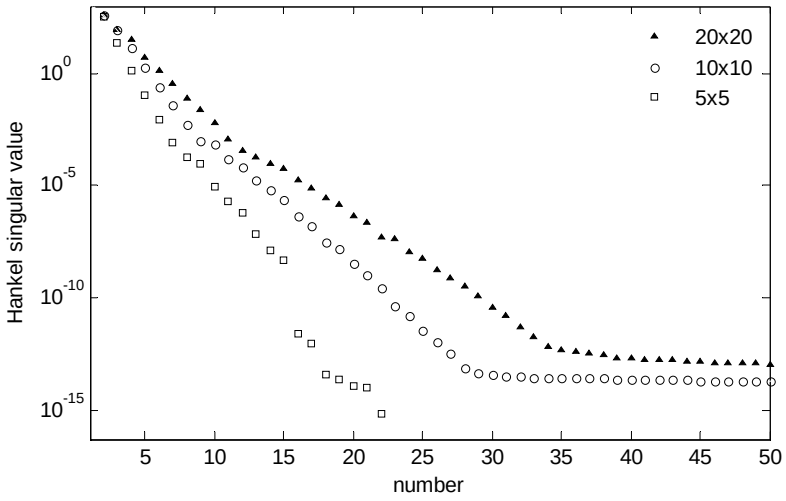

Figure 4.2 Behavior of HSVs for the heterogeneous fine-scale model and two different coarse-scale representations of that for Test Case (1).

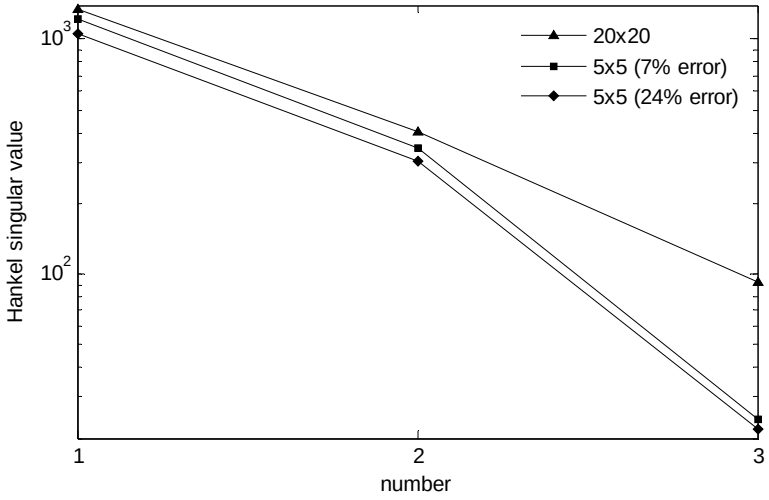

Figure 4.3 The first three HSVs of the heterogeneous fine-scale model and two coarse-scale representations of that for Test Case (1).

To illustrate the effect of the upscaling error on the controllability and the observability and, consequently, the HSVs of the system, we compared the HSVs of Test Case (1) obtained from two different coarse-scale models with those of the original fine-scale model. Both coarse models have 5×5 grid blocks, however, one is obtained by a local upscaling technique with relative cumulative production error (Eq. 4.14) of 7.6%, while the other one is calculated by an arithmetic averaging with 24.1% error. Figure 4.3 shows

the result for the first 3 HSVs. Evidently, for this example, the coarse-scale model with smaller upscaling error gives HSVs closer to those of the fine-scale model.

4.1.3. Control-relevant grid-based upscaling

By control-relevant grid-based upscaling we aim at obtaining a coarse-scale model that reproduces the original fine-scale input-output behavior as close as possible. To match the system properties, we propose to minimize the distance (error) between the input/output behaviors of the fine- and coarse-scale models in terms of several system norms, which are based on the observability and controllability properties of the system. The advantage of this control-relevant upscaling (CRU) approach is that it focuses on the observable/controllable state variables and, therefore, relies on those grid blocks that are most important to the input/output behavior of the model. A possible application of the CRU algorithm would be in closed-loop reservoir management (see Chapter 1), in which use is made of an ensemble of high-order geological models that are scaled up to low-order coarser representations for the actual flow simulations, the continuous model-based optimization, and model updating or data assimilation. To simplify our study, we focus on a single-phase-flow case that is described by a LTI system.

In the next sections, we describe the CRU algorithm and illustrate its performance by several numerical examples. The material is mainly based on Vakili-Ghahani et al. (2008), and Vakili-Ghahani & Jansen (2010a).

4.2. CRU algorithm

4.2.1. CRU problem

Consider the fine-scale reservoir model $\Sigma := (\mathbf{ABCD})$ with parameters $\boldsymbol{\theta}$, where $\mathbf{A} \in \mathbb{R}^{n \times n}$, $\mathbf{B} \in \mathbb{R}^{n \times m}$, $\mathbf{C} \in \mathbb{R}^{p \times n}$, and $\mathbf{D} \in \mathbb{R}^{p \times m}$. We search for coarse-scale parameters $\tilde{\boldsymbol{\theta}}$ that give a coarse-scale (lower dimensional) model $\tilde{\Sigma} := (\tilde{\mathbf{A}}\tilde{\mathbf{B}}\tilde{\mathbf{C}}\tilde{\mathbf{D}})$, where $\tilde{\mathbf{A}} \in \mathbb{R}^{r \times r}$, $\tilde{\mathbf{B}} \in \mathbb{R}^{r \times m}$, $\tilde{\mathbf{C}} \in \mathbb{R}^{p \times r}$, $\tilde{\mathbf{D}} \in \mathbb{R}^{p \times m}$ and $r < n$, such that $\tilde{\Sigma}$ reproduces the input-output behavior of the original system as close as possible. Figure 4.4 schematically depicts the CRU problem.

To solve the CRU problem, we start with an initial guess for coarse-scale parameters that can be obtained from a simple averaging technique, for example, or a local upscaling method. Then, we define $J(\tilde{\boldsymbol{\theta}})$, not as the direct difference between the outputs of the fine- and the coarse-scale models (i.e., $\|\mathbf{y} - \tilde{\mathbf{y}}\|$), but as a measure (i.e. some norm in terms of system properties) of the difference between the input-output behaviors of two systems . Mathematically, we formulate the CRU problem as

$$\tilde{\boldsymbol{\theta}} = \underset{\tilde{\boldsymbol{\theta}}_{lb}<\tilde{\boldsymbol{\theta}}<\tilde{\boldsymbol{\theta}}_{ub}}{\arg\min} \left\| \Sigma(\boldsymbol{\theta}) - \tilde{\Sigma}(\tilde{\boldsymbol{\theta}}) \right\| = \underset{\tilde{\boldsymbol{\theta}}_{lb}<\tilde{\boldsymbol{\theta}}<\tilde{\boldsymbol{\theta}}_{ub}}{\arg\min} J(\tilde{\boldsymbol{\theta}}), \tag{4.1}$$

i.e. we search for optimum coarse-scale parameters $\tilde{\boldsymbol{\theta}}$ (bounded by $\tilde{\boldsymbol{\theta}}_{lb}$ and $\tilde{\boldsymbol{\theta}}_{ub}$), such that the cost function $J(\tilde{\boldsymbol{\theta}})$ is minimized. We investigate various choices for $J(\tilde{\boldsymbol{\theta}})$ as we explain different CRU methods.

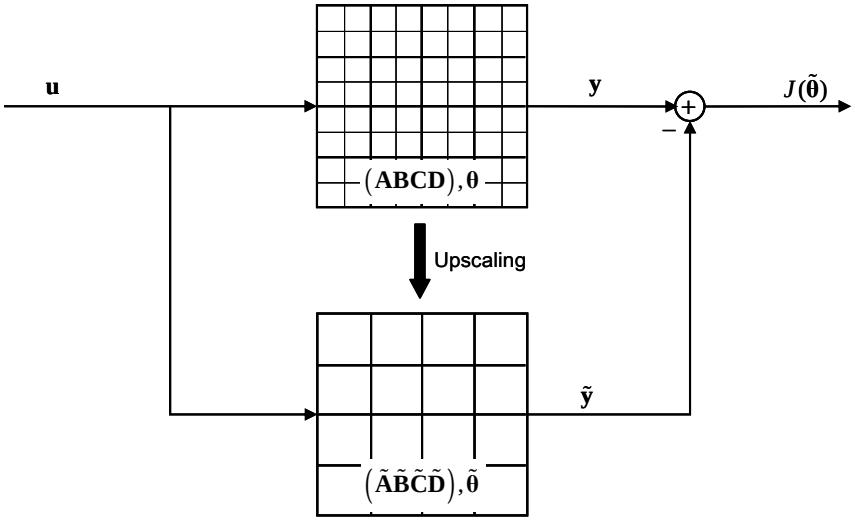

Figure 4.4 Schematic representation of the CRU problem. The aim is to find an equivalent coarse-scale model with an input-output behavior as close as possible to that of the original fine-scale model.

4.2.2. CRU methods

A key aspect of the CRU approach is that we can perform the minimization without performing any fine- or coarse-scale simulation and that the results do not depend on a specific input. This is achieved by making use of the fact that the dynamic system behavior is completely characterized by the elements of the four matrices $(\mathbf{A},\mathbf{B},\mathbf{C},\mathbf{D})$ in the dynamic system equations (Eqs. 3.14 and 3.15). Therefore, we can quantify the input-output behavior of the system with the aid of a system norm that is directly expressed in terms of these matrices. We can then define a cost function $J(\tilde{\boldsymbol{\theta}})$ as a system norm of an error model (CRU method 1), or we may formulate the cost function as the difference between input/output behaviors of the fine and the coarse models expressed in terms of

different system norms (CRU methods 2)[15]. To recall the system-theoretical notations used here, the reader is referred to chapter 3.

CRU Method (1)

In this method, we consider an 'error model' depicted by the dashed rectangle in Figure 4.5. The state-space representation of this new system $\Sigma' := (\mathbf{A}'\mathbf{B}'\mathbf{C}'\mathbf{D}')$ is obtained by subtracting the fine- and coarse-scale representations, written as

$$\Sigma' = \Sigma - \tilde{\Sigma}, \tag{4.2}$$

where

$$\mathbf{A}' = \begin{bmatrix} \mathbf{A} & 0 \\ 0 & \tilde{\mathbf{A}} \end{bmatrix}, \tag{4.3}$$

$$\mathbf{B}' = \begin{bmatrix} \mathbf{B} \\ \tilde{\mathbf{B}} \end{bmatrix}, \tag{4.4}$$

$$\mathbf{C}' = \begin{bmatrix} \mathbf{C} & -\tilde{\mathbf{C}} \end{bmatrix}, \tag{4.5}$$

$$\mathbf{D}' = \mathbf{D} - \tilde{\mathbf{D}}, \tag{4.6}$$

$$\mathbf{y}' = \mathbf{y} - \tilde{\mathbf{y}}. \tag{4.7}$$

The input vector **u** remains the same for all three systems (Σ, $\tilde{\Sigma}$, and Σ′). The CRU problem is now to find the coarse-scale parameters $\tilde{\boldsymbol{\theta}}$, such that the cost function $J(\tilde{\boldsymbol{\theta}})$ is minimized, where $J(\tilde{\boldsymbol{\theta}})$ is defined as a system norm of the error model Σ′. We investigated three different norms defined by Eqs. (3.39), (3.40) and (3.41). The cost function $J(\tilde{\boldsymbol{\theta}})$ is, therefore, chosen as

$$J(\tilde{\boldsymbol{\theta}}) = \left\| \Sigma - \tilde{\Sigma} \right\|_{\mathrm{H_2/HSH/H}} = \left\| \Sigma' \right\|_{\mathrm{H_2/HSH/H}}. \tag{4.8}$$

The expression and interpretation of each system norm is also given in section 3.5 and Table 3.2.

[15] For reasons of clarity, we present here a slightly different classification of the CRU methods from the one given in Vakili-Ghahani et al (2008) and Vakili-Ghahani & Jansen (2010a). However, the theory behind them remains the same.

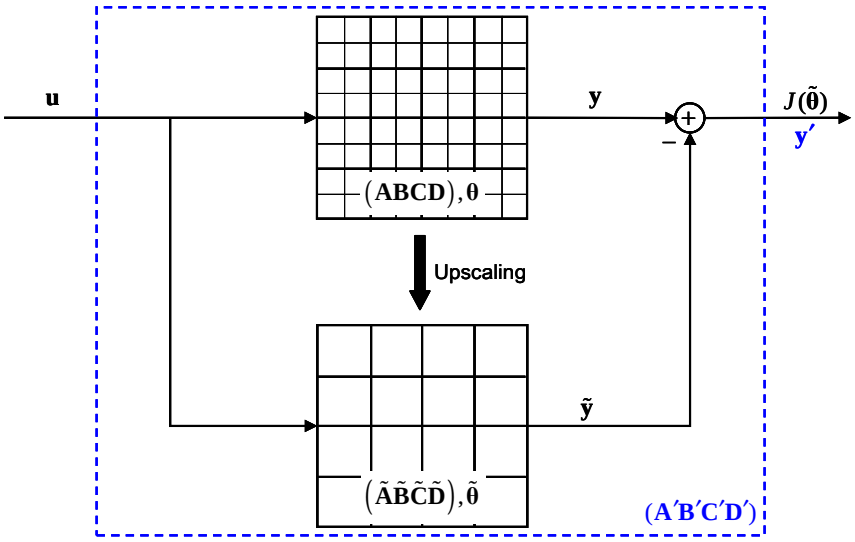

Figure 4.5 Schematic representation of the CRU problem with the error model depicted by the dashed rectangle.

CRU Method (2)

For this method, the 'distance' between the input-output behaviors of the fine- and the coarse-scale models is represented by the difference between their Markov parameters, or their system norms. Consider the fine-scale and coarse-scale models Σ and $\tilde{\Sigma}$. For an arbitrary $\mathbf{u}$ and a zero initial state, we can use Eq. 3.36 to write the output signals of two systems at time step k as

$$\mathbf{y}_k = \begin{bmatrix} \mathbf{D} & \mathbf{CB} & \cdots & \mathbf{CA}^{k-1}\mathbf{B} \end{bmatrix} \begin{bmatrix} \mathbf{u}_k & \mathbf{u}_{k-1} & \ldots & \mathbf{u}_0 \end{bmatrix}^T, \tag{4.9}$$

$$\tilde{\mathbf{y}}_k = \begin{bmatrix} \tilde{\mathbf{D}} & \tilde{\mathbf{C}}\tilde{\mathbf{B}} & \cdots & \tilde{\mathbf{C}}\tilde{\mathbf{A}}^{k-1}\tilde{\mathbf{B}} \end{bmatrix} \begin{bmatrix} \mathbf{u}_k & \mathbf{u}_{k-1} & \ldots & \mathbf{u}_0 \end{bmatrix}^T. \tag{4.10}$$

Seeing that the inputs of two systems are equal, we need to match the elements of the sequence $\begin{bmatrix} \mathbf{D} & \mathbf{CB} & \cdots & \mathbf{CA}^{k-1}\mathbf{B} \end{bmatrix}$ and $\begin{bmatrix} \tilde{\mathbf{D}} & \tilde{\mathbf{C}}\tilde{\mathbf{B}} & \cdots & \tilde{\mathbf{C}}\tilde{\mathbf{A}}^{k-1}\tilde{\mathbf{B}} \end{bmatrix}$, i.e., the Markov parameters of two systems to obtain the same outputs. Therefore, systems Σ and $\tilde{\Sigma}$ are equivalent (i.e., $\tilde{\mathbf{y}} = \mathbf{y}$ for any $\tilde{\mathbf{u}} = \mathbf{u}$) if their Markov parameters are equal [i.e., if $\mathbf{M}(\boldsymbol{\theta}) = \tilde{\mathbf{M}}(\tilde{\boldsymbol{\theta}})$][16]. Another interpretation is possible by expanding the transfer function (Eq. 3.38) for large z, i.e. in the neighborhood of infinity:

[16] We emphasize that, in general, the fine- and coarse-scale Markov parameters are not equal, since the inevitable upscaling errors may lead to a slightly different system, compared to the original fine-scale one. Moreover, it is not (easily) possible to find a projection between the coarse- and fine-scale models, such that we can formulate the errors. Nevertheless, we try to find coarse-scale parameters that result in coarse-scale Markov parameters 'as close as possible' to those of the fine-scale ones.

$$\mathbf{H}(z) = \mathbf{C}(z\mathbf{I} - \mathbf{A})^{-1}\mathbf{B} + \mathbf{D} + \mathbf{CB}z^{-1} + \mathbf{CAB}z^{-2} + ... + \mathbf{CA}^{k-1}\mathbf{B}z^{-k} + ..., \quad (4.11)$$

Accordingly, matching the Markov parameters is equivalent to the matching of the high-frequency moments of the system. Therefore, we can define the cost function as

$$J\left(\tilde{\boldsymbol{\theta}}\right) = \left\|\mathbf{M}(\boldsymbol{\theta}) - \tilde{\mathbf{M}}(\tilde{\boldsymbol{\theta}})\right\|. \quad (4.12)$$

However, the direct match of the Markov parameters for large systems might be numerically problematic, resulting in a non-convex problem (see Vakili-Ghahani et al. 2008). This is probably because the power calculation of the matrices may introduce a large numerical error, in particular, for Markov parameters with widely ranging values. For this reason, we use, instead, the energy norm of the Markov parameters of the system (i.e. H_2-norm), as defined by Eq. (3.39). Alternatively, we may choose the cost function as the difference between the HSH-norm or H-norm of the two systems. The cost function $J(\tilde{\boldsymbol{\theta}})$ is then defined as

$$J\left(\tilde{\boldsymbol{\theta}}\right) = \left\|\Sigma\right\|_{\mathrm{H_2/\ H/HSH}} - \left\|\tilde{\Sigma}\right\|_{\mathrm{H_2/H/\ HSH}}. \quad (4.13)$$

Note that the choice of $J(\tilde{\boldsymbol{\theta}})$ in Method 1 implies that we take a norm in terms of system properties of the error model Σ', whereas in Methods 2, we take the difference of two norms in terms of system properties of the models Σ and $\tilde{\Sigma}$.

4.2.3. Algorithm

1) Divide the fine-grid model into a coarser mesh. The degree of coarsening can be roughly determined by inspecting the behavior of Hankel singular values of the system.
2) Construct the state-space formulation of the coarse-scale system, using an initial guess for the equivalent permeability values $\tilde{\boldsymbol{\theta}}$. A local upscaling or a simple averaging technique can be used to obtain a fast initial guess.
3) Define $J(\tilde{\boldsymbol{\theta}})$ according to one of the methods described above.
4) Calculate the equivalent coarse-scale parameters from the solution of a minimization algorithm that minimizes $J(\tilde{\boldsymbol{\theta}})$, by changing the parameter values of the coarse model.

Remarks

- The upscaled permeability for each coarse grid block is bounded by the arithmetic and harmonic averages of the corresponding fine-scale

permeability values (according to the Wiener bounds). For the sake of simplicity, we considered an isotropic, and therefore scalar, permeability value for each grid block. However, we foresee that the CRU approach can be extended to the case of anisotropic or full tensor permeabilities, although the latter may require a somewhat more advanced minimization algorithm.

- In the examples presented, the well indices were computed following either the standard Peaceman method for block-centered wells or the method of Abou Kassem and Aziz (1985) for wells located at the corner of a gridblock. In both cases, the permeability in the well model was updated at every iteration.
- We performed the minimization using 'fmincon' routine in Matlab. To speed up the convergence of the minimization problem, we added a so-called Tikhonov regularization term $\alpha \| \boldsymbol{\theta} - \tilde{\boldsymbol{\theta}} \|$ to the objective function $J(\tilde{\boldsymbol{\theta}})$, where α is a small positive number.
- We note that, although our approach is based on optimally representing input/output data, we do not consider the reservoir entirely as a 'black box'. In particular, the use of a numerical reservoir simulator implies adherence to physical relations, such as mass conservation and Darcy's law. Moreover, we constrain the permeability values to stay between the Wiener bounds, which could be interpreted as incorporating a form of geological information. In theory, it may be possible, therefore, to include other constraints and prior information to ensure adherence to geological data and interpretations (e.g., in the form of geostatistical relationships or other quantitative measures).

4.3. Results and discussion

In this section, we will illustrate the performance of the CRU algorithm for two numerical examples. To evaluate the upscaling performance, we compare the upscaled results to those from a given high fidelity fine-scale model through a 'relative error' relation, defined as

$$e_{\mathbf{z}} = \frac{\left\| z_{fine} - z_{coarse} \right\|}{\left\| z_{fine} \right\|} \times 100\%, \tag{4.14}$$

where **z** may be chosen to represent a particular variable of interest. In particular, we will choose **z** to represent the pressure field in all time steps:

$$\mathbf{p} = \begin{bmatrix} \mathbf{p}_1^T & \mathbf{p}_2^T & \cdots & \mathbf{p}_K^T \end{bmatrix}^T, \tag{4.15}$$

where $\mathbf{p}_k$ is a $1\times r$ vector of the averaged fine-scale pressures in all r coarse grid blocks at time step k and K is the total number of time steps, such that in this case $n_z = rK$. The corresponding coarse-scale measure is then simply the vector of pressures in all coarse grid blocks at time step k. As a second measure, we chose **z** to represent the cumulative total production:

$$q_{cum}^p = \sum_{k=1}^{K} q_k^p \Delta t_k, \tag{4.16}$$

where the superscript p is used to indicate that we only consider production wells, and where $\mathbf{q}_k$ is the vector of well flow rates in time step k. Therefore, we introduce e_p and $e_{q,cum}$ as the relative errors between fine- and coarse-scale pressure fields and cumulative production rates, respectively. In general, according to the correctness criterion of an upscaling procedure (see subsection 2.2.1), the coarse model should be capable of reproducing the main aspects of the fine-scale flow behavior, among which an accurate prediction of the cumulative production, which is also one of the main objectives of most reservoir simulations.

Finally, to show the relative size of each coarse model, we define the '*n*-ratio' as the ratio of the number of the grid blocks in each model to that of the original fine-scale one, written as

$$n\text{-ratio} = \frac{n_{coarse}}{n_{fine}}. \tag{4.17}$$

This ratio also relates to the number of linear solves and, accordingly, gives a rough estimation of the computational time that is needed to simulate each reservoir model, compared to that of the fine-scale one. Clearly, the *n*-ratio for the fine-scale model is equal to 1.

4.3.1. Example 4.1

In this example, we study the reservoir system presented as Test Case (1) in subsection 3.3.1. Reservoir parameters and fluid properties are given in Table (3.1). The original fine-scale reservoir model has 20×20×1 grid blocks with a heterogeneous and isotropic

permeability field, depicted in Figure 3.2. We consider a production scenario with one injector and one producer that are located on the northwest and southeast corners of the reservoir, resembling a quarter five-spot pattern. The injection rates in the injection well and the bottomhole pressures in the production well are the system inputs (controls). The output vector then contains the bottomhole pressures in the injector and the production rates in the producer. The bottomhole pressure in the producer is set to 2.5e7 Pa and the injection rates versus time are shown in Figure 4.6.

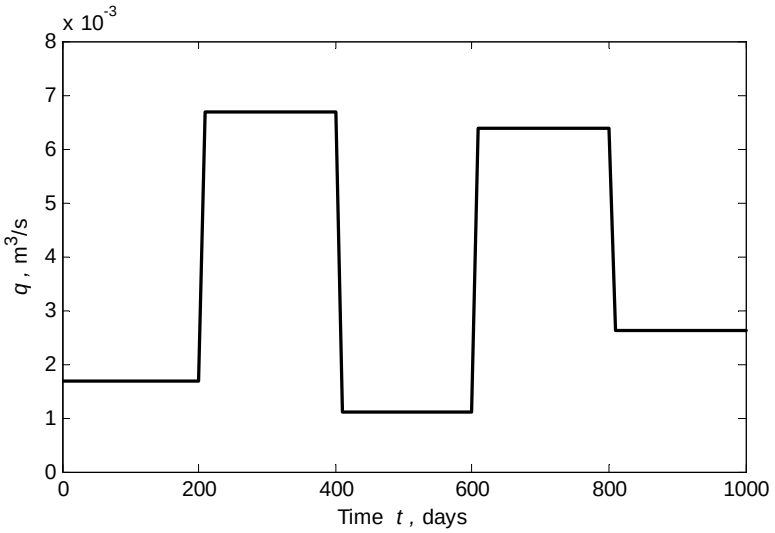

Figure 4.6 Prescribed injection rates for the injector in Example 4.1.

We scaled up the original 20×20 model of Example 1 to a 5×5 coarse model using different CRU algorithms and compared the results to those of the local-upscaling and the geometric-averaging techniques (see also Chapter 2 for a review of different upscaling techniques). For all CRU methods, geometric averaging was used as an initial guess and, during the minimization process, the coarse-scale permeability values were bounded by the Wiener bounds. Figure 4.7 shows the upscaled permeability field, obtained by the CRU method, and Table 6.1 presents the upscaling errors for different methods.

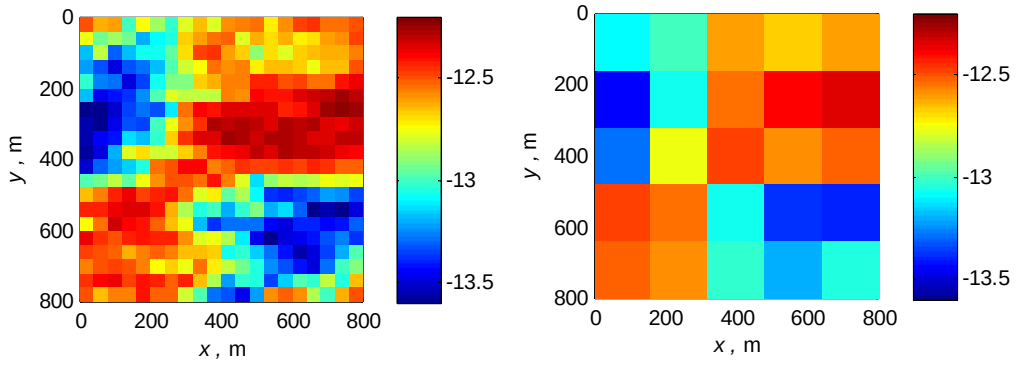

Figure 4.7 Log10 permeability fields for Example 4.1. Left: fine-scale permeability field from Test Case (1). Right: coarse-scale permeabilities, calculated by the CRU method.

Table 4.1 CRU performance for Example 4.1.

	geometric	local	CRU1-H2	CRU1-HSH	CRU1-H	CRU2-M	CRU2-H2	CRU2-HSH	CRU2-H
e_p (%)	1.5	1.5	0.9	0.9	0.9	1.0	1.4	1.1	1.1
$e_{q,cum}$ (%)	7.9	7.6	0.5	0.5	0.5	4.5	6.3	0.6	0.6
n-ratio	0.0625	0.0625	0.0625	0.0625	0.0625	0.0625	0.0625	0.0625	0.0625

In this table, CRU 1–2 refer to the CRU methods 1 and 2 described in the preceding section, where H2, HSH, H and M refer to H2-norm, HSH-norm, H-norm and the Markov parameters, respectively. We observe from the middle row that all CRU methods give superior results compared to the local and geometric-averaging techniques. This is true for the errors in the average pressures as well as for the errors in the cumulative production. Moreover, different system norms in Methods 1 give identical results[17].For Method 2; however, only the HSH-norm and the H-norm give comparable results to Method 1. We will discuss the computational and system-theoretical aspects of different methods in subsections 4.3.3 and 4.3.4.

4.3.2. Example 4.2

In this example, we consider a larger system with 220×60×1 grid blocks (i = 1, 2, …, 220 ; j = 1, 2, …, 60 and k = 1), referred to as Test Case (2). Reservoir parameters and fluid properties are given in Table 5.2. We choose a standard five-spot pattern with one

[17] We note, however, that this identity occurs only for small models, as will be discussed in more detail later.

injector located at the center of the grid block with (*i*,*j*,*k*) coordinates (110,30,1) and four producers at the outside corners of the four corner grid blocks. Injection rates in the injector and bottomhole pressures in the producers were considered as system inputs. We chose two different permeability fields taken from Layers 30 and 80 of the SPE 10 Comparative Solution Project (Christie and Blunt 2001). The fine-scale permeability realizations of these two layers are shown in the left parts of Figure 4.8 and Figure 4.9, respectively.

Table 4.2 Reservoir parameters and fluid properties for Test Case (2).

parameter	value	unit
reservoir length	700	m
reservoir width	400	m
reservoir height	2	m
fluid density	1000	kg/m^3
fluid viscosity	3.0e-04	Pa s
porosity	0.3	-
total compressibility	5.8e-07	1/Pa
initial reservoir pressure	4.1e07	Pa

We scaled up the original 220×60 model to a 22×6 coarse-scale one. Similar to Test Case (1), we compared the relative errors of average pressures and cumulative production for different upscaling methods. Because of computational reasons, discussed in more detail later, we considered only CRU Method 2 (by using the HSH-norm of the fine and the coarse models). Table 4.3 and Figure 4.9 summarize the upscaling results for Layers 30 and 80, respectively. It turns out that, for both cases, the CRU method gives superior results in reducing the upscaling error for cumulative production compared to the geometric-averaging and local methods. The differences in the pressure errors are less pronounced. Most notable is the good performance of the CRU method to predict the cumulative production from Layer 80. This is a strongly channelized system for which the geometric-averaging and the local methods result in very large upscaling errors because they cannot resolve the permeability connectivities between different coarse blocks. The CRU method gives the smallest error for this test case, which, because of strong large-scale flow paths in the channels, is a difficult problem for upscaling. The

error of approximately 20% is still considerable, but we note that we applied a coarsening factor of 100. For such large coarsening factors, a large part of the error is because of the numerical diffusion resulting from the coarse discretization rather than from calculation of the upscaled parameters (Durlofsky 2005). The coarse-scale permeability fields of Test Case 2 as obtained with CRU Method 2 have been displayed at the right-hand sides of Figure 4.8 and Figure 4.9.

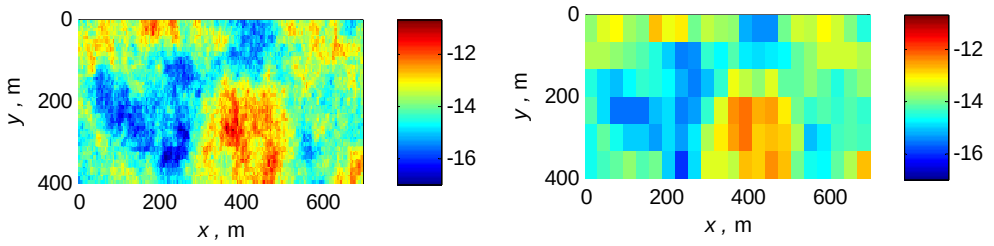

Figure 4.8 Log10 permeability fields for Example 4.2. Left: fine-scale permeability field from Test Case (2), SPE10 layer 30. Right: coarse-scale permeabilities, calculated by the CRU method.

Table 4.3 CRU performance in Example 4.2 (layer 30).

	geometric	local	CRU2-HSH
e_p (%)	5.69	5.52	3.93
$e_{q,cum}$ (%)	79.73	75.44	31.93
n-ratio	0.01	0.01	0.01

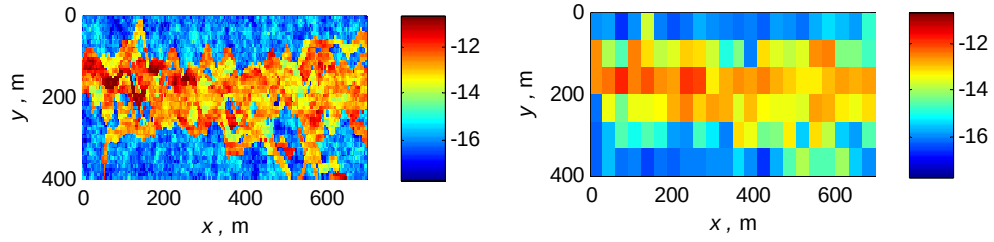

Figure 4.9 Log10 permeability fields for Example 4.2. Left: fine-scale permeability field from Test Case (2), SPE10 layer 80. Right: coarse-scale permeabilities, calculated by the CRU method.

Table 4.4 CRU performance in Example 4.2 (layer 80).

	geometric	local	CRU2-HSH
e_p (%)	1.82	2.39	1.57
$e_{q,cum}$ (%)	413.37	315.64	20.44
n-ratio	0.01	0.01	0.01

4.3.3. Computational Aspects

Figure 4.10 shows the values of the cost function for 15 iterations of the CRU minimization problem in Eq. (4.1), corresponding to different CRU methods in Table 6.1. As follows from the plots in this figure, the CRU algorithm converges after only a few iterations for the given small example. We also tried different initial guesses to upscale Test Case (1), including different averaging methods and a local upscaling technique. For this small reservoir, they all lead to almost the same solution[18]. However, calculating Hankel singular values and controllability and observability Gramians requires the solution of Lyapunov equations (Eqs. 3.25 and 3.26) using standard algorithms in Matlab, which is an expensive task, particularly for large systems. In most cases, we can reduce the computational cost of the method by some further modifications. For instance, in CRU method 1, the order (i.e., the number of states) of the error model is equal to the sum of the orders of the fine and the coarse models, which makes the computation of the Gramians even more expensive than the original fine-scale model. However, we can write the controllability Gramian of the error system as

$$\mathbf{W}_e' = \begin{bmatrix} \mathbf{W}_{e,11} & \mathbf{W}_{e,12} \\ \mathbf{W}_{e,21} & \mathbf{W}_{e,22} \end{bmatrix}. \tag{4.18}$$

Subsequently, from Eqs. (4.3), (4.4) and (3.25) we obtain

$$\begin{bmatrix} \mathbf{A} & 0 \\ 0 & \tilde{\mathbf{A}} \end{bmatrix} \begin{bmatrix} \mathbf{W}_{e,11} & \mathbf{W}_{e,12} \\ \mathbf{W}_{e,21} & \mathbf{W}_{e,22} \end{bmatrix} \begin{bmatrix} \mathbf{A}^T & 0 \\ 0 & \tilde{\mathbf{A}}^T \end{bmatrix} + \begin{bmatrix} \mathbf{B} \\ \tilde{\mathbf{B}} \end{bmatrix} \begin{bmatrix} \mathbf{B}^T & \tilde{\mathbf{B}}^T \end{bmatrix} = \begin{bmatrix} \mathbf{W}_{e,11} & \mathbf{W}_{e,12} \\ \mathbf{W}_{e,21} & \mathbf{W}_{e,22} \end{bmatrix}. \tag{4.19}$$

Therefore, $\mathbf{W}_{e,11}$ and $\mathbf{W}_{e,22}$ satisfy the DT Lyapunov (Stein) equations

$$\mathbf{A}\mathbf{W}_{e,11}\mathbf{A}^T + \mathbf{B}\mathbf{B}^T = \mathbf{W}_{e,11}, \tag{4.20}$$

$$\tilde{\mathbf{A}}\mathbf{W}_{e,22}\tilde{\mathbf{A}}^T + \tilde{\mathbf{B}}\tilde{\mathbf{B}}^T = \mathbf{W}_{e,22}, \tag{4.21}$$

and, hence, they are equal to the Gramians of the fine- and coarse-scale systems, respectively. In addition, from Eq. (4.19), $\mathbf{W}_{e,12}$ satisfies the DT Sylvester equation

$$\mathbf{A}\mathbf{W}_{e,12}\tilde{\mathbf{A}}^T + \mathbf{B}\tilde{\mathbf{B}}^T = \mathbf{W}_{e,12}. \tag{4.22}$$

[18] Note that in the case of using a local upscaling technique to obtain the initial guess, we obtain a directional permeability tensor as an initial guess. Therefore, for some CRU methods, we needed a few more iteration to converge.

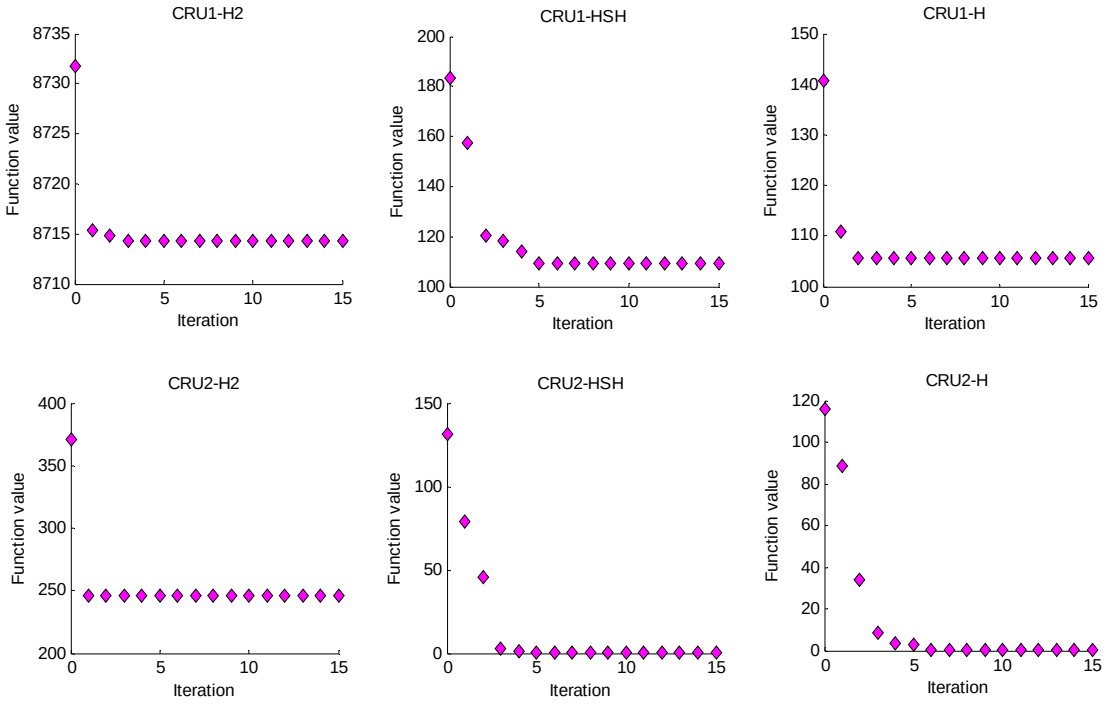

Figure 4.10 Cost function values corresponding to different CRU methods in Table 4.1.

Finally, since the Gramians are symmetric, $\mathbf{W}_{e,21} = \mathbf{W}_{e,12}$. Therefore, instead of computing the high-order controllability Gramian of the error system in each iteration, we only update $\mathbf{W}_{e,22}$ and $\mathbf{W}_{e,12}$ in Eq. (4.18) by solving the low-order equations (4.21) and (4.22). The same procedure is used to calculate the observability Gramian of the error system (see also Bunse-Gerstner et al. 2010).

Another improvement in the computational efficiency can be achieved by computing only the first few largest HSV'a of the system. That is because, in most reservoir systems, the HSVs are rapidly decreasing, indicating that the system dynamics can be described by only a few modes, i.e. those corresponding to the largest HSVs (see e.g. Figure 4.2). As an example, we calculated the HSH-norm (given by Eq. 3.40) for the fine-scale model in Example 4.1. Figure 4.11 shows the calculated value using different number of HSVs. Clearly, the HSH-norm can be accurately obtained from less than 10 HSVs instead of 400 HSVs.

Despite the above-mentioned modifications, standard methods for calculating the exact full-rank Gramians have to be replaced by some approximation techniques to solve the Lyapunov equations, such that we can apply CRU to realistic reservoir models. The description of some approximation methods and their complexity analysis is given in

sections 6.4 and 6.5. An alternative approach to reduce the computational burden involves replacing the fine-scale model by a reduced-order realization of that model (see also Vakili-Ghahani et al. 2008). This approach, which is referred to as 'reduced-order CRU' is discussed in section 6.3. Finally, instead of a control-relevant upscaling on uniform coarse grid blocks, we can perform a sort of selective coarsening based on the controllability and the observability of the system. The latter is the topic of the next chapter.

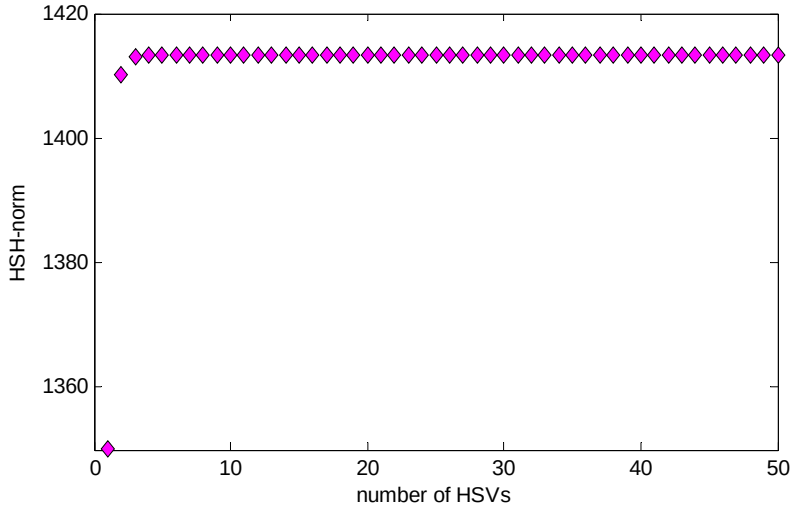

Figure 4.11 HSH-norm vs. number of Hankel singular values for the fine-scale model in example 4.1.

4.3.4. System-Theoretical Aspects

The definition of the objective function $J(\tilde{\boldsymbol{\theta}})$ in Method 1, Eq. (4.8), is theoretically correct in the sense that it is defined directly in terms of the error model, such that reduction of $J(\tilde{\boldsymbol{\theta}})$ to zero implies equality between the fine-scale and the coarse-scale models. However, the computational disadvantage of Method 1 is that the order of the error model is equal to the sum of the orders of the fine and the coarse models, which makes it less attractive for large models, although its computational efficiency can be improved, as we discussed before.

On the other hand, although CRU Method 2 is computationally more attractive, the definition of $J(\tilde{\boldsymbol{\theta}})$ by Eq. (4.13), in terms of the differences between two system norms, is theoretically less sound. That is because the equality of these norms does not necessarily imply the equivalence of the corresponding systems. However, in practice, the results of Method 2 is comparable to those of the Method 1, at least in those cases where we could compute their values (i.e., for small examples). For instance, in Example

4.1, both methods, when using the HSH-norm, give almost equal relative errors (see Table 6.1). Even the HSVs of the resulting coarse-scale-models are almost identical (see Figure 4.12).

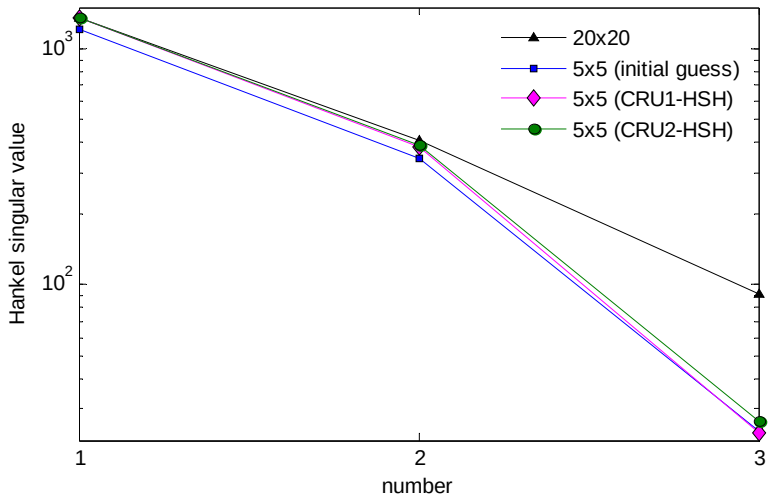

Figure 4.12 The first 3 HSVs of the fine-scale and three different coarse-scale models in example 4.1.

The good performance of CRU Method 2, despite its theoretical deficiency, may be the result of starting from a 'reasonable' guess in the form of a geometric average in combination with the requirement that the results stay within the Wiener bounds. In addition, the fixed structure of the parameter-estimation problem in the form of a banded system matrix **A** with to-be-estimated parameters and matrices **B**, **C**, and **D** with known parameters may also play an important role. Note that Method 2 in case of the direct use of the Markov parameters performs poorly for larger examples (see Vakili-Ghahani et al. 2008), most likely because of the widely ranging values of the Markov parameters and associated large numerical errors in matrix power calculations.

Finally, we used three different system norms in both CRU Method 1 and 2. Unlike the H2-norm, the HSH-norm and the H-norm are input-output invariant as they depend on the product of the Gramians (see sections 3.3 and 3.5). The H2-norm can be obtained by only computing one of the Gramians; however, it is not input-output invariant, and hence, the performance of the CRU method, when using the H2-norm, might depend on the chosen coordinates. Further research is required to understand the performance of these norms under different circumstances and to assess alternatives.

4.4. Summary

As a first step in developing grid-based upscaling techniques that take account of the amount of available control and measurements, we studied the possibility of implementing a single-phase control-relevant upscaling technique. In this method, the coarse-scale-model parameters are calculated as the solution of an optimization problem that minimizes the distance between the input/output behaviors of the fine- and coarse-scale models. This distance is measured in terms of different system norms, in which we use Hankel singular values as a measure of the combined controllability and observability and Markov parameters as a measure of the response of the system, respectively.

The CRU approach considers more realistic boundary conditions in comparison with most conventional upscaling techniques, as it considers the given well configuration. Therefore it is particularly attractive to scale up simulation models in flooding-optimization or history-matching studies for a given configuration of wells. Furthermore, it focuses on the observable and controllable state variables and, therefore, relies on those grid blocks that are most important to the input/output behavior of the model. Since these grid blocks are generally close to the well locations, the near-well effects are also better captured. We emphasize that the CRU approach is a global method in the sense that it relies on the system properties of the entire reservoir but that it does not require any forward simulation either of the full or of the upscaled model. It also does not depend on a particular control strategy but instead uses the dynamical system equations directly.

The price to pay, however, is that any change in the well configuration (including both well locations and the number of inputs and outputs) requires a (partial) repetition of the upscaling procedure. Moreover, computational issues in applying CRU to large-scale reservoir models form another limitation of this method. Nevertheless, current developments addressing the approximate solution of high-order Lyapunov equations (section 6.4) and a combination with model-order reduction techniques (section 6.3) may to a large extent solve the computational issues. Another alternative is to use a control-relevant selective coarsening approach, which is discussed in the next chapter.

5. CHAPTER: CONTROL-RELEVANT SELECTIVE COARSENING (CRSC)

In this chapter, we present a multi-level selective grid coarsening method to allow treatment of very large models with a high degree of heterogeneity in their parameter fields. In this control-relevant method, the criterion for grid size adaptation is based on the spatial quantification of the controllability and observability of the reservoir system.

5.1. Introduction

In most reservoir systems, there are only a limited number of degrees of freedom in the input-output dynamics for a given configuration of wells. This means that a large number of combinations of the state variables (pressure and saturation values) are not actually controllable and observable from the wells, and accordingly, they are not affecting the input-output behavior of the system. Thus, the complexity level of a model should be adjusted to the amount of available information and the extent of control that is possible in the reservoir system. In Chapter 4, we therefore proposed a single-phase control-relevant upscaling methodology that uniformly coarsens[19] the reservoir model based on the relevant level of information and control. However, the formulation as presented in Chapter 4 is restricted to fine-scale models with a maximum of around 10^5 grid blocks because of current limits on the computation of the underlying system norms.

In section 6.3, we will propose techniques to somewhat overcome the computational limit by combining CRU with model-order reduction techniques (see also Vakili-Ghahani et al. 2008). Here, we follow a different route and present a multi-level selective (i.e. non-uniform) grid coarsening method to allow treatment of very large models with a high degree of heterogeneity in their parameter fields. In this control-relevant selective coarsening (CRSC) method, the criterion for grid size adaptation is based on the controllability and observability properties of the reservoir system. The multi-level CRSC algorithm starts from a uniformly coarsened grid and then adaptively refines it to various degrees in the most controllable and observable parts of the reservoir. In addition to a computational advantage, the selective coarsening/refinement is also expected to be more

[19] Note that we use the terms ‘upscaling’ and ‘coarsening’ interchangeably.

accurate, in the sense that a selectively upscaled model is expected to introduce smaller upscaling errors than a uniformly upscaled model with the same number of grid blocks. The CRSC method is attractive for use in computer-assisted flooding optimization or history matching studies for a given configuration of wells, and in particular for the combined use of optimization and history matching in a closed-loop reservoir management setting.

This chapter is mainly based on Vakili-Ghahani & Jansen (2009), and Vakili-Ghahani & Jansen (2010b) and its main contribution is to present a control-relevant criterion for grid adaptation, and use it in a selective (non-uniform) coarsening/refinement approach that is applicable to arbitrarily large fine-scale models. Therefore, in the next sections, we will first explain the spatial quantification and visualization of the controllability and observability as a motivation to perform a selective coarsening. Thereafter, we will describe the CRSC algorithm and demonstrate its performance using two numerical examples. For background information on the system-theoretical concepts and notations used here, the reader is referred to Chapter 3.

5.2. Spatial quantification of controllability and observability

As discussed in Chapter 3, we can quantify the controllability and the observability of a linear reservoir system by computing the Gramians $\mathbf{W}_c$ and $\mathbf{W}_o$. The square roots of the eigen values of $\mathbf{W}_c\mathbf{W}_o$ are then equal to the Hankel singular values (HSVs) of the system (Moore 1981). Recall that the HSVs give a measure of the combined controllability and observability of the balanced states of the system. In Chapter 4 we used this analysis to develop a uniform control-relevant upscaling (CRU) method that indirectly focuses on the most controllable and observable states of the system. Here, in addition to the HSVs, we also consider the singular vectors, which are obtained by a singular value decomposition of

$$\mathbf{W}_c\mathbf{W}_o = \mathbf{U}\boldsymbol{\Sigma}^2\mathbf{V}^T, \tag{5.1}$$

where $\boldsymbol{\Sigma}$ contains the HSVs and $\mathbf{U}$ contains the corresponding singular vectors as columns. Using Eqs. (3.29), (3.30) and (3.31), we obtain

$$\mathbf{W}_c\mathbf{W}_o = \mathbf{T}^{-1}\bar{\mathbf{W}}_c\bar{\mathbf{W}}_o\mathbf{T} = \mathbf{T}^{-1}\boldsymbol{\Sigma}^2\mathbf{T}. \tag{5.2}$$

Consequently, for a balanced realization of the system, the singular vectors are equivalent to the columns of $\mathbf{T}^{-1}$, where $\mathbf{T}$ is a balancing transformation matrix that gives equal and diagonal Gramians.

As demonstrated by Example 3.1, in most reservoir cases, the magnitude of HSVs are rapidly decreasing, indicating that a large number of the states are weakly controllable/observable, hence, they weakly influence the input-output behavior of the system. Considering that, we can rewrite Eq. (5.1) as

$$\mathbf{W}_e \mathbf{W}_o = \begin{bmatrix} \mathbf{U}_1 & \mathbf{U}_2 \end{bmatrix} \begin{bmatrix} \mathbf{\Sigma}_1^2 & \mathbf{0} \\ \mathbf{0} & \mathbf{\Sigma}_2^2 \end{bmatrix} \begin{bmatrix} \mathbf{V}_1^T \\ \mathbf{V}_2^T \end{bmatrix}, \tag{5.3}$$

where $\mathbf{\Sigma}_1 = diag(\sigma_1, \sigma_2, \cdots, \sigma_r)$ contains the first *r* HSVs of the system (corresponding to the most controllable/observable states), which are significantly larger than the HSVs in $\mathbf{\Sigma}_2 = diag(\sigma_{r+1}, \sigma_{r+2}, \cdots, \sigma_n)$. Note that each column of $\mathbf{U}$ has *n* entries that are related to *n* states, which are in turns connected to *n* grid blocks. Moreover, the first *r* columns of $\mathbf{U}$, corresponding to the first *r* HSVs, are representing the most controllable/observable subspace of the state-space and, consequently, are related to those combination of the states that are most controllable/observable. Therefore, the singular vectors related to the first few HSVs of the system can be used to spatially quantify the controllability and the observability concepts (see also Zandvliet et al. 2008; Van Doren 2010). We illustrate the procedure by the following example.

5.2.1. Example 5.1

As an illustration of our approach consider a single-phase two-dimensional (2D) reservoir system, referred to as Test Case (3). Reservoir model parameters and fluid properties are given by Table 5.1, and the permeability field is shown in Figure 5.1. The permeability values vary between 5 mD and 1000 mD. There is one injector in the middle and four producers surrounding the injector, resembling an inverted five-spot pattern (see Figure 5.1). All wells are controlled by prescribed bottom-hole pressures. The time-varying bottom-hole pressure for injector 1 is shown in Figure 5.2. Note that the placement of a well in a low-permeable area is not a common practice. We did this, nevertheless, for producer 4 to illustrate the controllability/observability variation for different well placements. Moreover, due to relatively poor resolution of seismic data, in practice the exact location of the channels may be uncertain or unknown.

The fine-scale reservoir model has 16384 grid blocks, and therefore 16384 (pressure) states. Figure 5.3 displays the first 130 diagonal entries of the balanced Gramians, i.e. the Hankel singular values, for this reservoir system. The rapid decline in the magnitude of these values implies that the number of combinations required to describe the input/output behavior of the system is much smaller than 16384.

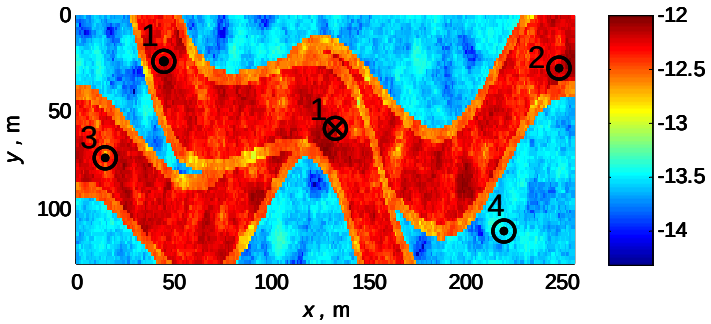

Figure 5.1 Log10 permeability field for Test Case (3), and locations of the injector (cross) and the producers (dots) in Example 5.1.

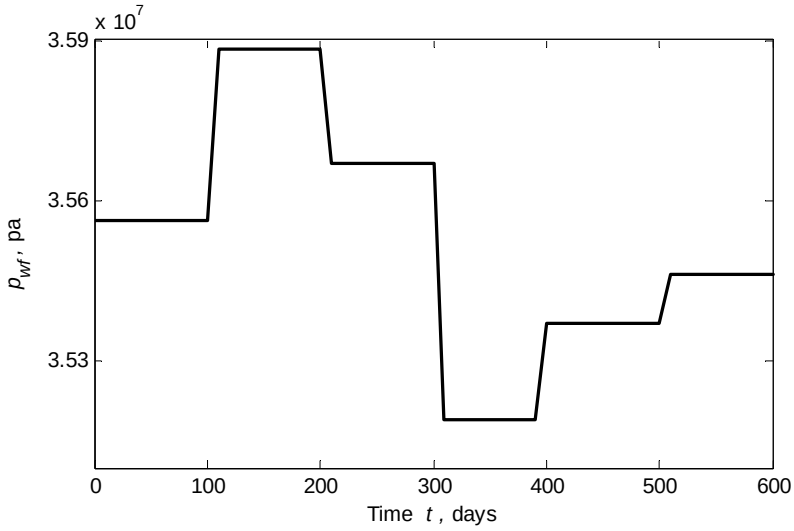

Figure 5.2 Prescribed well bottom-hole pressures in Example 5.1.

Table 5.1 Reservoir model parameters and fluid properties for Test Case (3).

parameter	value	unit
reservoir length	256	m
reservoir width	128	m
reservoir height	2	m
fluid density	1000	kg/m^3
fluid viscosity	3.0e-04	Pa s
porosity	0.3	-
total compressibility	5.8e-08	1/Pa
initial reservoir pressure	3.0e07	Pa

To visualize the controllability/observability, we consider 'directions' $\mathbf{u}_1, \mathbf{u}_2, ..., \mathbf{u}_6$, corresponding to the six largest HSVs of the system. Patterns 1 to 6 in Figure 5.4 show the directions mapped onto the computational grid. Because each component of the state represents the pressure in a grid block, this mapping allows us to quantify the variation of the controllability and observability of the system over the spatial domain in the form of 'patterns'. For a better visualization in Figure 5.4, we have sorted the grid blocks based on their importance (the magnitude of their non-zero values). Colors from red to blue, therefore, represent the 'grid importance'; i.e. the variation from strongly controllable/observable to weakly controllable/observable areas.

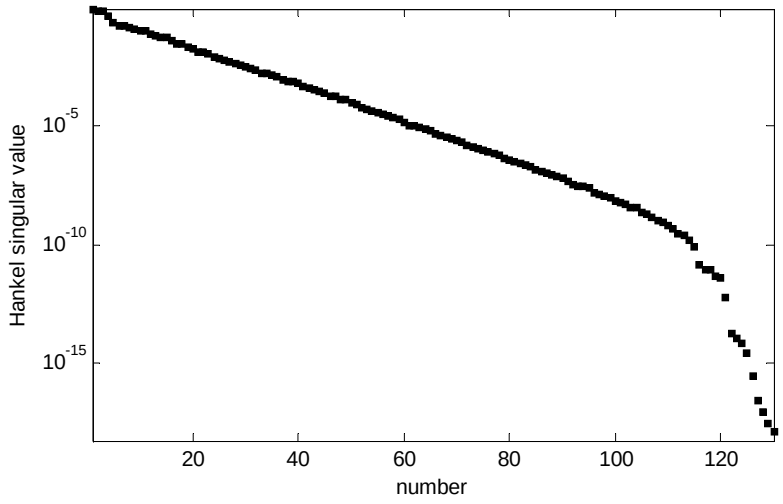

Figure 5.3 Hankel singular values for Example 5.1.

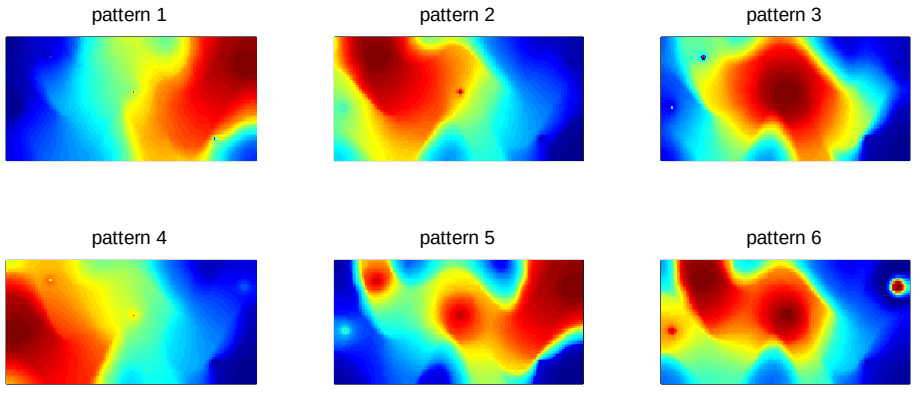

Figure 5.4 Patterns 1 to 6 represent the singular vectors corresponding to the six largest Hankel singular values of the system in Example 5.1. Colors from red to blue represent the grid importance.

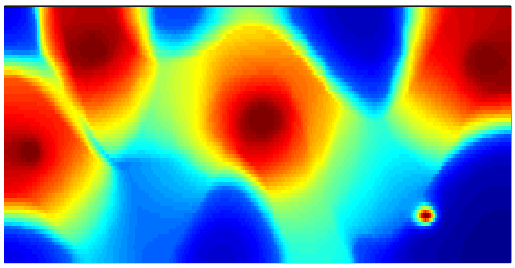

Figure 5.5 Visualization of the dominant pattern for controllability and observability variation over the spatial domain for Example 5.1; the Gramians were obtained with the LR-ADI algorithm. Colors from red to blue represent the grid importance obtained from the scaled weighted sum of the singular vectors corresponding to the first sixty Hankel singular values of the system.

The significance of each mapped pattern is proportional to the magnitude of the related Hankel singular value. The vector sum of all patterns, each weighted with its corresponding singular value, therefore gives the 'dominant' pattern that represents the spatial variation of the combined controllability and observability of the system. However, because of the rapid decay of the singular values, only a few patterns related to $\mathbf{\Sigma}_1$ in Eq. (5.3) need to be taken into account to accurately capture this combined controllability and observability. Accordingly, the dominant pattern is given by

$$\bar{\mathbf{u}} = \sum_{i=1}^{r} \frac{\sigma_i}{\sigma_1} \mathbf{u}_i . \tag{5.4}$$

Here, we use the weighted sum of the first 60 patterns. However, according to Figure 5.3, we could have chosen an even smaller number of patterns. Figure 5.5 presents the resulting dominant pattern. Recall that colors from red to blue represent the grid importance obtained by sorting all grid blocks based on the magnitude of their non-zero values. From this figure and for the given example, the most controllable and observable regions are in the vicinity of the wells and in high-permeable areas connected and close to the wells. The blue areas in Figure 5.5 are weakly controllable/observable. Note that the area in the vicinity of producer 4 is less controllable/observable, compared to other producers, because it is located in a low-permeable part of the reservoir.

The spatial quantification of the observability and controllability of a reservoir model forms the basis for our CRSC algorithm. The basic idea is to perform grid coarsening only in the weakly controllable and observable areas, i.e. in those areas that have the least effect on the input/output behavior of the system.

5.3. CRSC algorithm

The general idea behind selective (non-uniform) coarsening is to only coarsen those parts of the spatial domain that are the least important for the flow simulation according to some predefined criterion. In our CRCS application, we use a control-relevant criterion based on the quantification of the controllability and observability subspaces over the spatial domain. Other selective gridding methods have been proposed, sometimes with an adaptive, i.e. time-dependent, strategy for selective refinement and coarsening based on different criteria. In particular, adaptive gridding is often applied to maintain a fine grid in areas of high permeability or in areas where high saturation or concentration gradients occur; see e.g. Berger & Colella (1989), or Gerritsen & Lambers (2008) and references therein.

5.3.1. Algorithm

The CRSC algorithm includes three main steps:

1. Obtain a uniform coarse-scale model with a method of choice.
2. Spatially quantify the combined controllability and observability of the system using either fine- or coarse-scale Gramians.
3. Selectively refine the domain depending on the level of combined controllability and observability.

A schematic overview of the procedure is depicted in Figure 5.6. In the following, we will explain the algorithm in more detail:

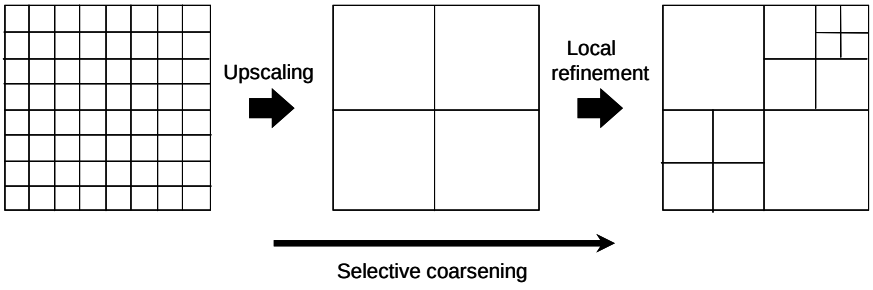

Figure 5.6 Control-relevant multi-scale gridding through uniform initial coarsening and subsequent selective refinement.

Step (1)

We choose an upscaling technique to generate a coarse-scale model. A fast and simple upscaling method is a so called local upscaling technique (see subsection 2.3.3), in which coarse-scale parameters are calculated from local flow calculations subject to some generic boundary conditions (Warren & Price 1961). An alternative technique is a local-global approach, in which the generic boundary conditions are only used to obtain an initial coarse-scale flow solution. The interpolation of the coarse-scale solution then gives more accurate local boundary conditions to find the new coarse-scale parameters and the process is iterated until the solution converges (Chen et al. 2003, Gerritsen & Lambers 2008). The accuracy of the coarse-scale approximation at this step is of limited importance, as long as it can be used to conduct the controllability and observability analysis in the next step.

Step (2)

To spatially quantify the most controllable/observable patterns, we first need to compute the balanced Gramians of the system by solving Lyapunov equations (Eqs. 3.25 and 3.26). A brief overview of different methods to compute the exact and approximate solution of these equations is given in section 6.4. The diagonal entries of the balanced Gramians (HSVs) and the corresponding direction are then used to quantify the variation of the system's controllability and observability properties over the spatial domain (see Figure 5.5). Finally, the coarse-scale grid blocks that are located in the areas corresponding to highly controllable/observable states (red areas in Figure 5.5), are flagged to be refined in the next step. A grid block is flagged if the following condition holds:

$$\frac{\overline{u}_i}{\|\overline{\mathbf{u}}\|} > \varepsilon, \tag{5.5}$$

where ε is a threshold value. A zero threshold value means that all the grid blocks should be flagged and the corresponding coarse-scale grid blocks need to be refined, while a unit threshold value means no refinement. From our experience and for the following examples, we found out that setting a threshold value of about 0.005 produced accurate coarse-scale results, while significantly reducing the number of grid blocks. However, the optimal choice of the threshold value is still an open question.

An alternative and faster approach to spatially quantify the controllability/observability is to use the coarse-scale Gramians from the approximated coarse-scale model of Step 1. However, Steps 2 and 3 may need to be iterated a few times to obtain a more accurate approximation of the controllable/observable subspaces. The use of the coarse-scale

model in this way is somehow similar to the adaptive local-global approach of Chen & Durlofsky (2006), in which they use a coarse-scale simulation to find areas for which the initial local upscaling with generic boundary conditions needs to be repeated with specific boundary conditions related to a particular flow scenario.

Step (3)

The last step is to refine the flagged coarse-scale grid blocks to finer ones, or even back to the initial fine-scale grid blocks. The result is a system of non-uniform grid blocks as depicted in Figure 5.7. To discretize partial differential flow equations over non-matching grid blocks, we choose a cell-centered finite volume technique. The interface fluxes for each control volume are calculated by using a two-point flux approximation method (Edwards 1996, Aavatsmark 2002). For instance, the flux between grid blocks 2 and 1 in Figure 5.7 is given by

$$q_2 = -\left(\frac{1}{\mu}\frac{2k_2k_1}{\Delta x_2 k_1 + \Delta x_1 k_2}\Delta y_2\right)(p_2 - p_{a2}), \tag{5.6}$$

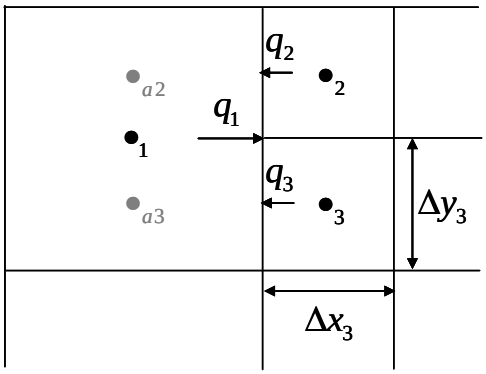

Figure 5.7 Non-uniform grid blocks.

where k_1 and k_2 are the permeability values of grid blocks 1 and 2, p_2 and p_{a2} are pressure values at points 2 and $a2$, μ is the fluid viscosity, and Δx and Δy are the grid block dimensions. An issue here is to calculate the pressure values at the auxiliary points like $a2$ and $a3$. Although there are various ways to do so, for simplicity we assume that they are equal to the average pressure for the entire grid block. However, to maintain the accuracy around the interface, we require that each grid block may only be refined once in each direction, i.e. at each refinement level, a grid block may contain up to four sub grid blocks. More accurate pressure calculations at the auxiliary points can be found in e.g. Gerritsen & Lambers (2008), Khattri et al. (2007), Nilsson et al. (2005), and Edwards (1996). Spatial and temporal discretization of the flow equation over the non-uniform

grid blocks leads to a system of equations that can be written in the state-space form given by Eqs. 3.14.

5.4. Results and discussion

We demonstrate the performance of CRSC with the aid of two numerical test cases. The first one concerns a channelized reservoir with relatively small permeability fluctuations, while the second one concerns a strongly channelized system. In both cases, we assume single-phase flow subject to no-flow boundary conditions. The liquid flow into and out of the reservoir is therefore through the wells. We consider a fixed configuration of the wells which are controlled by a prescribed variable bottom-hole pressure, while production and injection rates are recorded as the output of the system. The bottom-hole pressure is related to the grid block pressure by using a well index which is a function of the grid block geometry and permeability (Peaceman 1983). Like in the CRU algorithm, we use the relative error (Eq. 4.14) in terms of the averaged pressures and the cumulative production rates to compare the performance of the non-uniform coarse model obtained by the CRSC algorithm with those of the original fine-scale model and the uniformly coarsened model. Furthermore, we use the '*n*-ratio' defined by Eq. 4.17, to compare the size, and roughly the computational time that is needed to simulate a coarse-scale reservoir model, to that of the fine-scale one.

5.4.1. Example 5.2

In this example we consider the reservoir system of Test Case (3) with the production scenario described in Example 5.1. The permeability field and well locations are depicted in Figure 5.1. We chose factors of 8 in each direction to scale up the 256×64 fine-scale model to a uniform 32×8 coarse model by using a local upscaling technique. The grid refinement for this example was then based on the quantification of the state's controllability and observability over the spatial domain of the fine-scale model (FS-CRSC), as illustrated in Figure 5.5. The level of refinement for each flagged coarse grid depends on its 'importance' compared to other grid blocks. Thus, in red grid blocks that correspond to the most controllable/observable areas, we perform three levels of refinement to return to the original fine-scale model. Figure 5.8 shows the selectively coarsened grid obtained by the CRSC algorithm. Clearly the refinement around producer 4 is less than around the other wells because this producer is located in a low-permeable part of the reservoir and it has less effect on the input-output behavior of the system.

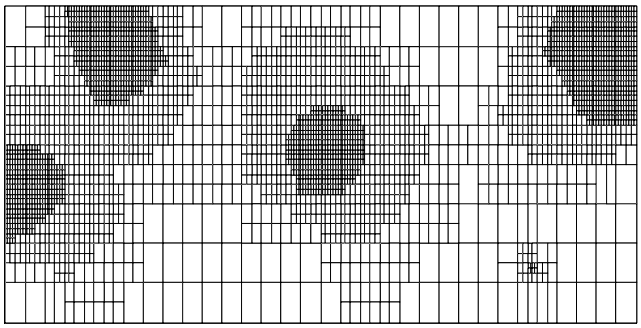

Figure 5.8 Selectively coarsened grid in Example 5.2. The refinement is based on the spatial quantification of the controllability/observability of the fine-scale model.

Table 5.2 CRSC performance for Example 5.2 using fine-scale Gramians.

	fine-scale	coarse (32×8)	FC-CRSC	coarse (128×32)
e_p (%)	0	0.6	0.1	0.4
$e_{q,cum}$ (%)	0	28.9	0.6	13.8
n-ratio	1	0.02	0.23	0.25

Table 5.2 represents the relative error and *n*-ratio for the simulation of Test Case (1) with different models. Although the uniform coarse model (32×8) gives a very fast simulation with an *n*-ratio of 0.02, the CRSC algorithm vastly outperforms the uniformly coarsened grid in terms of accuracy. More interestingly, the CRSC model with 3794 grid blocks even gives a much smaller error than the uniform coarse model (128×32) with 4096 cells. This illustrates that, for this example, in addition to a computational advantage, the selective coarsening is also more accurate than a uniformly upscaled model with the same number of grid blocks.

We can also use the Gramians of the initial coarse-scale model for spatial quantification of the controllability/observability, and thus for flagging the most controllable and observable parts of the reservoir. We set the threshold value such that the resulting *n*-ratio is comparable to that of the CRSC-FS model using the fine-scale Gramians. Table 5.3 gives the results after two iterations. Surprisingly, we observe that, for this example, the errors are comparable to the result of FS-CRSC (even without any iteration), while the computational time that is needed to compute the CRSC grid is decreased from 115 seconds for the FS-CRSC to 48 seconds for CS-CRSC with one iteration, and to 10 seconds for CS-CRSC without any iteration. Note that there is no change in the results after two iterations.

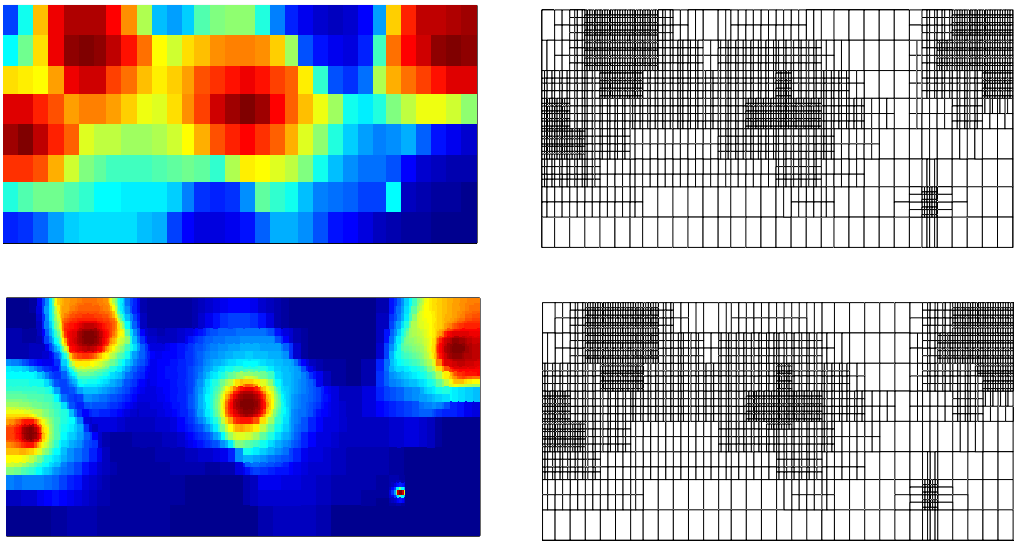

Figure 5.9 Dominant patterns (left) and selectively coarsened grid (right) in Example 5.2, using coarse-scale Gramians. The first row: iteration 0; the second row: iteration 1.

Table 5.3 CRSC performance for Example 5.2 using coarse-scale Gramians.

	CRSC-CS		
iteration	0	1	2
e_p (%)	0.16	0.16	0.16
$e_{q,cum}$ (%)	0.81	0.80	0.80
Number of grid blocks	3794	3824	3824
gridding time (s)	10	48	81

Nevertheless, the spatial quantification of the controllability/observability using fine-and coarse-scale Gramians and, consequently, the resulting CRSC grids are slightly different. This is evident from Figure 5.9, in which we show the dominant patterns (left) and the corresponding CS-CRSC grids (right). The spatial visualization of the controllability/observability in Figure 5.9 is different from the one in Figure 5.5, indicating that the spatial quantification of the controllable/observable subspaces based on the coarse-scale model is less accurate.

Finally, we compare the HSV plots of all uniform and non-uniform coarse models of Example 5.2 in Figure 5.10. As expected, the HSV plots of the CRSC models are much closer to the HSV plot of the fine-scale model. This illustrates again that the selective

coarsening is more accurate than a uniformly upscaled model with a similar number of grid blocks.

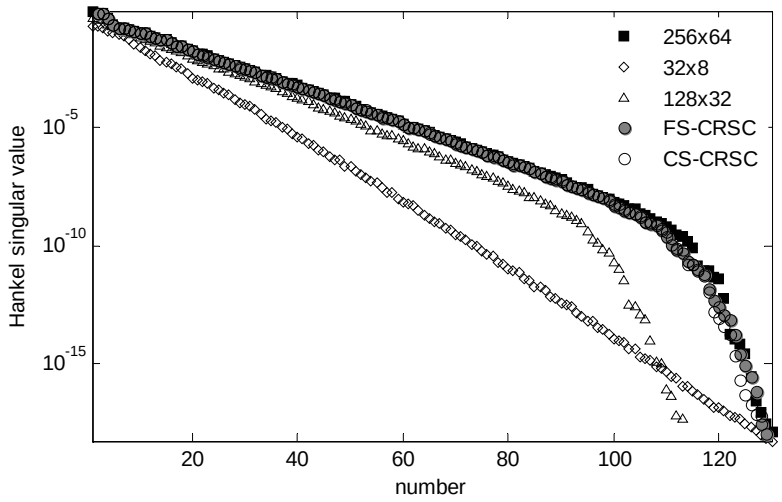

Figure 5.10 HSV plots for the fine-scale, uniform coarse-scale, and CRSC models in Example 5.2.

5.4.2. Example 5.3

As the second example, we consider again the reservoir system of Test Case (2) in Chapter 4 with reservoir model parameters given in Table 4.2. The permeability field is taken from layer 44 of the SPE10 comparative solution project (Christie & Blunt 2001), which represents a channelized reservoir with permeability values between 0.0001 mD and 17000 mD. The fine-scale reservoir model has 220×60 grid blocks with one injection and two production wells controlled by prescribed bottom-hole pressures. The permeability field and the well locations are depicted in Figure 5.11. Figure 5.12 illustrates the dominant pattern obtained from the weighted sum of the Hankel singular vectors corresponding to the first 60 HSVs of the system. Recall that the red grid blocks are the most relevant ones in terms of input/output behavior. We observe again that the highly controllable/observable states correspond to the grid blocks in the vicinity of the wells and of adjacent connected high-permeable zones. Interestingly, the high permeable areas in the upper left and lower right corners, which are either disconnected or far away from the wells, are weakly controllable/observable.

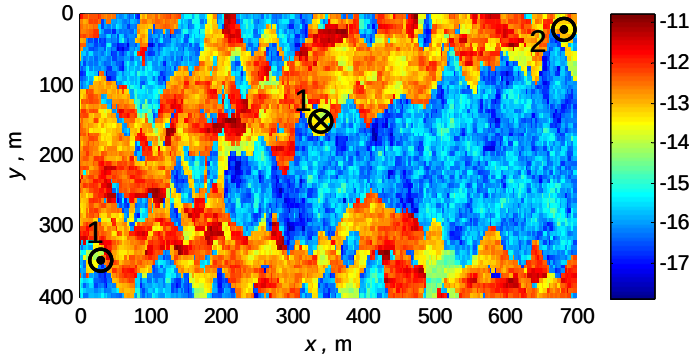

Figure 5.11 Log10 permeability field from Test Case (2), SPE10 layer 44, and locations of the injector (cross) and the producers (dot) in Example 5.3.

We scaled up the fine-scale model to a 15×55 coarse model using a local upscaling technique. Subsequent refinement of the grid blocks corresponding to the most controllable/observable parts of Figure 5.12 lead to a pattern of selectively coarsened grid blocks shown in Figure 5.13. The original fine-scale grid, the uniformly coarsened grids (15×55) and (30×110), and the CRSC grids were used to simulate the flow behavior in the reservoir. Table 6.1 gives the simulation results for different models in terms of cumulative production error and *n*-ratio. As in Example 5.2, it turns out that the CRSC method appropriately reproduces the fine-scale results, and clearly outperforms both uniformly coarsened models obtained with a local upscaling technique. Note that in highly channelized cases local techniques are well known not to resolve the permeability connectivities between different coarse blocks and, therefore, to result in large upscaling errors.

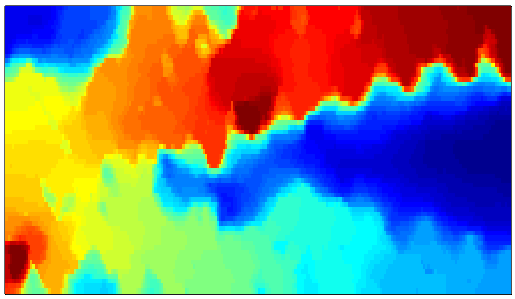

Figure 5.12 Visualization of the dominant pattern for controllability and observability variation over the spatial domain in Example 5.3. Colors from red to blue represent the grid importance obtained from the scaled weighted sum of the singular vectors corresponding to the Hankel singular values of the system.

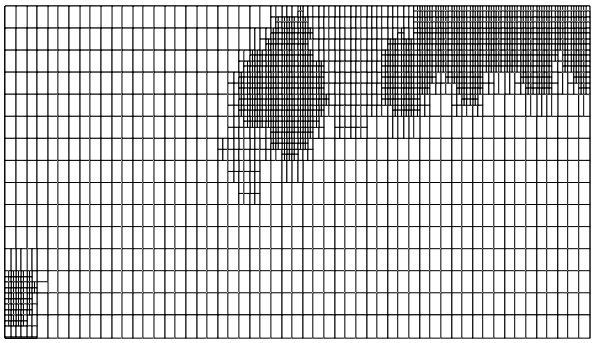

Figure 5.13 Selectively coarsened grid in Example 5.3.

Table 5.4 CRSC performance for Example 5.3.

	fine-scale	coarse (15×55)	CRSC	coarse (30×10)
e_p (%)	0	2.2	0.3	0.8
$e_{q,cum}$ (%)	0	76.2	0.4	39.6
n-ratio	1	0.06	0.20	0.25

5.4.3. Computational aspects

Similar to the CRU method, the most expensive operation in CRSC algorithm is to compute the Gramians of the system. Therefore, standard methods for calculating the exact full-rank Gramians in Matlab, which are intended for small systems (with less than 10^4 grid cells) have to be replaced by approximation techniques for large systems. The description of several approximation methods and their complexity analysis is given in sections 6.4 and 6.5. Alternatively, using the coarse model to compute the Gramians allows the application of the CRU algorithm to very large systems, although the spatial quantification of the controllable/observable subspaces is then less accurate (see Example 5.2).

To have a computationally more efficient multi-level refinement procedure and similar to Gerritsen & Lambers (2008), we applied an unstructured data approach to store the grid block and interface data. In this method, each grid block requires the storage of its geometrical and physical data, interface information and neighbor's indices. This allows a fast and easy accessibility to grid block data, regardless its level of coarsening. A detailed description of the unstructured data approach can be found in Ham et al. (2002).

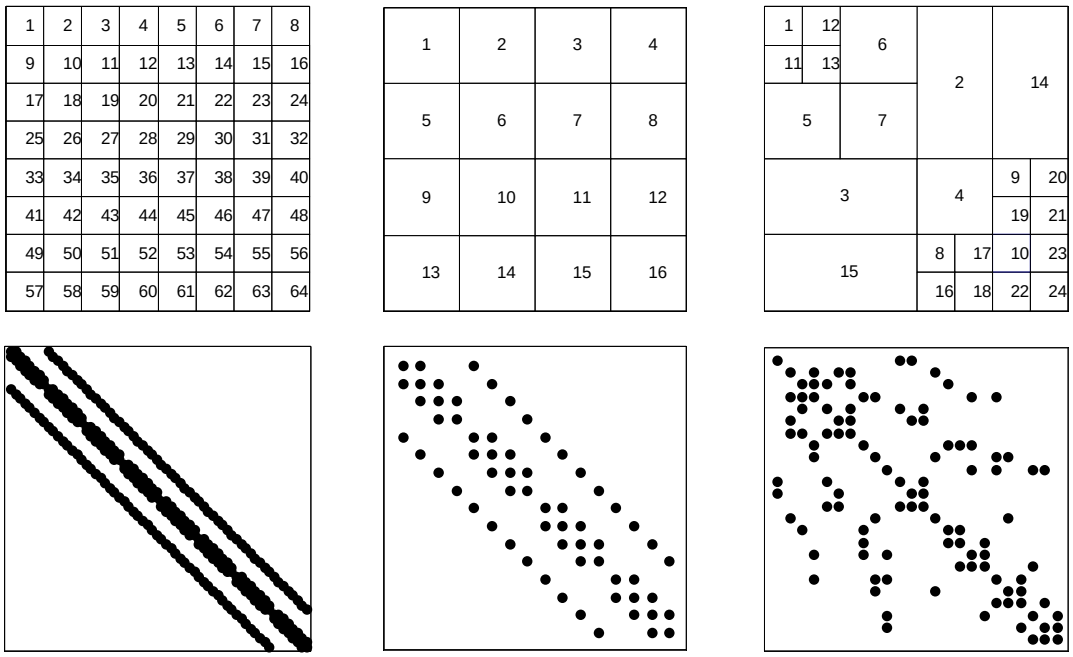

Figure 5.14 Uniform and non-uniform grid systems (first row) 'spy plots' of the corresponding system matrices (second row).

Furthermore, we used the *n*-ratio to compare the relative size and, consequently, the required computational time for solving a linear system of pressure equations in different models. However, computing the pressure solution over the CRSC grid is more expensive than over a uniform coarse grid with the same number of grid blocks. This is because the bandwidth[20] of a CRSC system matrix is larger compared to the one for a uniform grid (see Figure 5.14). This bandwidth can be optimized by an appropriate renumbering of the grid blocks as well as reordering the elements of the system matrix to produce a matrix with a significantly smaller bandwidth. For instance, reordering the elements of the system matrix **A** using the reverse Cuthill-McKee (RCM) ordering in Matlab gives a much narrower bandwidth, as the right spy plot in Figure 5.15 shows. Such a reordering can often make some operations like LU decomposition, which is used in the linear solver, sparser and faster. Note that the cost of the bandwidth optimizer is negligible, compared to the total CPU time of the solver and , therefore, the *n*-ratio can still roughly represent the relative CPU time spent to solve the pressure equations of the CRSC model.

[20] The bandwidth of a matrix is computed as the maximum bandwidth of each row of the matrix. The bandwidth of a row of the matrix is the number of matrix entries between the first and last nonzero entries in the row.

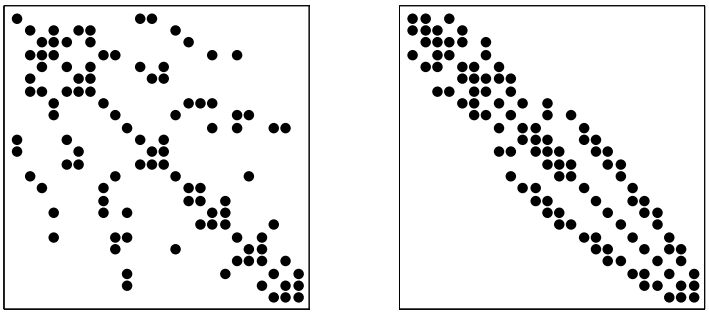

Figure 5.15 Spy plot of a system matrix before (left) and after (right) the bandwidth optimization by RCM.

In summary, for large systems, the CRSC grid can be efficiently obtained by using approximation methods to compute the Gramians, applying a proper grid block numbering, optimizing the bandwidth of the system matrix, and using the unstructured data approach to optimize the grid data storing and loading during the simulation. Note that the CRSC grid blocks need to be obtained only once and in an offline part of the simulation, whereas simulation of the flow equation over the CRSC grid blocks might be performed many times in different applications.

5.4.4. Remarks

- For the sake of simplicity, we used simple gridding and discretization techniques, and we implemented them in MATLAB. Alternative gridding and discretization strategies might further improve the CRSC performance in terms of both accuracy and computational efficiency.
- The CRSC method can conceptually simply be extended to 3D applications.
- In this Chapter, we developed a single-phase upscaling technique (CRSC method), which is based on single-phase flow equations. Nevertheless, the resulting CRSC grids are expected to outperform the uniform coarse grids even in two-phase flow applications. Furthermore, the CRSC algorithm can also be extended to two-phase flow simulations. However, for nonlinear two-phase flow cases, we need to either linearize the system, or compute the controllability and observability Gramians empirically (for the empirical calculations of the Gramians see subsection 6.4.3). The other important issue in two-phase flow is to deal with moving saturation fronts. Since the saturations are only controllable along the front and only observable after water breakthrough in the wells (Van Doren 2010), the performance of CRSC algorithm would be improved by adding grid adaptations to resolve the strongly controllable/observable areas along the moving saturation

fronts. Further research is required to evaluate the computational benefits of the CRSC approach in multi-phase flow applications.

- Other possible solution to treat saturations in a two-phase flow simulation might be applying a multi-scale framework, in which the CRSC grid blocks are only used to solve the pressure equation while the saturation equation is solved over the fine-scale grid blocks.

5.5. Summary

We proposed a multi-level CRSC method to allow treatment of very large models with a high degree of heterogeneity in their parameter fields. In this control-relevant selective coarsening method, the criterion for grid size adaptation is based on the spatial quantification of the controllability and observability properties of the reservoir system and, hence, the level of refinement for each coarse grid block depends on its 'importance' compared to other grid blocks. We applied our algorithm to two numerical examples and found that it can accurately reproduce results from the corresponding fine-scale simulations, while significantly speeding up the simulation. In addition to a computational advantage, the selective coarsening/refinement is also more accurate, compared to a uniformly upscaled model with the same number of grid blocks. That is the case because the most controllable/observable areas, which appear to be in the vicinity of the wells and in high-permeable areas close to and connected to the wells, remain unchanged and, therefore, global flow patterns and permeability contrasts of the fine-scale model are better preserved by the CRSC algorithm.

Similar to the CRU approach, the CRSC technique considers the global flow effects by relying on the system properties of the entire reservoir but it does not depend on a particular control strategy. However, it should be (partially) repeated if the well configuration is changed.

6. CHAPTER: REDUCED-ORDER CONTROL-RELEVANT UPSCALING

In this chapter, we explain several system-theoretical reduction techniques followed by investigating the potential benefits of using them in combination with our control-relevant upscaling approach. Thereafter, several approximation methods to compute the Gramians are discussed and a brief complexity analysis of different operations is presented.

6.1. Introduction

The main concern about CRU and CRSC algorithms is their applicability, in terms of required computational power, to more realistic and large reservoir systems. The most expensive phase of numerical calculations associated with both methods is the computation of the Gramians which requires the solution of (large) Lyapunov equations (Eqs. 3.25 and 3.26). On the other hand, the standard exact methods in Matlab (e.g., Bartels-Stewart algorithm) are intended for small systems (with an order of 10^4 cells), and they are computationally too expensive or even intractable for larger systems. Therefore, the main focus of this chapter is to investigate possible approaches to improve the computational efficiency of CRU and CRSC methods.

The first attempt is made by performing our control-relevant upscaling method on a low-dimensional approximation of the original fine-scale system obtained by a system-theoretical model reduction technique, so that lower-order Lyapunov equations are to be solved. The second approach is to use computationally efficient algorithms to solve large Lyapunov equations. Alternatively, a fast approximation of the Gramians can be obtained from sufficient snapshots of the simulation data in time. The latter is mainly based on the same principles that are used in common model reduction techniques. In the following sections, first, we present a short description of several model reduction techniques and then explain both above-mentioned approaches. Moreover, we investigate the possibility of using the spatial quantification of the controllability and observability of the system in developing a missing point estimation approach for model reduction. At the end, we discuss the computational complexity of different operations that are needed to perform the CRU and CRSC upscaling.

6.2. Model reduction

System-theoretical model reduction provides a systematic tool to reduce the complexity of large-scale models. Consider a linear reservoir model with a state-space representation given by Eq. (3.14) and (3.15). To derive a reduced-order model of the system, we project[21] the state vector onto a subspace defined by bi-orthogonal projection matrices (bases) $\mathcal{V}$ and $\mathcal{W}$, so that $\mathcal{W}^T\mathcal{V} = \mathbf{I}$ and $\mathbf{x} = \mathcal{V}\hat{\mathbf{x}}$. We can partition the transformed state as

$$\hat{\mathbf{x}} = \begin{bmatrix} \hat{\mathbf{x}}_r \\ \hat{\mathbf{x}}_2 \end{bmatrix}, \tag{6.1}$$

where $r<<n$ and the states in $\hat{\mathbf{x}}_r$ are corresponding to r columns of $\mathcal{V}$ that represent the dominant basis vectors (functions). The basis functions are chosen appropriately, such that the system dynamics are captured accurately by the resulting reduced-order model. The states in vector $\hat{\mathbf{x}}_2$ are considered 'unimportant', and explicitly set to zero. Therefore we can write

$$\mathbf{x} = \mathcal{V}\hat{\mathbf{x}} \approx \mathcal{V}_r\hat{\mathbf{x}}_r. \tag{6.2}$$

In most model reduction techniques, we proceed with some variation of a Petrov-Galerkin projection [22] to construct the reduced-order model. The r^{th}-order low-dimensional approximation of the original n^{th}-order model is then written as

$$\dot{\hat{\mathbf{x}}}_{r,k+1} = \hat{\mathbf{A}}_r\hat{\mathbf{x}}_{r,k} + \hat{\mathbf{B}}_r\mathbf{u}_k, \tag{6.3}$$

$$\mathbf{y}_{r,k} = \hat{\mathbf{C}}_r\mathbf{x}_{r,k} + \mathbf{D}\mathbf{u}_k, \tag{6.4}$$

where $\hat{\mathbf{A}}_r = \mathcal{W}_r^T\mathbf{A}\mathcal{V}_r$, $\hat{\mathbf{B}}_r = \mathcal{W}_r^T\mathbf{B}$, and $\hat{\mathbf{C}}_r = \mathbf{C}\mathcal{V}_r$. The performance of the reduced system depends on the choices of $\mathcal{V}_r$ and $\mathcal{W}_r$. In the following, we will discuss balanced truncation (BT), proper orthogonal decomposition (POD), and balanced POD (BPOD) approaches to obtain the bases.

Note that the material presented in this section is based on well-established system-theoretical reduction techniques developed and applied in different disciplines such as electrical circuit analysis, mechanical system design, weather forecasting and

[21] There is another category of model reduction methods that involves no projections. Examples of those methods are Hankel optimal model reduction (Glover 1984) and singular perturbation approximation (Liu & Anderson 1989).

[22] If $\mathcal{W} = \mathcal{V}$ the projection is orthogonal and it is called a Galerkin projection, otherwise it is an oblique (Petrov-Galerkin) projection.

oceanography. The most widely used reduction methods are BT, moment matching (Krylov methods), POD, BPOD, and trajectory-based piecewise linear (TPWL) approximation, where the last three can be also used for nonlinear models. For a general overview of different methods see Antoulas (2005) and references therein. For recent applications of model reduction techniques to reservoir modeling see Markovinović et al. (2002), Heijn et al. (2004), Gildin et al. (2006), Cardoso et al. (2009), Cardoso & Durlofsky (2010a, 2010b) and Markovinović (2009).

6.2.1. Balanced truncation (BT)

The concept of BT, introduced by Moore (1981), is closely related to the definition of balanced realization described in section 3.3 (see also Glover 1984). The idea is to use the combined knowledge of both inputs and outputs to determine the state variables that can be truncated in a reduced-order representation of the system. In a balanced realization, these states are related to the least controllable/observable subspaces described by the singular vectors corresponding to small HSVs of the system. Therefore, we can define the projection subspaces as the dominant eigen spaces of the product of controllability and observability Gramians. The balanced realization[23], as proposed by Laub et al. (1987), can be obtained by Cholesky factorizations of the Gramians, i.e., $\mathbf{W}_c = \mathbf{L}_c\mathbf{L}_c^T$ and $\mathbf{W}_o = \mathbf{L}_o\mathbf{L}_o^T$, followed by a singular value decomposition of

$$\mathbf{L}_o^T\mathbf{L}_c = \mathbf{U}\boldsymbol{\Sigma}\mathbf{V}^T = \begin{bmatrix}\mathbf{U}_1 & \mathbf{U}_2\end{bmatrix}\begin{bmatrix}\boldsymbol{\Sigma}_1 & \mathbf{0} \\ \mathbf{0} & \boldsymbol{\Sigma}_2\end{bmatrix}\begin{bmatrix}\mathbf{V}_1^T \\ \mathbf{V}_2^T\end{bmatrix}, \tag{6.5}$$

after which the balancing transformation matrices are defined as $\mathbf{T} = \mathbf{L}_c\mathbf{V}\boldsymbol{\Sigma}^{-1/2}$ and $\mathbf{T}^{-1} = \boldsymbol{\Sigma}^{-1/2}\mathbf{U}^T\mathbf{L}_o^T$. The partition $\boldsymbol{\Sigma}_1$ contains the r largest HSVs of the system corresponding to the most controllable/observable combinations of states, i.e. the combinations that have the largest contribution to the input-output behavior of the system. Therefore, for the BT procedure, we choose $\mathcal{V}_r = \mathbf{L}_c\mathbf{V}_1\boldsymbol{\Sigma}_1^{-1/2}$ and $\mathcal{W}_r^T = \boldsymbol{\Sigma}_1^{-1/2}\mathbf{U}_1^T\mathbf{L}_o^T$. The HSVs corresponding to the truncated states give an a-priori error bound on the output (Enns 1984), written as

$$\left\|\mathbf{y} - \mathbf{y}_r\right\| \le 2\sum_{i=r+1}^{n}\sigma_i\left\|\mathbf{u}\right\|. \tag{6.6}$$

[23] Contrary to the balancing procedure described in section 3.3, this approach uses the Cholesky factors of the Gramians which can be directly computed, i.e., without explicitly forming the Gramian matrices.

This makes the BT approach a rigorous reduction technique, for which the accuracy is guaranteed. However, the computation of the Gramians for large systems such as reservoir models is often impractical.

6.2.2. Proper orthogonal decomposition (POD)

A model reduction method based on POD[24] uses the spatial correlation in the states (pressures and saturations) to compute a limited number of spatial patterns (directions) in the state-space coordinates, which can be used to characterize the dominant dynamical variations of the system. These dominant patterns are obtained by selecting the leading eigen vectors of the covariance matrix obtained from several fine-scale simulation data. The covariance matrix is defined as

$$\bar{\bar{\mathbf{X}}} = \bar{\mathbf{X}}\bar{\mathbf{X}}^{\mathrm{T}}, \tag{6.7}$$

where $\bar{\mathbf{X}} = [\mathbf{x}_1 - \bar{\mathbf{x}} \quad \mathbf{x}_2 - \bar{\mathbf{x}} \quad \ldots \quad \mathbf{x}_N - \bar{\mathbf{x}}]$ is a shifted snapshot matrix containing N shifted snapshots of the fine-scale solution at different points in time for a particular set of wells and boundary conditions, with $\bar{\mathbf{x}} = (1/N)\sum_{i=1}^{N}\mathbf{x}_i$ representing the average state. Often a simplification is introduced by operating directly on the snapshot matrix $\mathbf{X} = [\mathbf{x}_1 \quad \mathbf{x}_2 \quad \ldots \quad \mathbf{x}_N]$, i.e. without shifting the snapshots. Sirovich (1987) proposed the 'method of snapshots' that avoid the explicit calculation of the correlation matrix. In this method, we compute a singular value decomposition of $\mathbf{X} = \mathbf{U}\boldsymbol{\Sigma}\mathbf{V}^{\mathrm{T}}$, Where $\mathbf{U}$ and $\mathbf{V}$ are orthogonal matrices, and $\boldsymbol{\Sigma}$ is a diagonal matrix containing the singular values of the snapshot matrix[25]. In most applications, these singular values decay rapidly and only r of them are significant ($r << n$). The reduced bases are then chosen as

$$\mathscr{V}_r = \mathscr{U}_r = \boldsymbol{\Phi}_r, \tag{6.8}$$

where $\boldsymbol{\Phi}_r$ contains the leading r left singular vectors in matrix $\mathbf{U}$. Note that $\boldsymbol{\Phi}_r{}^T\boldsymbol{\Phi}_r = \mathbf{I}$. We choose r POD basis functions based on the definition of a relative 'energy level' that is present in the snapshots, given by

$$\left(\sum_{i=1}^{r}\sigma_i^2 \Big/ \sum_{i=1}^{N}\sigma_i^2\right) \le \alpha, \tag{6.9}$$

[24] Depending on the area of application, POD is also known as Karhunen-Loeve (K-L) and Principal Component Analysis (PCA).

[25] The columns of $\mathbf{U}$ are also the eigenvectors of the data covariance matrix $\mathbf{X}\mathbf{X}^{\mathrm{T}}$, and the diagonal $\boldsymbol{\Sigma}$ contains the square-roots of the corresponding eigen values.

where σ_i represent the POD singular values and α is a fraction of 'energy' that we need to retain. The bases $\mathcal{V}_r$ and $\mathcal{W}_r$ can be substituted in Eqs. (6.3) and (6.4) to construct the reduced-order model.

POD can be used to obtain efficient projection matrices for large systems resulting in a reduction level of the several orders of magnitude. However, unlike the BT, it has no quality guaranties and the range of validity of the resulting low-order model is restricted to the region of the state-space, where the data have been collected. For a more detailed description of the POD method see e.g. Antoulas (2005).

6.2.3. Balanced POD (BPOD)

BPOD is based on the idea of combining BT and POD to perform an approximate balanced truncation, in which the Gramians are approximated by the method of snapshots. Therefore, the method is tractable for very large systems (Willcox & Peraire 2002; Rowely 2005). As is shown in Lall et al. (1999, 2002) for the time domain and in Willcox & Peraire (2002) for the frequency domain, the POD modes of the impulse response of the system are equivalent to the dominant eigen vectors of the controllability Gramian and, accordingly,

$$\mathbf{W}_c \approx \mathbf{X}\mathbf{X}^T, \tag{6.10}$$

If the snapshots are generated with inputs other than impulses, as is often the case in our application, Eq. (6.10) gives an approximation to the controllability Gramian over the chosen region of state-space, where the data have been collected (Willcox & Peraire 2002; Bui-Thanh & Willcox 2005). Note that in a multiple-input case, the snapshots are obtained for each input in turn and they are all stacked in one snapshot matrix[26]. Similarly, the observability Gramian[27] can be approximated by

$$\mathbf{W}_o \approx \mathbf{Z}\mathbf{Z}^T, \tag{6.11}$$

where $\mathbf{Z}$ is the snapshot matrix of an adjoint (dual) system which for a continuous-time linear system, is defined as

$$\dot{\mathbf{z}} = \mathbf{A}_c^T\mathbf{z} + \mathbf{C}_c^T\mathbf{u}_a, \tag{6.12}$$

[26] In case of a large number of inputs (outputs), we can also compute a POD input (output) projection basis and apply the BPOD technique to the resulting system with reduced number of inputs (outputs) (see Bui-Thanh & Willcox 2005; Rowley 2005).

[27] The observability Gramian of a system is equivalent to the controllability Gramian of its adjoint (dual) system (see e.g. Antoulas 2005).

where $\mathbf{A}_c$ is the continuous-time system matrix, $\mathbf{C}_c$ is the continuous-time output matrix and $\mathbf{u}_a$ represents the adjoint input.

Computing the approximate Gramians for a particular set of well and boundary conditions involves several training simulations of the forward and the adjoint systems. Subsequently, a sufficient number of snapshots of the forward and the adjoint run are stored in the snapshot matrices $\mathbf{X}$ and $\mathbf{Z}$. Similar to the BT method and using the 'method of snapshots', we compute the singular value decomposition $\mathbf{Z}^T\mathbf{X} = \mathbf{U}\boldsymbol{\Sigma}\mathbf{V}^T$. The balanced transformation matrices are written as $\mathscr{V} = \mathbf{X}\mathbf{V}\boldsymbol{\Sigma}^{-1/2}$ and $\mathscr{W}^T = \boldsymbol{\Sigma}^{-1/2}\mathbf{U}^T\mathbf{Z}^T$, where the diagonal entries of $\boldsymbol{\Sigma}$ give the Hankel singular values of the system. Now we can choose

$$\mathscr{V}_r = \mathbf{X}\mathbf{V}_1\boldsymbol{\Sigma}_1^{-1/2}, \tag{6.13}$$

$$\mathscr{W}_r^T = \boldsymbol{\Sigma}_1^{-1/2}\mathbf{U}_1^T\mathbf{Z}^T, \tag{6.14}$$

where $\boldsymbol{\Sigma}_1$ contains the r largest HSVs of the system and $\mathbf{U}_1$ and $\mathbf{V}_1$ contain the corresponding singular vectors as columns.

Note that BT and BPOD are both related to the most controllable/observable subspaces of the system. However, from a computational point of view, the BT approach is only applicable to small system (order of 10^4 grid blocks). Therefore, the main advantage of BPOD is that using the method of snapshots we can calculate an approximate balanced transformation without requiring the explicit computation of the Gramians, and since it only involves matrix-vector operations, it can be applied to very large systems. Moreover, unlike BT, this method can also be used for nonlinear systems such as two-phase flow models. However, BPOD requires several training simulations, with different input sequences, of the forward and adjoint systems.

6.3. Model reduction and Control-relevant upscaling

6.3.1. Reduced-order CRU

As discussed in Chapter 4, the CRU algorithm tries to reduce the distance between the coarse- and fine-scale models by changing the coarse-scale parameters. Since this distance is measured by a system norm that represents the controllability and observability properties of the system, the CRU algorithm indirectly focuses on system parameters that are related to most controllable/observable states of the system. The basic idea of reduced-order CRU is to apply the CRU technique to a reduced-order subspace of the system that represents to the most controllable/observable subspace of the system (see

also Vakili-Ghahani et al. 2008). Therefore, in the reduced-order CRU algorithm, we replace the original n^{th}-order fine-scale system by an r^{th}-order low-dimensional approximation, where $r<<n$. The schematic representation of the CRU problem in Figure (4.4) is then replaced by the one in Figure 6.1. Otherwise, the reduced-order CRU algorithm is the same as the full-order version that was described in section 4.2. The main improvement here is that the minimization problem (Eq. 4.1) is accelerated since lower-order Lyapunov equations have to be solved.

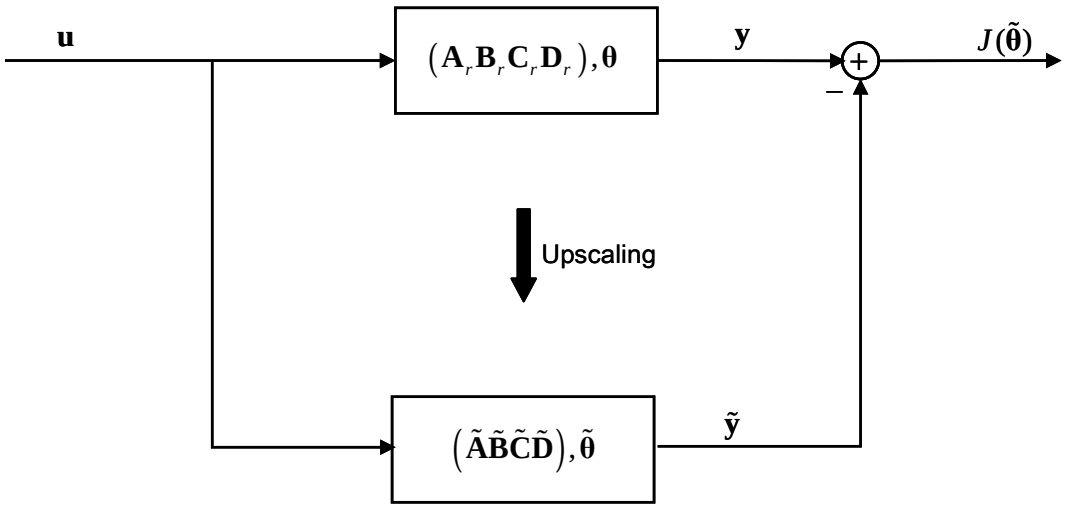

Figure 6.1 Schematic representation of the reduced-order CRU problem.

To determine a reduced-order model we can use the model reduction techniques based on POD or BPOD methods described in the previous section. Note that, while BPOD is related to the most controllable/observable subspaces of the system, the POD modes approximate only the most controllable subspace. Therefore, in applications, for which the observability of the system is important, BPOD is recommended. On the other hand, BPOD requires several training simulation of the forward and adjoint systems, while the POD approach only requires several simulations of the forward model. In both cases, the results of POD and BPOD are only valid for a region of state-space, from which the snapshots are collected.

In summary, reduced-order CRU enables the use of the control-relevant upscaling approach for large models. However, unlike the original full-order CRU, it requires forward simulations and, in case of BPOD, also adjoint simulations of the fine-scale model. We illustrate the performance of reduced-order CRU by the following example.

6.3.2. Example 6.1

We consider the reservoir system of Test Case (1) with the production scenario described in Example 4.1. To illustrate the performance of reduced-order CRU, we rerun the CRU algorithm for Example 4.1, while replacing the fine-scale model with a reduced-order representation obtained by POD. The POD bases are computed using 100 snapshots of a forward training simulation. The corresponding POD singular values have been plotted in Figure 6.2. We chose 6 basis functions to simulate the reduced-order model, such that the retained 'energy' according to Eq. (6.9) is 99.9999 %. The results in terms of the relative error in the average pressure and the cumulative production are given in Table 6.1.

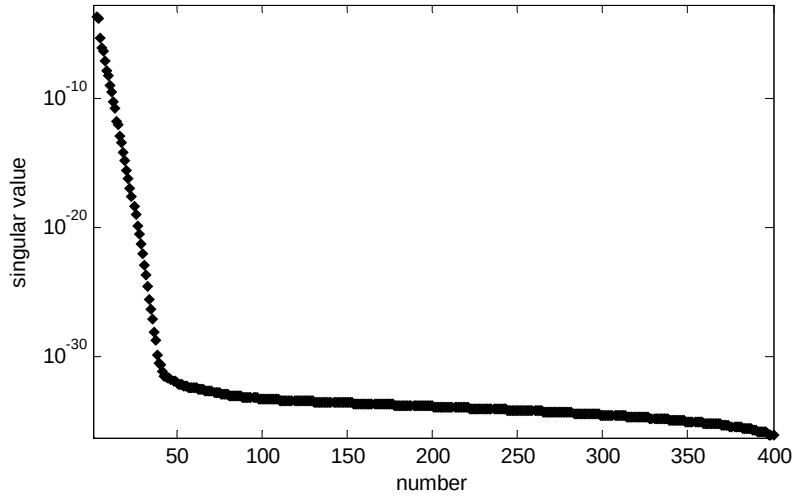

Figure 6.2 Singular values corresponding to the POD bases in Example 6.1.

Table 6.1 Reduced-order CRU performance for Example 6.1.

	CRU1-H2	CRU1-HSH	CRU1-H	CRU2-M	CRU2-H2	CRU2-HSH	CRU2-H
e_p (%)	0.7	0.7	0.6	1.4	1.8	1.1	1.1
$e_{q,cum}$ (%)	0.4	0.5	0.5	5	6.3	0.6	0.6
Reduced CRU time (s)	10	15	11	10	10	14	12
CRU time (s)	139	1518	281	10	10	18	13

Comparing Table 6.1 with Table 4.1 shows that, for this example, reduced-order CRU gives almost identical results to full-order CRU. A slightly smaller error for some of the CRU methods is probably due to a better-conditioned minimization problem when we work with a smaller system in the reduced-order case. However, according to rows 3 and

4 of Table 6.1, reduced-order CRU can significantly speed up the CRU procedure, particularly, for CRU method 1. This is because, using reduced-order CRU, we need to solve the Lyapunov equations for a much smaller error system in each iteration. For CRU method 2, full-order and reduced-order CRU give identical results so that for CRU2-HSH and CRU2-H even the cost function values in each iteration are equal (see Figure 6.3). Note that in case of a larger system, for which the exact computation of the Gramians is intractable, reduced-order CRU would be beneficial for both CRU methods.

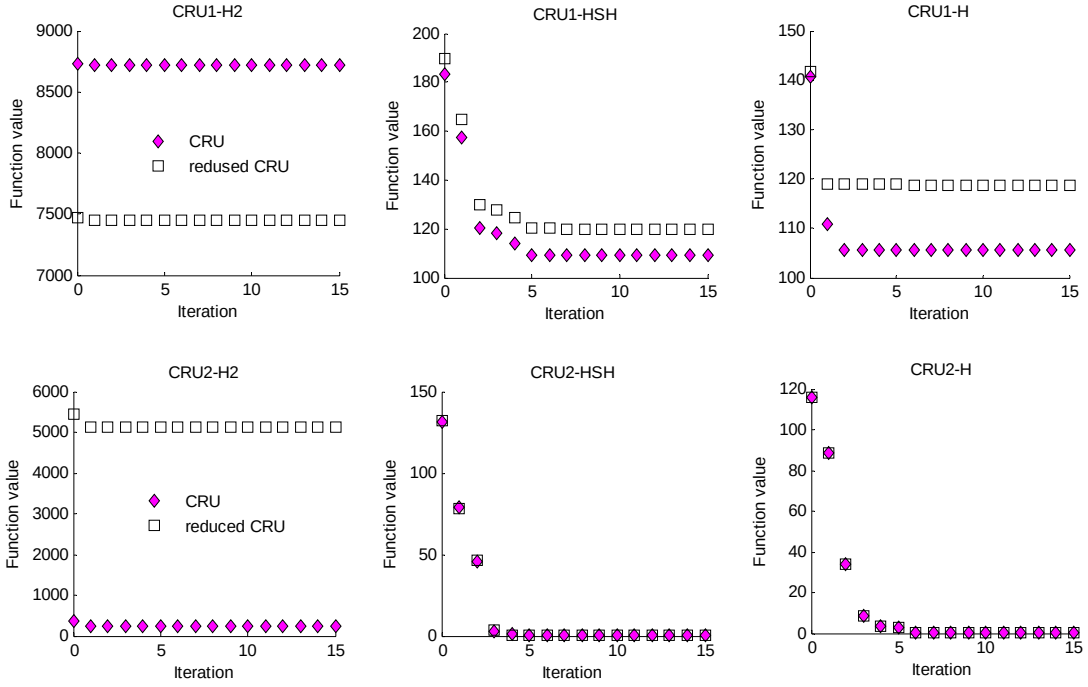

Figure 6.3 Cost function values corresponding to different CRU methods in Table 4.1 and 6.1.

As explained in Chapter 4, the CRU algorithm indirectly focuses on the grid blocks which are related to the more controllable/observable subspaces of the system. Therefore, in general, using BPOD bases, which also consider the observability of the system, is expected to be more accurate compared to ordinary POD bases, which only represent the most controllable subspace of the system. Nevertheless, for this example, the most controllable directions are sufficient as the controllable and observable directions are equivalent. This is evident from Figure 6.4, where we project the first two singular vectors (directions) of the controllability Gramian, the observability Gramian and the product of them on the spatial grid. Mathematically, this is valid when in Eqs. (3.25) and (3.26), $\mathbf{A}^T\mathbf{A} = \mathbf{A}\mathbf{A}^T$ (Farrell & Ioannou 1993). Then, for such a system, $\mathbf{W}_c$ and $\mathbf{W}_o$

have the same singular vectors and the POD directions are equivalent to the balancing directions as demonstrated by Figure 6.4 for Example 6.1. For our application this implies that control and observation should be exercised at the same points in the reservoir. If this is not the case, e.g. when there are only a limited number of wells in which rates or bottomhole pressures can be observed, there may be a significant difference between the controllable and unobservable subspaces, in which case the use of BPOD may have benefits.

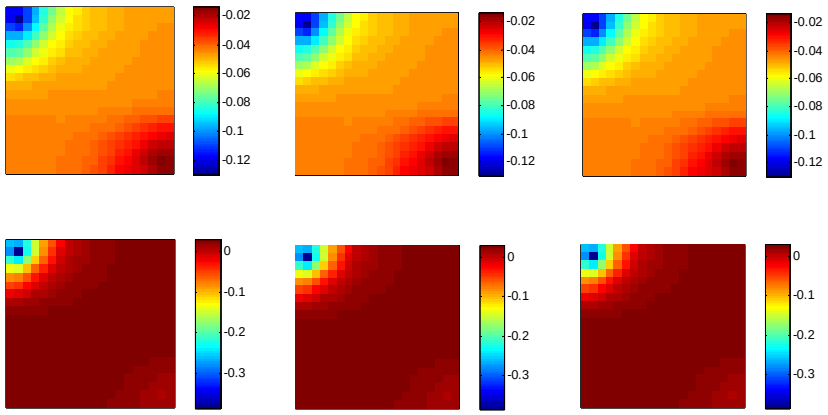

Figure 6.4 The first two singular vectors (directions) of the Controllability Gramian (column 1), observability Gramian (column 2) and the product of them (column 3) in Example 6.1.

6.3.3. Control-relevant missing point estimation

As explained in section 6.1, we can construct a reduced-order model of a given high-order system by projecting the state-space onto a lower-dimensional space using the projection matrices $\mathcal{V}_r$ and $\mathcal{W}_r$. The columns of $\mathcal{V}_r$ and $\mathcal{W}_r$ give r basis vectors with the length of n, where n is the number of grid blocks. Therefore, the construction cost of the reduced-order model and, in particular, $\mathcal{W}_r^T \mathbf{A} \mathcal{V}_r$ (in terms of both computational time and storage requirement) can be further reduced, if we can also reduce the length of the basis functions by selecting a number of grid points of the spatial domain[28]. This idea, known as Missing Point Estimation (MPE), was first proposed by Astrid et al. (2004) to model a glass feeder. Later Cardoso et al. (2009) applied the MPE approach to reservoir flow simulation. In their work, they used a condition number criterion to select the most important l grid blocks and, accordingly, they obtained POD basis functions of length l

[28] Reducing the construction cost of $\mathcal{W}_r^T \mathbf{A} \mathcal{V}_r$ (equivalent to $\mathcal{W}_r^T \mathbf{J} \mathcal{V}_r$, where $\mathbf{J}$ is the Jacobian matrix) is even more significant in two-phase flow simulations, where there are more than one state variables per grid block resulting in high construction time and storage requirement due to a large Jacobian matrix (see Cardoso et al. 2009).

instead of length n where $l < n$. More specifically, for the POD bases the relation $\boldsymbol{\Phi}_r{}^T\boldsymbol{\Phi}_r = \mathbf{I}$ holds, meaning that the condition number of matrix $\boldsymbol{\Phi}_r{}^T\boldsymbol{\Phi}_r$ is equal to one. The idea of MPE is to remove a number of grid blocks and the corresponding rows from the basis matrix $\boldsymbol{\Phi}_r$, while allowing the condition number to increase to a specific number. The grid blocks are sorted and selected based on their contribution to deviating from the unit condition number.

In a similar approach, here, we consider another criterion to select the relevant grid blocks and, subsequently, relevant rows of the basis functions for the input/output behavior. In our control-relevant MPE (CR-MPE) approach, we use the spatial quantification of controllability and observability (see section 5.2) to select the grid blocks related to the most controllable and observable regions of the spatial domain. The overall procedure of CR-MPE is as follows. First, the dominant pattern $\bar{\mathbf{u}}$ is obtained by Eq. (5.4) and the grid blocks are sorted based on the magnitude of the corresponding elements (rows) of $\bar{\mathbf{u}}$. Then, the l grid blocks that satisfy Eq. (5.5), i.e. those that are located in areas corresponding to highly controllable/observable states are selected. This approach can be applied to both POD and BPOD basis functions. To perform the CR-MPE using POD or BPOD bases, we replace the $r \times n$ matrices $\mathcal{V}_r$ and $\mathcal{W}_r$ by $r \times l$ matrices $\mathcal{V}_{r,l}$ and $\mathcal{W}_{r,l}$, where the l rows of $\mathcal{V}_{r,l}$ and $\mathcal{W}_{r,l}$ are related to the selected grid blocks. (Note that for the POD bases $\mathcal{V}_{r,l} = \mathcal{W}_{r,l}$). The MPE and CR-MPE performances are demonstrated by the following numerical example.

6.3.4. Example 6.2

Consider again the reservoir system of Test Case (1) with one injector and one producer that are controlled by time-variant bottomhole pressures. The permeability field and the well locations are described in the left part of Figure 6.5. From 100 snapshots of the solution of a training simulation, we compute 7 POD basis functions with a length of 400 elements each. The bases are stacked in the columns of matrix $\boldsymbol{\Phi}_r$. We applied both original MPE approach (Astrid et al. 2004) and CR-MPE method to select the relevant grid blocks. Figure 6.5 and Figure 6.6 show the results for MPE and CR-MPE, respectively. In these figures, the first column depicts the log10 permeability field and the well locations, the second column shows the grid block importance based on the MPE or CR-MPE criteria and the third column illustrates 200 selected grid blocks. In both cases, we replace the 400×7 bases matrix $\boldsymbol{\Phi}_r$ by a 200×7 one. Recall that colors from red to blue in the middle part of Figure 6.6 also represents the spatial variation of the controllability and the observability of the system.

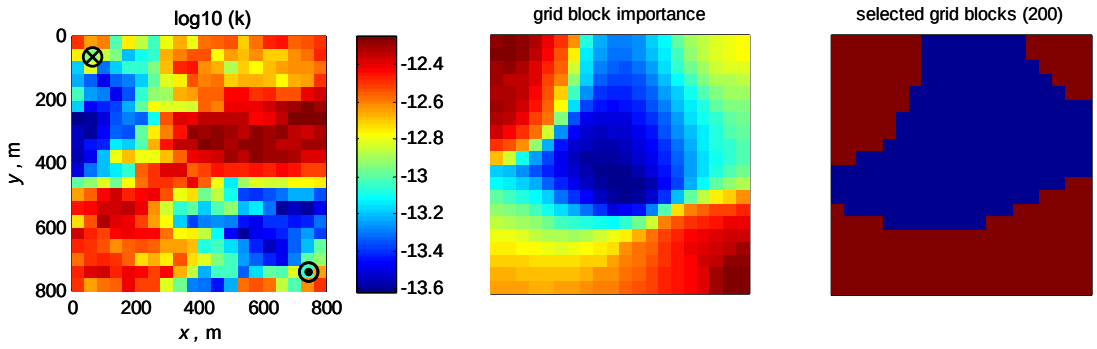

Figure 6.5 Left: Log10 permeability field and locations of one injector (cross) and one producer (dot) for Test Case (1) in Example 6.2. Middle: grid importance from red to blue based on condition number. Right: selected grid blocks using the original MPE method.

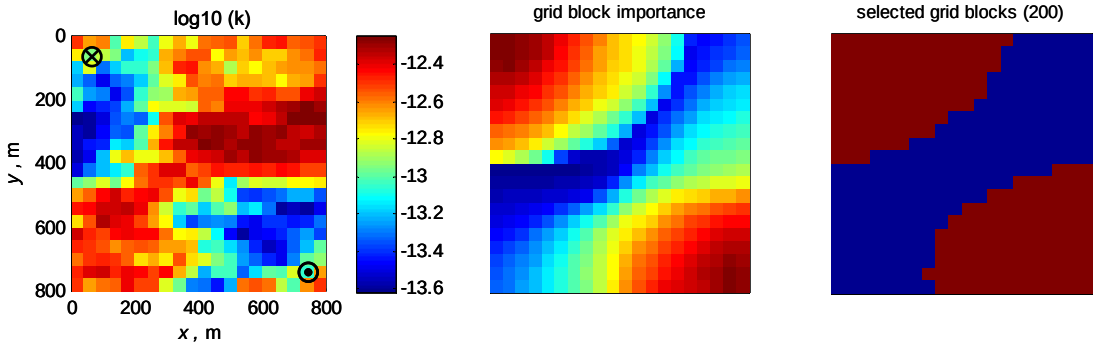

Figure 6.6 Left: Log10 permeability field and locations of one injector (cross) and one producer (dot) for Test Case (1) in Example 6.2. Middle: grid importance from red to blue based on controllability and observability. Right: selected grid blocks using the CR-MPE method.

Comparing Figure 6.5 with Figure 6.6, we observe that both methods correctly select the grid blocks close to the wells, which are more relevant in terms of input-output behavior. However, the MPE method also selects some additional grid blocks on the corners far from the wells that are related to weakly controllable/observable states (c.f. the middle part of Figure 6.6). Opposedly, the CR-MPE method selects only the input-output relevant grid blocks. Therefore, as shown in Figure 6.7, the CR-MPE method slightly outperforms the MPE method in simulating the production rates of the system, when compared to the original high-order model.

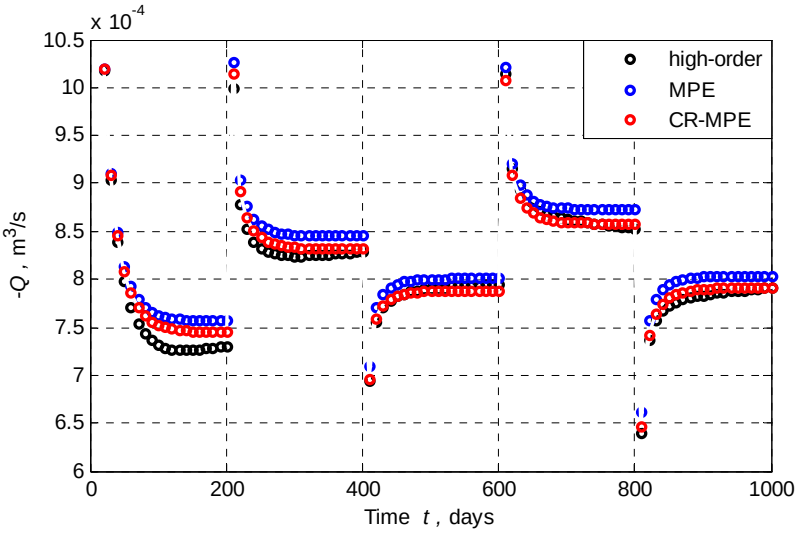

Figure 6.7 Production rates in Example 6.2 from the simulation of the original high-order model and two reduce-order representations obtained by MPE and CR-MPE.

6.4. Approximation of the Gramians

To study the controllability and observability of a reservoir system in either the CRU or the CRSC method, we first need to compute the Gramians of the system by solving the Lyapunov equations (Eqs. 3.25 and 3.26). Therefore, in this section, we briefly explain three different methods to compute the Gramians. An extensive overview of different techniques to compute the exact and approximate solutions of these equations can be found in Antoulas (2005), Penzl (2006), Markovinović (2009) and the references therein.

6.4.1. Exact methods

The first method is to use direct algorithms for small dense Lyapunov equations, such as the Bartels-Stewart technique (Bartels and Stewart 1972) and Hammarling's method (Hammarling 1982), which are already implemented in Matlab as functions *lyap* and *lyapchol*. Such methods rely on an initial Schur decomposition of the system matrix **A** followed by additional factorizations of dense matrices (see Antoulas 2005). Therefore, an important shortcoming is a very high computational time and memory requirement that make them intractable for large systems (with an order larger than 10^4).

6.4.2. Low-rank iterative approximation of the Gramians

To overcome the computational shortcomings of the exact methods, one may use different iterative techniques to approximate the Gramians (see Penzl 2006). Here we only mention the alternating direction-implicit (ADI) algorithm that seeks **W** as the

solution of the continuous-time Lyapunov equation $\mathbf{AW}+\mathbf{WA}^T+\mathbf{BB}^T=\mathbf{0}$, in an iteration step of the form

$$\begin{aligned}\mathbf{W}_i = &(\mathbf{A}-\mu_i^*\mathbf{I})(\mathbf{A}+\mu_i\mathbf{I})^{-1}\mathbf{W}_{i-1}\left[(\mathbf{A}-\mu_i^*\mathbf{I})(\mathbf{A}+\mu_i\mathbf{I})^{-1}\right]^* \\ &-2\rho_i(\mathbf{A}+\mu_i\mathbf{I})^{-1}\mathbf{B}\mathbf{B}^*(\mathbf{A}+\mu_i^*\mathbf{I})^{-*},\end{aligned} \tag{6.15}$$

where $\mu_i \in \mathbb{C}^-$ ($i=1,2,3,...$) are the shift parameters, $\rho_i = \mathrm{Re}(\mu_i)$ and $\mathbf{W}_0=\mathbf{0}$. Furthermore, in many cases like in our applications, the eigen values of the Gramians are decaying very fast, indicating that there exist accurate low-rank approximations. For each Gramian, let $\mathbf{W}=\mathbf{L}\mathbf{L}^{\mathrm{T}}$, where $\mathbf{L}$ is the Cholesky decomposition (square root) of the Gramian. For large systems we replace the full-rank Cholesky factor $\mathbf{L}$ by a low-rank approximation $\mathbf{L}_r$, where $r < n$ is a rank of $\mathbf{L}$ related to the order of the controllable and observable subspaces. Consequently, we only have to store the $n\times r$ matrix $\mathbf{L}_r$ instead of the dense $n\times n$ matrix $\mathbf{W}$. Therefore, in addition to reducing the computational cost, we reduce the memory requirements.

Rewriting Eq. (6.15) in terms of the low rank approximation of the Cholesky factors results in a low rank ADI (LR-ADI) approach. This approach, which has been implemented in LYAPACK[29], leads to an efficient algorithm that can approximate the system Gramians nearly up to machine precision (see example 6.3). The fast and reliable LR-ADI approach, therefore, was used to compute the Gramians in most examples in Chapter 4 and 5. For a detailed implementation of this method, see Penzl (1999, 2006).

6.4.3. Empirical Gramians

Instead of solving the Lyapunov equations, we may approximate the Gramians from the numerical simulation data for a particular set of inputs and initial conditions. The initial approach was proposed by Lall et al. (1999, 2002). However, they used direct POD methods to obtain approximate system Gramians, which is computationally expensive, in particular, for large systems as it leads to the construction of two $n\times n$ dense matrices. Therefore, we use here an alternative formulation that is based on the BPOD (Willcox and Peraire 2002; Rowely 2005). In this approach the approximate Gramians are computed as described by Eqs.(6.10) and (6.11) in subsection 6.2.3. Note that in our application, i.e. using spatial quantification of the controllability and the observability properties, we need the columns of $\mathbf{T}^{-1}$, which are equivalent here to the columns of $\mathcal{U}_r^T$

[29] LYAPACK is a Matlab toolbox for the solution of large-scale problems in control theory. It uses iterative algorithms and it is intended for solving large and sparse Lyapunov equations (see Penzl 1999). Note that LYAPCK only solves the continuous-time Lyapunov equations. However, the discrete- and continues-time Lyapunov equations have the same solutions (Antoulas 2005).

given by Eq. (6.14). Therefore, we never directly compute the Gramian matrices. In other applications a low rank approximation of the Gramians could be formed using $\mathbf{\Sigma}_1$, $\mathcal{Y}_f$ and $\mathcal{U}_f$ (see Willcox and Peraire 2002).

6.4.4. Example 6.3

To compare the approximate Gramians obtained by LR-ADI and BPOD to the exact Gramians, first we consider the small reservoir model of Test Case (1) (see Examples 6.1 and 4.1). For the LR-ADI method, the low-rank Cholesky factors are computed by LYAPACK and in BPOD case we use the snapshots from the solution of the forward and the adjoint models. Figure 6.8 shows the square root of first 200 singular values of the product of the Gramians (i.e., HSVs) computed by different methods. Evidently, the LR-ADI approach gives a much more accurate solution compared to the BPOD approach.

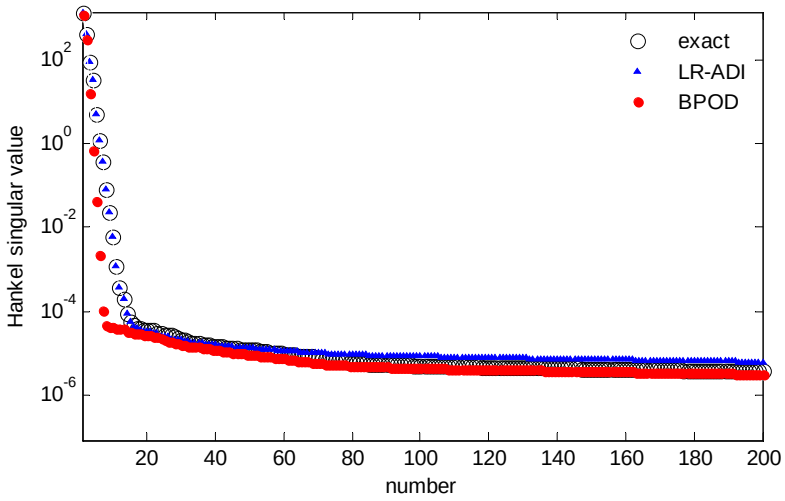

Figure 6.8 Hankel singular values computed by exact and approximate Gramians for test case (1) in Example 6.3.

Nevertheless, the accuracy in finding the more controllable/observable subspaces seems to be sufficient in applications such as the CRSC algorithm that only requires a rough approximation of these subspaces. This is illustrated by Figure 6.9 that depicts the dominant pattern obtained from the approximate BPOD Gramians for a larger reservoir system described in Example 5.1. The resulting mapping is very close to the one in Figure 5.5, which was obtained by the LR-ADI technique. In this case, the computational time for the LR-ADI and the BPOD methods are 105 s and 52 s, respectively. Note that

the BPOD method only involves matrix-vector operations and, therefore, it can be applied to very large systems.

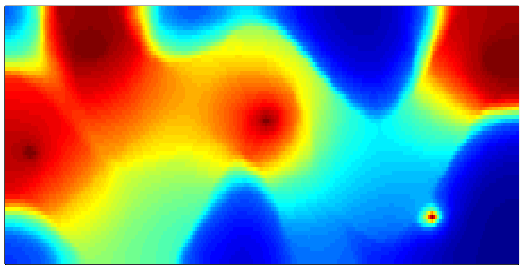

Figure 6.9 Visualization of the dominant pattern for controllability and observability variation over the spatial domain for Test Case (3); the Gramians were obtained using the 'method of snapshots'. Colors from red to blue represent the grid importance obtained from the scaled weighted sum of the singular vectors corresponding to the Hankel singular values of the system.

6.5. Complexity analysis

In order to obtain a rough approximation of the computational efficiency of the CRSC and CRU algorithms, we investigated the computation of the most expensive operations. This includes the computation of the Gramians and the calculation of the Hankel singular values (balancing). The balancing step as described in section 3.3 requires a singular value decomposition of operation of order n^3. However, in practice, we only perform it for the first k largest singular values and therefore the computational overhead is in the order of k^3, where $k \ll n$. In particular, using the formulation described in subsection 6.2.1 in combination with low-rank Cholesky decomposition, we may implement the SVD on very large matrices. Therefore, the limiting part in the application of CRSC and CRU algorithms to large systems is the computation of the Gramians, i.e. the solution of Lyapunov equations.

6.5.1. Computation of the Gramians

In case of direct Lyapunov solvers, as described in subsection 6.4.1, the solver requires arithmetic operations in the order of n^3 and storage of several dense matrices of order n, i.e., n^2 storage. The high storage requirement is because, in addition to producing dense Gramians, these methods are based on Schur decomposition of the sparse system matrix which produces dense matrices. Consequently, these methods are only applicable to systems with an order of $<10^4$.

The second approach is the LR-ADI method, for which the operation requirement is in the order of rn where r is the number of columns that are used for the computation.

Moreover, the storage cost for this method is much smaller (also in the order of *rn*). The reason is that here we directly work with low-rank Cholesky factors of the Gramians, compared to direct methods, in which we need to store the full-rank dense Gramians (in the order of n^2). Therefore, this is the method that can be also applied to very large systems. In particular, for large systems in which the input and output matrices **B** and **C** have a low numerical rank, i.e. for small numbers of inputs and outputs, the eigen values of the Gramians are decaying very fast, indicating that there exist accurate low-rank approximations. For instance, Figure 5.3 shows that the Hankel singular values for Test case (3) are rapidly decreasing. This means that for this example (n=16384), k can be chosen around 100 or even less (note that the y-axis is represented on a logarithmic scale). Therefore, the use of the LR-ADI method for this example can considerably reduce the computational time and storage requirement, compared to direct methods.

The last approach was to approximate the Gramians from the method of snapshots or BPOD. In this case, the Lyapunov equations are never solved and to approximate the Gramians only one SVD is needed of a matrix with dimension $N_f \times N_a$, where N_f and N_a are the number of snapshots from the forward and the adjoint simulations. Therefore, assuming $N_f = N_a$, the computational overhead is in the order of N_f^3, where often $N_f \ll n$. Interestingly, the size of the SVD problem here is independent of *n* (the number of grid blocks) and, therefore, this method can be applied to very large systems. However, it requires also several flow simulations over the original fine-scale model and the associated adjoint model with operations in the order of *n*. Note that for large systems it is more efficient to use an iterative method to solve this system of equations. For a more detailed complexity analysis of different methods for computation of the Gramians, the reader is referred to Antoulas (2005) and Markovinovic (2009).

6.5.2. CRU versus CRSC

In general, CRSC is a faster approach since it requires no iterations (unless we use an approximate initial coarse-scale model to spatially quantify the controllability/observability). Moreover, the CRU minimization algorithm requires the computation of the gradient of the cost function with respect to the coarse-scale parameters which can be very expensive particularly when we use an error system, i.e., in CRU method 1, in combination with perturbation-based gradients (We note that computation of the gradients can be performed much more efficiently using adjoint-based methods but we did not pursue this possibility here). On the other hand, the resulting grid from the CRSC algorithm implies the solution of the flow equation on multi-level non-uniform grids, which requires more computational time and memory space, compared to

the flow simulation on uniform cells. In this case, the effective bandwidth of the system matrix can be optimized by an extra operation, for which the extra computational cost can be neglected particularly for larger systems (see subsection 5.4.3). The other steps in the simulation are similar for CRU and CRSC grid systems and the simulation cost is roughly related to *O(n)* for both cases.

Note that, in any case, the upscaled model needs to be obtained only once (or a few times in case of changes in the well configuration) and in an offline part of the simulation, whereas many forward simulations of the flow equations may be required in applications such as computer-assisted history matching or flooding optimization under uncertainty.

6.6. Summary

We investigated the potential benefits of using a model reduction technique (POD) in combination with the CRU method. In the example considered, a reduced-order model based on POD could accelerate the upscaling procedure particularly for CRU method 1. Note that, in general, POD only considers the relation between the inputs and the states (controllability), while the goal of simulation is often to predict an accurate output. Moreover, a reduction based on only inputs or outputs might be strongly dependent on a particular scaling of the states (state-space coordinate), whereas a balanced case is coordinate-invariant. Further research is required to address the computational aspects of CRU, and the potential use of other model-order reduction techniques in combination with our control-relevant upscaling approach.

The computational efficiency can be also improved by using approximate Gramians. The solution of the Lyapunov equations can be approximated by iterative methods followed by a low rank Cholesky factorization of the Gramians (e.g., LR-ADI method). Alternatively, the Gramians can be approximated from the snapshots of the trajectories (states) that the forward system and its adjoint follow when simulating some training inputs. The approximate techniques to obtain the Gramians can improve the computational efficiency of both CRU and CRSC algorithms, which increases their applicability to realistic, large-scale reservoir models.

7. CHAPTER: CONCLUSIONS & RECOMMENDATIONS

In this thesis, we developed control-relevant uniform and selective upscaling algorithms, which are based on the controllability and observability of the reservoir system for a given well configuration. This chapter presents the conclusions of the thesis and gives several recommendations for future research.

7.1. Conclusions

Geological subsurface models often represent the subsurface heterogeneity with 10^6 to 10^9 parameters. The major issues with such high-order (large-scale) systems are related to both computational and system-theoretical aspects (Chapter 1). In this research, we approached the upscaling problem from a system-theoretical perspective and we developed two control-relevant upscaling algorithms. In the end, the following remarks and conclusions are emphasized:

- Although different upscaling techniques are available in reservoir simulation, most of them lack generality and case independency, as they are only valid under certain reservoir and boundary conditions. Moreover, in most techniques, it is assumed that the computed coarse-scale parameters, based on a specified set of boundary conditions often with no sink/source terms, will be applicable to all other flow scenarios. The validity of this assumption is not warranted, seeing that in a real reservoir the global flow is often driven by wells rather than by fixed-pressure or fixed-rate boundary conditions (Chapter 2).

- For a given configuration of wells, there are only a limited number of degrees of freedom in the input-output dynamics of a reservoir system. From a system-theoretical point of view, this means that a large number of combinations of the state variables are not actually controllable and observable from the wells, and accordingly, they are not affecting the input-output behavior of the system (Chapter 3).

- HSVs of a system can indicate those linear combinations of the states that represent the most important input-output characteristics of the system, and consequently determine the order of the input-output dynamics. Accordingly, they can be used to adjust (reduce) the level of the model complexity (or model order) to the available amount of control and information for a given configuration of wells. Note that the controllability and observability of a linear system is independent of the specific values of time-variant inputs, but dependent on well configurations (Chapter 3).
- We introduced a single-phase control-relevant upscaling (CRU) technique that minimizes the difference between a fine-scale and a coarse-scale reservoir model in terms of system norms that characterize the input/output behavior for a given configuration of wells. We defined two CRU methods with three system norms to quantify the difference between the fine-scale and the coarse-scale models. The definition of the objective function in Method 1 is theoretically more justified, while Method 2 is computationally more attractive. In addition, based on the examples, the HSH-norm and the H-norm seem to have a better performance compared to the H2-norm (Chapter 4).
- Computation of the largest Hankel singular values of a reservoir model and mapping the corresponding directions on the reservoir grid allows for a spatial quantification of the combined controllability and observability. For a given configuration of wells, the most controllable/observable areas appear to be in the vicinity of the wells and in high-permeable areas close to and connected to the wells (chapter 5).
- Control-relevant selective coarsening (CRSC) can be achieved by initial uniform coarsening and subsequent selective refinement in areas of highest combined controllability and observability. We proposed a multi-level CRSC method to allow treatment of very large models with a high degree of heterogeneity in their parameter fields. Based on the numerical examples, CRSC can accurately reproduce the flow response of the fine scale models for time varying inputs. In addition to giving a computational advantage, the selective coarsening gives also

more accurate results than a uniformly upscaled model with the same number of grid blocks (Chapter 5).

- For large systems, the CRSC grid can be efficiently obtained by using appropriate approximation methods to compute the Gramians, applying a proper grid block numbering, optimizing the bandwidth of the system matrix, and using the unstructured data approach to optimize the grid data storing and loading during the simulation (Chapter 5).

- Both CRU and CRSC are global methods in the sense that they rely on the system properties of the entire reservoir. However, they do not require any forward simulation either of the full or of the upscaled model. They also do not depend on a particular control strategy but instead use the dynamical system equations directly. However, any change in the well configuration (including both well locations and the number of inputs and outputs) requires a (partial) repetition of the upscaling procedure. Accordingly, these methods are attractive for use in computer-assisted flooding optimization or history matching studies for a given configuration of wells, and in particular for the combined use of optimization and history matching in a closed-loop reservoir management setting, but unattractive in applications like well placement optimizations.

- The use of CRU in conjunction to a model-order reduction technique seems promising to obtain a reduced-order CRU algorithm that to a large extent solves the computational issues in applying CRU to large-scale reservoir models. On the other hand, the spatial quantification of controllability and observability can be used to define a new criterion for selecting only the input-output relevant grid blocks in a missing point estimation (MPE) process, where we can reduce the computational and storage cost of the model reduction procedure by retaining only those rows of the basis functions that are corresponding to the selected grid blocks (Chapter 6).

- Current developments addressing the approximate solution of high-order (i.e. fine-scale) Lyapunov equations make it likely that CRU and CRSC will be applicable to realistic reservoir models with up to 10^6 grid blocks. Alternatively, a

fast approximation of the Gramians can be obtained from sufficient snapshots of the simulation data in time. Conceptually, this approach is applicable to any realistic large-scale reservoir. However, it requires several high-order training simulations, while the resulting low-order model is restricted to the region of state-space from which the data have been collected (Chapter 6).

- Note that in any case the upscaled model from CRU or CRSC needs to be obtained only once and in an offline part of the simulation, whereas simulation of the flow equation over the resulting coarse-scale grid blocks might be repeated many times in different applications.
- This research was primarily concerned with the system-theoretical aspects of upscaling in reservoir simulation. Therefore, the computational efficiency of the presented algorithms was not optimized. However, despite its preliminary character, the research reported here may offer a new insight into the upscaling problem from a system-theoretical perspective.

7.2. Recommendations

- The coarse-scale models obtained by single-phase CRU and CRSC can be also used for two-phase simulations. Nevertheless, the performance of the methods needs to be tested. Moreover, the algorithms can be extended to include two-phase flow controllability and observability analysis that includes also the saturation equation. However, for nonlinear two-phase flow cases, we need to either linearize the system, or compute the controllability and observability Gramians empirically. The other important issue in two-phase flow cases is to deal with moving saturation fronts. Since the saturations are only controllable along the front and only observable after water breakthrough in the wells, the performance of the CRSC algorithm might be improved by adding (partial) dynamic grid adaptations to resolve the strongly controllable/observable areas along the moving saturation fronts. Further research is required to evaluate the computational benefits of applying the CRSC approach to multi-phase flow applications.

- Another possible solution to treat saturations in a two-phase flow simulation might be applying a multi-scale framework, in which the CRSC grid blocks are only used to solve the pressure equation while the saturation equation is solved over the fine-scale grid blocks.
- To efficiently apply the CRU and CRSC algorithms to large reservoir models, we could also investigate a local-global framework, in which the reservoir domain is divided into several compartments, such that each compartment includes one well (or a couple of wells). CRU and CRSC could then be performed on each local compartment, for which the boundary conditions are derived from an approximate initial coarse-scale model. The procedure should probably be iterated to converge.
- The accuracy of the CRU and CRSC algorithms might increase by improving the controllability and observability of the reservoir system by adding more measurement points from monitoring wells, or adding data sources like time-lapse seismic. Moreover, adding a near-well upscaling technique would improve the results.
- Despite the presented discussions on the computational aspects of the CRU and the CRSC algorithms, further research is required to address undiscussed issues. Examples of those are the convergence of the CRU minimization algorithm for realistic large reservoirs, performance of the algorithm for gravity-driven or aquifer-driven flow, accuracy of the approximate Gramians for different systems, combination of CRU with other model reduction techniques (other than POD-based technique), alternative gridding and discretization strategies for CRSC (particularly, in reservoir applications with complex geologies and advanced multilateral well configurations), a systematic and optimal choice of the threshold value in the spatial quantification of controllability and observability, and extending the algorithms to 3D applications.

NOMENCLATURE

List of symbols

A	system matrix
B	input matrix
C	output matrix
D	direct-throughput matrix
dS	surface element
dV	volume element
E	energy
f	fractional flow function
g	acceleration of gravity, Lt^{-2}, m/s^2
G	arbitrary pressure gradient, $L^{-2}mt^{-2}$, Pa/m
H	transfer function
h	thickness, L, m
I	identity matrix
J	well index matrix, L^2t/m, $m^3/(Pa\ s)$
k	counter
k	permeability, L^2, m^2
K	permeability matrix
l	length, L, m
l	length of MPE basis function
L	Cholesky factor
M	matrix of Markov parameters
n	number of grid blocks
n	unit outward normal vector
N	number of snapshots
N	number of layers in a layered reservoir
p	pressure, $L^{-1}mt^{-2}$, Pa
p	proportion of permeable medium
p	pressure vector
q	volumetric flow rate, L^3t^{-1}, m^3/s

$\mathbf{q}$	flow rate vector
r	number of states in reduced-order model
S	phase saturation
t	time, t, s
T	transmissibility, $L^2M^{-1}t$, $m^3/(Pa\ s)$
$\mathbf{T}$	transmissibility matrix
u	phase velocity, Lt^{-1}, m/s
$\mathbf{u}$	input vector
$\mathbf{u}$	singular vector
$\mathbf{U}$	matrix of left singular vectors
V	grid block volume, L^3, m^3
$\mathbf{V}$	accumulation matrix
$\mathbf{V}$	matrix of right singular vectors
$\mathbf{W}$	Gramian
x	distance in the x-direction, L, m
$\mathbf{x}$	state vector
$\mathbf{X}$	snapshot matrix of forward model
y	distance in the y-direction, L, m
$\mathbf{y}$	output vector
z	distance in the z-direction, L, m
$\mathbf{z}$	adjoint state vector
$\mathbf{Z}$	snapshot matrix of adjoint model
$\mathcal{C}$	controllability matrix
$\mathcal{O}$	observability matrix
$\mathcal{H}$	Hankel matrix (impulse response matrix)
$\mathcal{V}$	left projection matrix
$\mathcal{W}$	right projection matrix
μ	shift parameter
ρ	real part of shift parameter
ε	threshold value
$\mathbf{\Phi}$	POD bases matrix
Ω	domain, L^3,m^3

Σ	system notation
$\mathbf{\Sigma}$	diagonal matrix containing singular values
ϕ	porosity
μ	viscosity, $L^{-1}mt^{-1}$, Pa s
μ	universal exponent
λ	eigenvalue
σ	singular value
ρ	density, $L^{-3}m$, kg/m^3
λ	mobility, $LM^{-1}t$, $m^2/(Pa\ s)$
α	small number

Subscripts

$\mathscr{c}$	controllability
$\mathscr{O}$	observability
ε	length scale parameter
a	adjoint
b	bulk volume
c	continuous-time
c	capillary
cum	cumulative
f	forward
f	fluid
h	Hankel
i	counter
k	counter
L	coarse-scale (observation) scale, L, m
l	permeability oscillation scale, L, m
o	oil
p	pressure
q	flow rate
r	reduced
r	relative
r	rock

t	threshold
w	water
x	x-direction
y	y-direction
α	fluid phase (oil or water)
α	auxiliary

Superscripts

*	coarse-scale parameter
c	coarse-scale variable
con	controllable
l	liquid
T	transpose
$unobs$	unobservable
ω	arbitrary exponent

Glossary

BPOD	Balanced Proper Orthogonal Decomposition
BT	Balanced Truncation
CR-MPE	Control-Relevant Missing Point Estimation
CRSC	Control-Relevant Selective Coarsening
CRU	Control-Relevant Upscaling
CT	Continuous-Time
DT	Discrete-Time
FVD	Finite Volume Discretization
HSH	Hilbert-Schmidt-Hankel norm
HSV	Hankel Singular Value
LR-ADI	Low-Rank Alternating Direction-Implicit
LTI	Linear Time-Invariant
MPE	Missing Point Estimation
POD	Proper Orthogonal Decomposition
RCM	Reverse Cuthill-McKee
TPFA	Two-Point Flux Approximation

BIBLIOGRAPHY

Aarnes J. (2004). On the use of a mixed multiscale finite element method for greater flexibility and increased speed or improved accuracy in reservoir simulation. *SIAM Multiscale modeling & simulation* **2**:421–39.

Aarnes, J., Kippe, V., Lie K.-A., and Rustad A.B. (2007a). Modeling of multiscale structures in flow simulations for petroleum reservoirs. *Geometric Modelling, Numerical Simulation, and Optimization Applied Mathematics at SINTEF*, Eds. G. Hasle, K.-A. Lie, and E. Quak, Springer Berlin Heidelberg, pp. 307-360.

Aarnes, J.E., Gimse, T. and Lie, K.-A. (2007b). An introduction to the numerics of flow in porous media using Matlab. *Geometric Modelling, Numerical Simulation, and Optimization Applied Mathematics at SINTEF*, Eds. G. Hasle, K.-A. Lie, and E. Quak, Springer Berlin Heidelberg, pp. 265-306.

Aavatsmark, I. (2002). An introduction to multipoint flux approximations for quadrilateral grids. *Computational Geosciences* **6** (3-4): 405-432.

Abou Kassem, J.H. and Aziz, K. (1985). Analytical well models for reservoir simulation. *SPE J.* **25** (4): 573-579.

Antoulas, A.C. (2005). *Approximation of large-scale dynamical systems*. Philadelphia, Pennsylvania: Advances in Design and Control, Society for Industrial and Applied Mathematics (SIAM).

Artus, V. and Noetinger, B. (2004). Up-scaling two-phase flow in heterogeneous reservoirs: current trends. *Oil & Gas Science and Technology - Rev. IFP* **59** (2): 185-195.

Astrid, P., Weiland, S., Willcox, K. and Backx, T. (2004). Missing point estimation in models described by proper orthogonal decomposition. *Proceeding* of 43rd IEEE Conference on Decision and Control **2**: 1767-1772.

Aziz, K. and Settari, A. 1979. *Petroleum reservoir simulation*. Essex, UK: Elsevier Applied Science Publishers.

Barker, J.W. and Thibeau, S. (1997). A critical review of the use of pseudo relative permeabilities for upscaling. *SPE Reservoir Engineering* **12** (2): 138-143.

Bartels, R.H. and Stewart, G.W. (1972). Solution of the matrix equation AX + XB = C Comm. of the ACM, **15** (9): 820-826.

Begg, S.H., Carter, R.R., Dranfield, P. (1989). Assigning effective values to simulator gridblock parameters for heterogeneous reservoirs. *SPE Reservoir Engineering* **4** (4): 455-463. SPE-16754-PA.

Berger, M.J. and Colella, P. (1989). Local adaptive mesh refinement for shock hydrodynamics. *Journal of Computational Physics* **82**: 64-84.

Berkowitz, B. and Balberg, I. (1993). Percolation theory and its application to groundwater hydrology. *Water Resources Research* **29** (4): 775-794.

Brouwer, D.R. (2004). *Dynamic water flood optimization with smart wells using optimal control theory*. PhD dissertation, Delft University of Technology.

Brouwer, D.R. and Jansen, J.D. (2004). Dynamic optimization of water flooding with smart wells using optimal control theory. *SPEJ* **9** (4): 391-402.

Brouwer, D.R., Nævdal, G., Jansen, J.D., Vefring, E.H. and van Kruijsdijk, C.P.J.W. (2004). Improved reservoir management through optimal control and continuous model updating, SPE 90149, SPE Annual Technical Conference and Exhibition, 26-29 September, Houston, Texas.

Bui-Thanh, T., Willcox, K. (2005). Model reduction for large-scale CFD applications using the balanced proper orthogonal decomposition. AIAA Paper 2005-4617, presented at 16th AIAA Computational Fluid Dynamics Conference, Toronto, Canada, 6-9 June.

Bunse-Gerstner et al. (2010). h2-norm optimal model reduction for large scale discrete dynamical MIMO systems. *Journal of Computational and Applied Mathematics* **233** (5): 1202-1216.

Cardoso, M.A., Durlofsky, L.J. and Sarma, P. (2009). Development and application of reduced-order modeling procedures for subsurface flow simulation. *International Journal for Numerical Methods in Engineering* **77** (9): 1322-1350.

Cardoso, M., Durlofsky, L.J. (2010a). Use of reduced-order modeling procedures for production optimization. *SPE J*, **15** (2): 426-435.

Cardoso, M.A., Durlofsky, L.J. (2010b). Linearized reduced-order models for subsurface flow simulation. *Journal of Computational Physics* **229** (3): 681-700.

Cardwell, W.T. and Parsons, R.L. (1945). Average permeabilities of heterogeneous oil sands. *Petroleum Transactions, AIME* **160**: 34-42.

Chen, Y. and Durlofsky, L.J. (2006). Adaptive local–global upscaling for general flow scenarios in heterogeneous formations. *Transport in Porous Media* **62**: 157–185.

Chen, Y. and Oliver, D.S. (2009). Ensemble-based closed-loop production optimization on Brugge field. Paper SPE 118962 presented at the SPE Reservoir Simulation Symposium, The Woodlands, Texas, USA, 2–4 February.

Chen, Y., Durlofsky, L.J., Gerritsen, M.G. and Wen, X.H. (2003). A coupled local-global upscaling approach for simulating flow in highly heterogeneous formations. *Advances in Water Resources* **26** (10): 1041-1060.

Christie, M.A. (1996). Upscaling for reservoir simulation. *Journal of Petroleum Technology* **48** (11): 1004-1010.

Christie, M.A. (2001). Flow in porous media - scale up of multiphase flow. *Current Opinion in Colloid & Interface Science* **6** (3): 236-241.

Christie, M.A. and Blunt, M.J. (2001). Tenth SPE comparative solution project: a comparison of upscaling techniques. *SPE Reservoir Evaluation & Engineering* **4** (4): 308-317.

Dale, M., Ekrann, S., Mykkeltveit, J. and Virnovsky, G. (1997). Effective relative permeability and capillary pressure for one-dimensional heterogeneous media. *Transport in Porous Media* **26** (3): 229-260.

Darman, N.H., Pickup, G.E. and Sorbie, K.S. (2002). A comparison of two-phase dynamic upscaling methods based on fluid potentials. *Computational Geosciences* **6** (1): 5-27.

Dasheng, Q. and Hesketh, T. (2005). An analysis of upscaling techniques for reservoir simulation. *Petroleum Science and Technology* **23** (7-8): 827-842.

DeCarlo, R.A. (1989). *Linear Systems: A state variable approach with numerical implementation.* Englewood Cliffs, New Jersey: Prentice Hall.

Deutsch, C. (1989). Calculating effective absolute permeability in sandstone/shale sequences. *SPE Formation Evaluation* **4** (3): 343-348.

Drummond, I.T. and Horgan, R.R. (1987). The effective permeability of a random medium. *Journal of Physics A: Mathematical and General* **20** (14): 4661-4672.

Durlofsky, L. J., Milliken, W. J. and Bernath, A. (2000). Scale-up in the near-well region, *SPE J.* **5**: 110-117.

Durlofsky, L.J. (1991). Numerical calculation of equivalent grid block permeability tensors for heterogeneous porous media. *Water Resources Research* **27** (5): 699-708.

Durlofsky, L.J. (1998). Coarse scale models of two phase flow in heterogeneous reservoirs: volume averaged equations and their relationship to existing upscaling techniques. *Computational Geosciences* **2** (2): 73-92.

Durlofsky, L.J. (2002). Upscaling of geological models for reservoir simulation: issues and approaches. *Computational Geosciences* **6** (1): 1-4.

Durlofsky, L.J. (2005). Upscaling and gridding of fine scale geological models for flow simulation. Paper presented at the 8th International Forum on Reservoir Simulation, Stresa, Italy, 20-24 June.

Edwards, M.G. (1996). Elimination of adaptive grid interface errors in the discrete cell centered pressure Equation. *Journal of Computational Physics* **126**: 356-372.

Edwards, M.G., Rogers, C.F. (1998). Finite volume discretization with imposed flux continuity for the general tensor pressure equation. *Computational Geosciences* **2** (4): 259-290.

Ekrann, S. and Aasen, J.O. (2000). Steady-State Upscaling. *Transport in Porous Media* **41** (3): 245-262.

Enns, D.F. (1984). Model reduction with balanced realizations: An error bound and a frequency weighted generalization. *Proceeding* of the 23rd IEEE conference on Decision and Control: 127-132.

Evensen, G. (2009). *Data assimilation. the ensemble Kalman filter*, second edition. Springer.

Farmer, L.J. (2002). Upscaling: a review. *International Journal for Numerical Methods in Fluids* **40** (1-2):63-78.

Farrell, B. F., Ioannou, P. J. (1993). Stochastic forcing of the linearized Navier-Stokes equations. *Physics of Fluids* **A5** (11): 2600-2609.

Gerritsen, M.G. and Durlofsky, L.J. (2005). Modeling fluid flow in oil reservoirs. *Annual Review of Fluid Mechanics* **37**:211–38.

Gerritsen, M.G. and Lambers, J.V. (2008). Integration of local-global upscaling and grid adaptivity for simulation of subsurface flow in heterogeneous formations. *Computational Geosciences* **12** (2): 193-208.

Gildin, E., Klie, H., Rodriguez, A., Wheeler, M.F., and Bishop, R.H. (2006). Development of low-order controllers for high-order reservoir models and smart wells. Paper SPE 102214 presented at the SPE Annual Technical Conference and Exhibition, San Antonio, Texas, USA, 24–27 September.

Glover, K. (1984). All optimal Hankel-norm approximations of linear multivariable systems and their L(infinity)-error bounds. *International Journal of Control* **39** (6): pp. 1115-1193.

Gueguen, Y., Ravalec, M. and Ricard, L. (2006). Upscaling: effective medium theory, Numerical Methods and the Fractal Dream. *Pure and Applied Geophysics* **163**: 1175-1192.

Ham, F.E., Lien, F.S. and Strong, A.B. (2002). A Cartesian grid method with transient anisotropic adaptation. *Journal of Computational Physics* **179** (2): 469-494.

Hammarling, S. 1982. Numerical solution of the stable, nonnegative definite Lyapunov equation. *IMA Journal of Numerical Analysis* **2** (3): 303-323.

Hanzon, B. (1992). The area enclosed by the (oriented) Nyquist diagram and the Hilbert-Schmidt-Hankel norm of a linear system. *IEEE Transactions on Automatic Control* **37** (6): 835–839.

Hartanto, L., (2004). *Different scales and integration of data in reservoir simulation*. PhD dissertation, Curtin University of Technology.

Hassanizadeh, S.M., Manthey, S., Dahle, H.K. and Celia, M.A. (2005). How effective are effective parameters? *Geophysical Research Abstracts* **7**: 05868.

He, C., Edwards, M. G. and Durlofsky, L.J. (2002). Numerical calculation of equivalent cell permeability tensors for general quadrilateral control volumes. *Computational Geosciences* **6** (1): 29-47.

Heijn, T., Markovinović, R., and Jansen, J.D. (2004). Generation of low-order reservoir models using system-theoretical concepts. *SPE J.* **9** (2): 202-218.

Holden, L. and Nelsen, B.F. (2000). Global upscaling of permeability in heterogeneous reservoir; the output least squares (OLS) method. *Transport in Porous Media* **40** (2): 115-143.

Hornung U. (1997). *Homogenization and porous media*. Springer.

Hou TY nad Wu XH. (1997). A multiscale finite element method for elliptic problems in composite materials and porous media. *J. Computational Physics* **134**:169-89.

Jafarpour, B. and McLaughlin, D. (2007). Efficient permeability parameterization with discrete cosine transform. Paper SPE 106453 presented at the SPE Reservoir Simulation Symposium, Houston, Texas, USA, 26-28 February.

Jansen, J.D. (2009). *System theory for reservoir management*. Lecture notes for course AES1490, Delft University of Technology.

Jansen, J.D., Bosgra, O.H. and Van den Hof, P.M.J. (2008). Model-based control of multiphase flow in subsurface oil reservoirs. *Journal of Process Control* **18** (9): pp. 846–855.

Jansen, J.D., Brouwer, D.R., Nævdal, G. and van Kruijsdijk, C.P.J.W. (2005). Closed-loop reservoir management. *First Break*, January, **23**:43-48.

Jansen, J.D., Douma, S.D., Brouwer, D.R., Van den Hof, P.M.J., Bosgra, O.H., and Heemink, A.W. (2009). Closed-loop reservoir management. Paper SPE 119098 presented at the SPE Reservoir Simulation Symposium, The Woodlands, Texas, USA, 2–4 February.

Journel, A. G., Deutsch, C. and Desbarats, A. J. (1986). Power averaging for block effective permeability. SPE paper 15128 presented at the 56th California Regional Meeting of SPE, April 2-4, Oakland, CA.

Kailath, T. (1980). *Linear systems*. Englewood Cliffs, New Jersey: Prentice Hall.

Khattri, S.K., Fladmark, G.E. and Dahle, H.K. (2007). Control volume finite difference on adaptive meshes. *Lecture Notes in Computational Science and Engineering* **55**: 629-636.

King, P.R. (1987). The use of field theoretic methods for the study of flow in a heterogeneous porous medium. Journal *of Physics A: Mathematical and General* **20** (12): 3935-3947.

King, P.R. (1989). The use of renormalization for effective permeability calculating. *Transport in Porous Media* **4** (1): 37-58.

King, P.R. (1996). Upscaling permeability: error analysis for renormalization. *Transport in Porous Media* **23** (3): 337-354.

King, P.R., Buldyrev, S.V., Dokholyan, N.V., Havlin, S., Lopez, E., Paul, G. and Stanley, H.E. (2002). Percolation theory. *DIALOG: London Petrophysical Society Newsletter* **10** (3).

Kyte, J.R. and Berry, D.W. (1975). Pseudo functions to control numerical dispersion. *SPE Journal* **15** (4): 269-276.

Lall, S., Marsden, J.E. and Glavaki, S. (1999). Empirical model reduction of controlled nonlinear systems. *Proc.* of the 14th IFAC World Congress: 473-478.

Lall, S., Marsden, J.E. and Glavaki, S. (2002). A subspace approach to balanced truncation for model reduction of nonlinear control systems. *International Journal of Robust and Nonlinear Control* **12** (6): 519-535.

Laub, A., Heath, M., Paige, C., and Ward, R. (1987). Computation of system balancing transformations and other applications of simultaneous diagonalization algorithms. *IEEE Transactions on Automatic Control* **32** (2): 115-122.

Li, R., Reynolds, A.C., and Oliver, D.S. (2003). History matching of three-phase flow production data. *SPE J.* **8** (4): 328-340.

Liu, Y. and Anderson, B.D.O. (1989). Singular perturbation approximation of balanced systems. *Proceeding* of the 28th IEEE Conference on Decision and Control, pages 1355-1360.

Mansoori, J. (1994). A review of basic upscaling procedures: advantages and disadvantages. Yarus, J.M. and Chambers R.L., editors, *Stochastic Modeling and Geostatistics, AAPG Computer Applications in Geology* **3**(chapter 7): 65-74.

Markovinović, R. (2009). *System-theoretical model reduction for reservoir simulation and Optimization*. PhD dissertation, Delft University of Technology.

Markovinović, R., Geurtsen, E.L., Heijn, T., and Jansen, J.D. (2002). Generation of low-order reservoir models using POD, empirical Gramians and subspace identification. *Proc*., 8th European Conference on the Mathematics of Oil Recovery (ECMOR VIII), Freiberg, Germany, 3–6 September.

Moore, B. (1981). Principle component analysis in linear systems: controllability, observability and model reduction. *IEEE Transactions on Automatic Control* **26** (1): 17-32.

Nævdal, G., Brouwer, D.R., and Jansen, J.-D. (2006). Waterflooding using closed-loop control. *Computational Geosciences* **10** (1): 37-60.

Nævdal, G., Johnsen, L.M., Aanonsen, S.I. and Vefring, E.H. (2005). Reservoir monitoring and continuous model updating using ensemble Kalman filter. *SPE J.* **10** (1): 66-74.

Neuweiler, I. and Cirpka, O.A. (2005). Homogenization of Richards equation in permeability fields with different connectivities. *Water Resources Research* **41** (2): W02009.

Nilsson, J., Gerritsen, M. and Younis, R. (2005). A novel adaptive anisotropic grid framework for efficient reservoir simulation. SPE 93243 presented at SPE Reservoir Simulation Symposium, 31 January-2 February, The Woodlands, Texas.

Noetinger, B., Artus, V. and Zargar, G. (2005). The future of stochastic and upscaling methods in hydrology. *Hydrogeology Journal* **13** (1):184-201.

Olsder, G.J. and van der Woude, J.W. (2005). *Mathematical systems theory*, third edition. VSSD, Delft, the Netherlands.

Pal, M, Edwards, M.G., and Lamb, A.R. (2006). Convergence study of a family of flux-continuous finite-volume schemes for the general tensor pressure equation. *International Journal for Numerical Methods in Fluids* **51**: 1177-1203.

Peaceman, D.W. (1977). *Fundamentals of numerical reservoir simulation*. Elsevier, New York.

Peaceman, D.W. (1983). Interpretation of well-block pressures in numerical reservoir simulation with nonsquare grid blocks and anisotropic permeability. *SPE J.* **23** (3): 531-543.

Peaceman, D.W. (1997). Effective transmissibilities of a gridblock by upscaling; comparison of direct methods with renormalization. *SPE Journal* **2** (3): 338-349.

Penzl, T. (1999). LYAPACK: A MATLAB toolbox for large Lyapunov and Riccati equations, model reduction problems, and linear-quadratic optimal control problems. SFB 393 Fakultät für Mathematik, TU Chemnitz.

Penzl, T. (2006). Algorithms for model reduction of large dynamical systems. *Linear Algebra and its Applications* **415** (2-3): 322-343.

Pickup, G. E. and Stephen, K. D. (2000). An assessment of steady-state scale-up for small-scale geological models. *Petroleum Geoscience* **6** (3): 203-210.

Polderman, J.W. and Willems, J.C., 1998. Introduction to mathematical systems theory. Springer.

Ramirez, W.F (1987). *Application of optimal control theory to enhanced oil recovery*. Elsevier.

Renard, Ph. and de Marsily, G. (1997). Calculating equivalent permeability: A review. *Advances in Water Resources* **20** (5–6): 253–278.

Romeu, R.K. and Noetinger, B. (1995). Calculation of internodal transmissivities in finite difference models of flow in heterogeneous porous media. *Water Resources Research* **31** (4):943-959.

Rommelse, J.R. (2009). *Data assimilation in reservoir management*. PhD dissertation, Delft University of Technology.

Rowely, C.W. (2005). Model reduction for fluids using balanced proper orthogonal decomposition. *International Journal of Bifurcation and Chaos* **15** (3): 997–1013.

Saez, A., Otero, C.J. and Rusinek, I. (1989). The effective homogeneous behavior of heterogeneous media. *Transport in Porous Media* **4** (3):213-238.

Sahni, I. and Horne, R.N. (2005). Multiresolution wavelet analysis for improved reservoir description, *SPE Reservoir Engineering and Evaluation* **8** (1): 53-69.

Salimi, H. and Bruining. H. (2009). Upscaling in vertically fractured oil reservoirs using homogenization. *Transport in Porous Media*.

Sarma, P., Aziz, K. and Durlofsky, L.J., (2005). Implementation of adjoint solution for optimal control of smart wells. Paper SPE 92864 presented at the SPE Reservoir Simulation Symposium, Houston, USA, 31 January – 2 February.

Sarma, P., Durlofsky, L.J., Aziz, K. and Chen, W.H. (2007) A new approach to automatic history matching using kernel PCA. Paper SPE 106176 presented at the SPE Reservoir Simulation Symposium, Houston, Texas, USA, 26-28 February.

Sarma, P., Durlofsky, L.J., Aziz, K., and Chen, W.H. (2006). Efficient real-time reservoir management using adjoint-based optimal control and model updating. *Computational Geosciences* **10** (1): 3–36.

Sirovich, L. (1987). Turbulence and the dynamics of coherent structures. Part 1: coherent structures. *Quarterly of Applied Mathematics* **45** (3): 561–571.

Skogestad, S. and Postlethwaite, I. (2005). *Multivariable feedback control: snalysis and design*, second edition. West Sussex, UK: John Wiley & Sons.

Vakili-Ghahani S.A. and Jansen, J.D. (2008). Control relevant upscaling. Paper SPE 113647 presented at the 2008 SPE Europec/EAGE Annual Conference and Exhibition, Rome, Italy, 9–12 June.

Vakili-Ghahani S.A., Markovinović, R. and Jansen, J.D. (2008). Upscaling of large reservoir systems by using a control-relevant approach. *Proc.* 11th European Conference on Mathematics in Oil Recovery (ECMOR X1), Bergen, Norway, 8-11 September.

Vakili-Ghahani, S.A. and Jansen, J.D. (2009). Control-relevant selective grid coarsening. Paper SPE 124581 presented at the SPE Annual Technical Conference and Exhibition, 4-7 October, New Orleans, USA.

Vakili-Ghahani, S.A. and Jansen, J.D. (2010a). Control-relevant upscaling. *SPE J.* **15** (2): 471-479. SPE-113647-PA. doi: 10.2118/113647-PA. Revised from paper SPE 113647 presented at the 2008 SPE Europec/EAGE Annual Conference and Exhibition, Rome, Italy, 9–12 June.

Vakili-Ghahani, S.A. and Jansen, J.D. (2010b). A system-theoretical approach to selective grid coarsening of reservoir models. Submitted to *Computational Geosciences*.

Van Doren, J.F.M. (2010). *Model structure analysis for model-based operation of petroleum reservoirs*. PhD dissertation, Delft University of Technology.

van Doren, J.F.M., van den Hof, P.M.J., Jansen, J.D., and Bosgra, O.H. (2008). Determining identifiable parameterizations for large-scale physical models in reservoir engineering. *Proc*., 17th Int. Fed. Autom. Control (IFAC) World Congress, Seoul, Korea, 6–11 July.

Van Duijn, C.J., Mikelic, A. and Pop, I.S. (2002) Effective equations for two-phase flow with trapping on the micro scale. *SIAM Journal on Applied Mathematics* **62** (5): 1531-1568.

Virnovsky, G.A., Friss, H.A. and Lohne, A. (2004). A steady-state upscaling approach for immiscible two-phase flow. *Transport in Porous Media* **54** (2): 167-192.

Warren, J.E. and Price, H.S. (1961). Flow in heterogeneous porous media. *SPE Journal* **1** (3): 153–169.

Wen, X.-H. and Gómez-Hernández, J.J. (1996). Upscaling hydraulic conductivities in heterogeneous media: An overview. *Journal of Hydrology* **183** (1–2): ix–xxxii.

Wen, X.H., Durlofsky, L.J. and Edwards, M.G. (2003). Use of border regions for improved permeability upscaling. *Mathematical Geology* **35** (5):521-547.

White, C.D. and Horne, R.N. (1987). Computing absolute transmissibility in the presence of fine-scale heterogeneity. Paper SPE 16011 presented at SPE Symposium on Reservoir Simulation, 1-4 February, San Antonio, Texas.

Willcox, K. and Peraire, J. (2002). Balanced model reduction via the proper orthogonal decomposition. *AIAA Journal* **40** (11): 2323-2330.

Yeo, I.W. and Zimmerman, R.W. (2001). Accuracy of the renormalization method for computing effective conductivities of heterogeneous media. *Transport in Porous Media* **45** (1) : 129-138.

Zandvliet, M. (2008). *Model-based lifecycle optimization of well locations and production settings in petroleum reservoirs*. PhD Dissertation, Delft University of Technology.

Zandvliet, M.J., van Doren, J.F.M., Bosgra, O.H., Jansen, J.D. and Van den Hof, P.M.J. (2008). Controllability, observability and identifiability in single-phase porous media flow. *Computational Geosciences* **12** (4) 605–622.

SUMMARY

Geological models often represent the subsurface heterogeneity by using a large number of parameters (10^6 to 10^9 voxels). Moreover, the uncertainty of the geological parameters is increasingly taken into account by simulating an ensemble of model realizations which significantly increases the computational demands, especially when it is also required to perform repeated simulations for computer-assisted flooding optimization or history matching (e.g., application of reservoir simulation in closed-loop reservoir management). This requires an 'upscaling/order-reduction' solution that transfers the relevant features of a geological model to a flow simulation model such that cost-efficient simulation, prediction and control of the fluid flow in the reservoir become feasible.

In addition to the computational issues, a more fundamental reason for upscaling/order-reduction is related to system-theoretical concepts like controllability and observability of the system which indicate how much of the state-space can be influenced through changing the input (i.e., the degree to which the system is 'controllable'), and how much of the internal behaviour of the system can be inferred from the output (i.e., the degree to which the reservoir is 'observable'). In most reservoir applications and for a given configuration of wells, there is only a limited amount of information (output) that can be observed from production data, while there is also a limited amount of control (input) that can be exercised by adjusting the well parameters. From a system-theoretical point of view, this means that a large number of combinations of the state variables (pressure and saturation values) are not actually controllable and observable from the wells, and accordingly, they are not affecting the input-output behavior of the system. In this research, therefore, we approach the upscaling problem from a system-theoretical perspective, and we aim at adjusting (reducing) the level of model complexity (order) to the level of relevant dynamics in terms of input-output behaviour.

As the first approach, we propose a control-relevant upscaling (CRU) algorithm, in which the coarse-scale-model parameters are selected such that the distance between input/output behaviors of the fine- and coarse-scale models is minimized. This distance is measured in terms of different system norms that characterize the input-output behavior of the system. The advantage of this approach is that it focuses on the observable/controllable state variables and, therefore, relies on those grid blocks that are most important to the input/output behavior of the model.

The second approach is a multi-level selective (i.e. non-uniform) grid coarsening method, in which the criterion for grid size adaptation is based on the spatial quantification of the controllability and observability properties of the reservoir system. In this control-relevant selective coarsening (CRSC) method the level of refinement for each coarse grid block depends on its importance compared to other grid blocks. Based on the numerical examples, the CRSC algorithm can accurately reproduce the flow response of the fine scale models. Moreover, the selective coarsening gives more accurate results than a uniformly upscaled model with the same number of grid blocks. That is the case because the most controllable/observable areas, which appear to be in the vicinity of the wells and in high-permeable areas close to and connected to the wells, remain unchanged and, therefore, global flow patterns and permeability contrasts of the fine-scale model are better preserved by the CRSC algorithm.

Both CRU and CRSC are global methods in the sense that they rely on the system properties of the entire reservoir. However, they do not require any forward simulation, neither of the full nor of the upscaled model. They also do not depend on a particular control strategy but instead use the dynamical system equations directly. However, any change in the well configuration (including well locations and the number of inputs and outputs) requires a (partial) repetition of the upscaling procedure. Accordingly, these methods are attractive for use in computer-assisted flooding optimization or history matching studies for a given configuration of wells, but unattractive in applications like well placement optimization.

The use of the CRU technique in conjunction with a model-order reduction method such as proper orthogonal decomposition promises CRU application to large-scale reservoir models. Alternatively, the computational efficiency of both CRU and CRSC algorithms is improved using approximate techniques to obtain the controllability and observability Gramians. However, this research was primarily concerned with the system-theoretical aspects of upscaling in reservoir simulation. Further research is required to evaluate the computational benefits of applying CRU and CRSC to realistic large reservoirs and also multi-phase flow applications. Despite its preliminary character, the research reported here may offer a new insight into the upscaling problem from a system-theoretical perspective.

SAMENVATTING

Het aantal modelparameters waarmee de heterogeniteit van de geologische ondergrond wordt gekarakteriseerd is vaak heel groot (10^6 to 10^9 voxels). Bovendien wordt de onzekerheid betreffende de geologische parameters in toenemende mate opgevangen door simulaties van een ensemble van modelrealisaties, hetgeen de vereiste rekenkracht significant doet toenemen. Dit is in het bijzonder het geval wanneer de (ensemble-)simulaties herhaaldelijk uitgevoerd dienen te worden in het kader van een computerondersteunde reservoiroptimalisatie of history matching (parameterschatting) zoals, bijvoorbeeld, in een “closed-loop reservoir management” toepassing. Dit vraagt om een “opschalings-/orde-reductie” oplossing die de relevante kenmerken van een geologisch model vertaalt naar een stromingsmodel, zodat een efficiënte simulatie, voorspeling, en beheersing van de vloeistofstroming in het reservoir haalbaar worden.

Behalve de rekenkundige aspecten zijn er ook meer fundamentele redenen voor opschaling/orde-reductie, die verband houden met systeem-theoretische concepten zoals ‘regelbaarheid’ en ‘waarneembaarheid’ van het systeem, waarmee respectievelijk aangegeven wordt hoeveel van de toestandsruimte vanaf de systeemingangen te regelen valt en hoeveel van het inwendig dynamisch gedrag van het systeem uit uitgangsmetingen bepaald kan worden. In de meeste reservoirtoepassingen en voor een gegeven puttenconfiguratie is er namelijk slechts een beperkte hoeveelheid informatie (uitgang) die uit productiedata waargenomen kan worden. Aan de andere kant is er ook slechts een beperkte mate van besturing (ingang) mogelijk door het regelen van de putparameters. Vanuit een systeemtheoretisch oogpunt betekent dit dat een groot aantal combinaties van de toestandsvariabelen (drukken- en saturatiewaardes) vanuit de putten feitelijk onregelbaar en onwaarneembaar zijn, met als resultaat dat ze het ingang-uitgang gedrag van het systeem niet beïnvloeden. In dit onderzoek wordt het opschalingsprobleem derhalve vanuit een systeemtheoretische perspectief benaderd, met als doel het verlagen van het complexiteitsniveau van het model (d.w.z. het reduceren van de modelorde) tot het niveau van relevante dynamica met betrekking tot het ingang-uitgang gedrag van het systeem.

In de eerste aanpak stellen we een “control-relevant” opschalingsalgorithme (CRU) voor, waarin de grove-rooster parameters zo geselecteerd worden dat de afwijking van het ingang-uitgang gedrag van het grove-rooster model ten opzichte van het gedrag van het fijne-rooster model geminimaliseerd wordt. De afwijking wordt gedefinieed met behulp

van verschillende systeemnormen die het ingang-uitgang gedrag van het systeem karakteriseren. Het voordeel van deze aanpak is dat het zich focust op de regelbare/waarneembare toestandsvariabelen/combinaties en zich derhalve op die roosterpunten richt die voor het ingang-uitgang gedrag van het model het meest belangrijk zijn.

De tweede aanpak is een multi-level selectieve (d.w.z., niet-uniforme) rooster-opschalingsmethode, waarin het roosteradaptatiecriterium gebaseerd wordt op de ruimtelijke kwantificatie van de regelbaarheids- en waarneemaarbaarheidseigenschappen van het reservoirsysteem. In deze control-relevante selectieve opschalingsmethode (CRSC) hangt het verfijningsniveau voor elk roosterpunt af van zijn gewicht in vergelijking tot andere roosterpunten. Numerieke voorbeelden geven aan dat met behulp van het CRSC algoritme de stromingsresponsie van het fijne-rooster model nauwkeurig gereproduceerd wordt. Bovendien levert de selectieve opschaling nauwkeuriger resultaten dan een uniform opgeschaald model met hetzelfde aantal roosterpunten. Dat is het resultaat van het feit dat de meest regelbare/waarneembare gebieden, dat wil zeggen de gebieden dichtbij de putten en in hoogdoorlatende zones dichtbij en verbonden met de putten, in een selectieve opschaling onveranderd blijven. Globale stromingspatronen en doorlatendheidscontrasten worden met het CRSC algoritme daardoor beter behouden.

Zowel CRU als CRSC zijn globale methoden in de zin dat ze berusten op systeemeigenschappen van het hele reservoir. Ze vereisen echter voorwaartse simulatie van noch het volle noch het opgeschaalde model. Ze zijn ook onafhankelijk van de regelstrategie en maken rechtsreeks gebruik van de vergelijkingen van de systeemdynamica. Elke wijziging in de putconfiguratie (zowel wat betreft putlocaties als het aantal van ingangen en uitgangen) vereist echter een (gedeeltelijke) herhaling van de opschalingsprocedure. Deze methoden zijn derhalve aantrekkelijk voor gebruik in computergesteunde optimalisatie of history matching studies voor een gegeven putconfiguratie, maar niet voor toepassingen in putplaatsingoptimalisatie.

Het gebruik van de CRU techniek in combinatie met een model-orde reductie methoden zoals “proper orthogonal decomposition” opent mogelijkheden voor het toepassen van CRU op grootschalige reservoir modellen. Als alternatief is de rekenefficiëntie van zowel CRU als CRCS algoritmen te verbeteren door gebruik te maken van benaderende technieken voor het verkrijgen van de regelbaarheids- en waarneembaarheids-Gram matrices. Het huidige onderzoek was primair gericht op de systeemtheoretische aspecten van opschaling in reservoirsimulatie, en verder onderzoek is nodig om de rekenvoordelen te evalueren van het toepassen van CRU en CRSC op realistisch grote reservoirs alsook

meerfasestroming toepassingen. Ondanks zijn voorlopige karakter levert het gerapporteerde onderzoek een nieuw inzicht op in het opschalingsprobleem vanuit een systeemtheoretische invalshoek.

ABOUT THE AUTHOR

Ali Vakili was born on June 6, 1979 in Ghom, Iran. He received his Bachelor degree in Chemical Engineering from Tehran University, Iran, in 2001. Afterward, he moved to the Netherlands in 2002, where he received his Master of Science degree in Petroleum Engineering from Delft University of Technology (TU Delft) in 2004. From mid 2004 to mid 2006, he was employed as a reservoir and production engineer in NIOC (National Iranian Oil Company). He moved again to the Netherlands in July 2006 to pursue his PhD study at TU Delft. The results of this study are reported in this thesis. In July 2010, he started a postdoc research in Reservoir Systems and Control at the department of Geotechnology, TU Delft.